Elastic Tensile Properties of Uncured Towpreg Composite Materials: Experiment and Modelling

Massimo Carboni

A Thesis

in

The Department

of

Mechanical, Industrial and Aerospace Engineering

Presented in Partial Fulfillment of the Requirements

For the Degree of Master of Applied Science in Mechanical Engineering at

Concordia University

Montreal, Quebec, Canada

August 2020

Concordia University

School of Graduate Studies

This is to certify that the thesis prepared

By: **Mr. Massimo Cabroni**

Entitled: **Elastic Tensile Properties of Uncured Towpreg Composite Materials: Experiment and Modelling**

and submitted in partial fulfillment of the requirements for the degree of

Master of Applied Science (Mechanical Engineering)

complies with the regulations of this University and meets the accepted standards with respect to originality and quality.

Signed by the final Examining Committee:

_____ Chair
Dr. Tsz Ho Kwok

_____ Examiner
Dr. Tsz Ho Kwok

_____ External Examiner
Dr. Anjan Bhowmick

_____ Supervisor
Dr. Mehdi Hojjati

Approved by

_____
Department Chair *Dr. Martin D. Pugh*

20th July, 2020

_____
Dr. Mourad Debbabi, Interim Dean
Gina Cody School of Engineering and Computer Science

Abstract

Elastic Tensile Properties of Uncured Towpreg Composite Materials: Experiment and Modelling

Massimo Carboni

Modern composite manufacturing techniques using Automated Fiber Placement (AFP) technology incorporates process modeling simulations to predict the path of the towpreg. One of the limiting factors in process modeling for AFP is the reliance on using cured composite material properties while in practice, the properties of the uncured state is required. Variability exists in the material properties between both states, with the properties of the uncured towpreg being significantly lower due the viscous matrix. One of those properties is the tensile modulus. Through experimental uniaxial tensile testing of uncured towpreg samples, the mechanical behavior of the material is analyzed in order to propose a model to accurately predict the modulus at varying loads and temperatures. Along with this data, the effects of fiber waviness on the tensile behavior of uncured towpreg are analyzed at the microscopic level. To support the experimentation, a finite element analysis (FEA) is performed to demonstrate the correlation at the micro and mesoscale levels between fiber waviness and the tensile response curve of uncured towpreg. A mathematical model is proposed derived from free body diagram analysis and classical lamination theory and based on the assumed sinusoidal wavelength of the fibers to predict how the fiber geometry affects the system.

Acknowledgements

My appreciation goes to my supervisor Dr. Mehdi Hojjati for his expert advice, encouragement and support throughout the writing on this thesis. The work would not be possible without his faith in the project.

I would like to also thank Dr. Daniel-Iosif Rosca and Dr. Heng Wang for their support in performing the experimentation necessary to complete this research. I would also like to thank all my friends and colleagues from Concordia for their collaboration and discussions on the topic, especially to Mr. Mohammad Hossein Ghayour, Mr. Mushan Belhaj and Mr. Ali Dodangeh.

Lastly my sincerest thanks go to my mother, my sister, and my girlfriend for the love and support they've shown me through this academic journey. I wouldn't have been able to complete this program without them.

Table of Contents

List of Figures

List of Tables

Chapter 1: Introduction

1.1 Background

Composites manufacturing has become more relevant in all forms of industry, with the aerospace industry being one of the major consumers in carbon fiber reinforced composites. Manufacturing of composites is typically done using sheets of unidirectional carbon fiber prepreg. Prepreg consists of unidirectional carbon fiber tows pre-impregnated with uncured epoxy resin. The prepreg system is then frozen as to halt the curing process of the resin. The final results are a malleable sheet of carbon fiber and uncured resin that can be placed along a preformed tool. Upon placement, the sheet of prepreg is malleable enough to conform to the shape of the tool while still maintaining its structural integrity. Once the part is completed and required number of sheets of carbon fiber are placed, curing of the resin can take place to produce the finished part. Traditionally, parts have been manufactured using hand lay-up and other manually operated manufacturing techniques. However, with the rise of smart factory and industry 4.0, the demand for automated manufacturing of composite parts has increased due to the benefits it possesses over manufacturing methods involving manual labor; thus leading to the emergence of Automated Fiber Placement (AFP) and Automated Tape Laying (ATL) manufacturing techniques. ATL and AFP manufacturing are similar processes that use an automated control arm to place tows of carbon fiber prepreg across a preformed tool. This arm applies a compaction force to the uncured prepreg, via a roller, to compress it onto the tool while the arm applies a tensile force to pull the prepreg taught, all the while continuously feeding more material as it moves along it's preprogrammed path. As the arm steers the prepreg along the surface of the tool, shear can also be introduced into the prepreg system, depending on the control path. Once the first layer of prepreg is laid down, the machine restarts the path over again to place down as many plies as needed. The main difference between ATL and AFP manufacturing lies in the width of the material being laid down on the tool. AFP manufacturing typically places several tows of prepreg at the same time, while ATL lays down a single tow.

These automated methods of composite manufacturing are faster, more cost-efficient and provide a viable alternative in manufacturing large complex structures. Several reviews on these new types of manufacturing methods have been published in recent years [1]–[6], highlighting the potential benefits of this manufacturing process. As presented in E. Oromiehie's review on AFP technologies, there has been a growing shift in recent years to replace traditional manufacturing methods, such as hand layup, with AFP based manufacturing. Figure 1.1 shows the percentage by which conventional manufacturing techniques have been replaced by AFP in recent years. While a large percentage of manufacturing is shifting to AFP methods, there still are some drawbacks associated with this automated process. It is possible for defects in the placement of material to occur that can negatively impact the mechanical performance of the finished lamina.

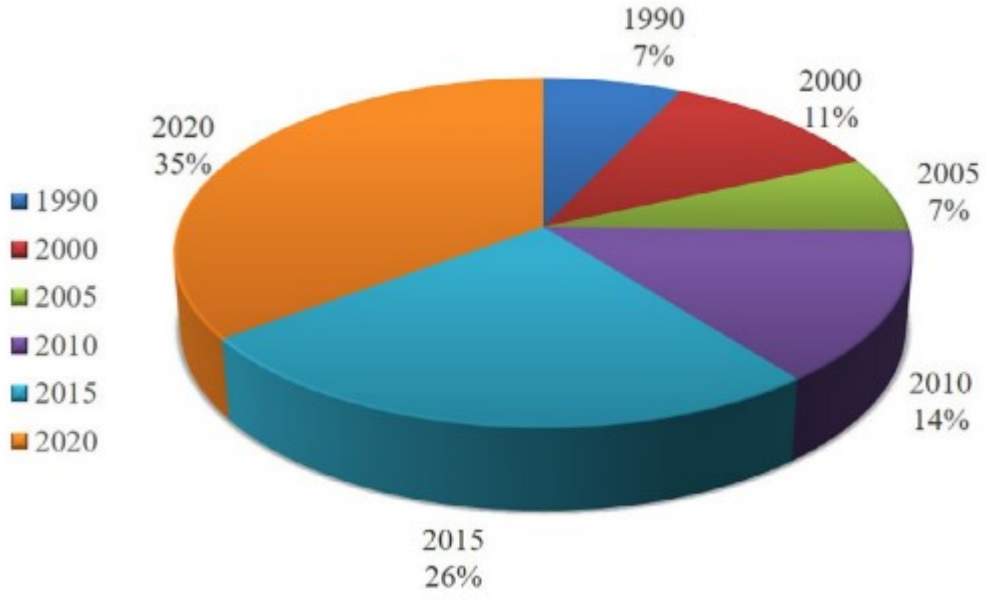

Figure 1.1: Adaption of AFP Based Composites Manufacturing over Traditional Methods [4]

Both AFP and ATL manufacturing techniques rely on process modeling simulations to predict the path of the fibers and to control the process parameters to avoid the formation of different types of defects. This process model is used to simulate the path of the machine head in order to predict how the prepreg will be laid down. While recent papers have published their findings into

the defects associated with AFP and ATL manufacturing [7]–[11], F. Heinecke's general study on imperfections in AFP [8] provides a clear overview on the recent work done in this field of study and on the major possible defects that can occur along with their potential sources. From this paper, it is most interesting to note that Heinecke states that while automated manufacturing has a high potential to replace manual manufacturing, the main hindrance for its implementation is machine downtime due to inspection and rework caused by defects in the prepreg deposition. One proposed solution to improve the automated process is to develop more accurate and detailed process models to better predict where and why defects occurs. Thus, with such process models the manufacturing parameters can be adjusted accordingly and the overall occurrence of defects can be reduced. Figure 1.2 represents the types of defects described by Heinecke et al. in their review of the automated fiber placement processes.

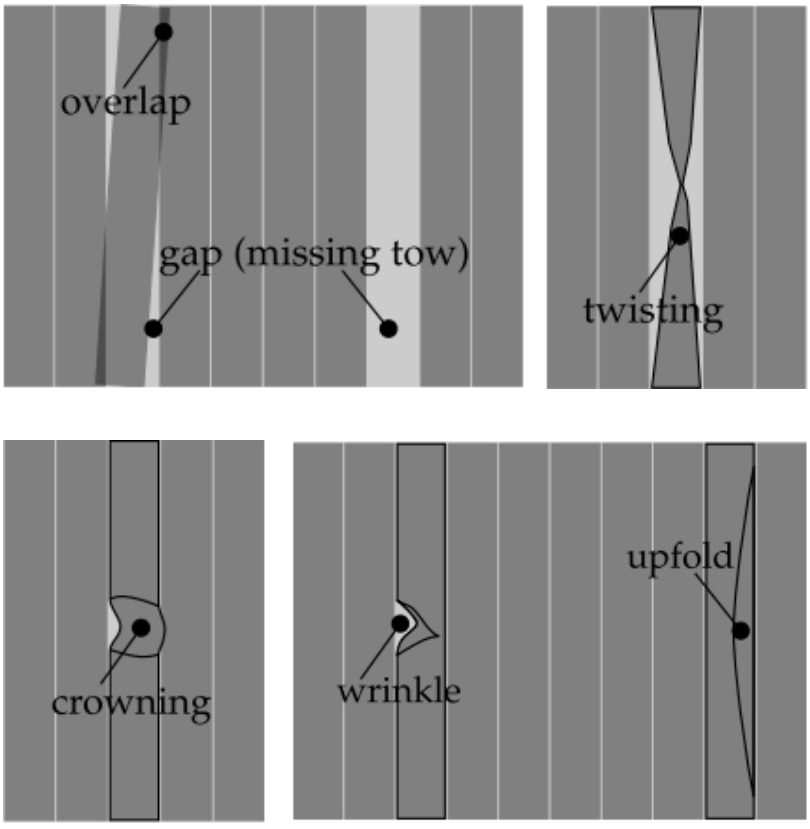

Figure 1.2: Most Common Types of Defects Found in AFP & ATL Manufacturing [8]

One of the limiting factors in process modeling for AFP and ATL is the reliance on using the cured composite material properties when the material properties for the uncured state is required. Variability exists in the material properties between both states, with the properties of the uncured state being significantly lower due the vicious matrix. This change in material properties between real world application and simulations can be attributed to a source of error in the AFP and ATL process modelling and defects such as tow misalignment, angle deviation, gaps and overlaps can occur during the manufacturing process as a result. Many studies have been done to investigate the material properties of uncured carbon fiber prepreg, specifically focusing on tensile, compression and shear behaviour of this material [6]–[22]; however, there is still more research to be done in this field.

1.2 Aim and Objective

The aim of this study is to close the knowledge gap concerning the tensile behavior of uncured carbon fiber used in AFP and ATL manufacturing. As Z. Wang et al. presented in their study on AFP tensioner control modulus [1], the tension imposed on the prepreg system has a significant impact on the quality of the final part. The instability in tension control results in the application of too little, or too great of a tensile force which will cause structural defects in the laminate. To gain a better understanding of the mechanical behavior of the uncured prepreg material, it's tensile performance will be analyzed, primarily through experimental testing, in order to propose a model to accurately predict the modulus of said material at varying loads. Along with this data, the effects of fiber waviness on the tensile behavior of uncured prepreg will also be determined. To support the experimentation, a finite element analysis (FEA) model will be developed to demonstrate the correlation at the micro and mesoscale between fiber waviness and the tensile response curve of uncured prepreg. A mathematical model will also be proposed based on the assumed sinusoidal wavelength of the fibers to predict how the geometry affects the force throughout the system. The results of this study will be applicable to process modeling of AFP manufacturing to reduce the number of defects occurring in the process due to the instability of applied tensile loads. The equations presented in the last sections of this thesis are

applicable for both FE modeling and hand calculations in determining the effective modulus of the uncured system.

1.3 Thesis Outline

This study is divided into eight chapters to form a complete thesis based on studying the tensile stiffness of uncured thermoset carbon fiber prepreg. The outline of each chapter is as follows:

Chapter 1: Introduction. In this chapter, a general introduction into automated fiber placement technologies is outlined. Specifically, the use of carbon fiber prepreg in manufacturing of composite materials. The motivation and aims of this thesis are also described.

Chapter 2: Literature Review outline. This section of the thesis focuses on evaluating the current work done in this field of study, focusing on the properties of uncured prepreg. Initial developments, testing methods and ideas stated in this chapter will be used as a basis for the work found in this study.

Chapter 3: Experimental Testing. This chapter will present the testing procedures and methodology that will be used in this thesis. The section will focus on the test setup and how the evolution of the material properties will be conducted. It presents the material that will be used throughout experimentation and all the testing apparatuses used.

Chapter 4: Results and Discussion. Following from the previous chapter, this section highlights and presents the recorded data and observations made through experimental testing. All plots, figures and tables obtained through testing of the material will be presented in this chapter and initial conclusions will be made about the driving properties of the uncured system.

Chapter 5: Finite Element Model. The finite element model created and simulated will be presented in this chapter of the thesis. Focusing on the development of ABAQUS simulations, comparisons between the tested and simulated results will be discussed here.

Chapter 6: Mathematical Model. To achieve the main goals of this thesis, the mathematical model to solve for the stiffness parameters of the uncured carbon fiber prepreg will be presented

in this chapter. Culminating the findings from all previous chapters and presenting a solution to the initial question, this final chapter will mathematically detail the effects occurring on the stiffness of the prepreg system.

Chapter 7: Conclusion. Serving as a summary of the thesis, this chapter will provide closing remarks on the proposed solution of this work. The aims and goals of the report will be answered here.

Chapter 8: Future Work. As the final chapter of this thesis, any future work or remaining uncertainties will be addressed in this section and considerations on improvements will be made.

Chapter 2: Literature Review

2.1 Review of Mechanical Behavior Test Methods

As one of the fundamental properties of any material, the tensile behavior of uncured carbon fiber prepreg must be known in order to have an accurate model for AFP and ATL simulations. During the ATL and AFP manufacturing process, a robotic arm applies a compaction force via roller on the uncured prepreg, pressing it down onto the tool. This compaction force is applied to allow a certain level of tackiness in the prepreg in order to hold the material in place as the robotic arm moves along the tool path. As the arm is moving, the prepreg being placed down is constantly under a uniaxial tensile force as it is being fed from the machine. If the tensile force applied by the automated arm is too great, the tackiness of the material will not be able to withstand the force and the prepreg will lift off from the tool. If the tensile force is too weak, there will be too much slack present in the prepreg which can result in unwanted defects. Thus, in process modeling, it is important to have an accurate representation of the tensile behavior of uncured prepreg in order to properly calibrate to machine and avoid unwanted defects in the part. Studying the tensile behavior of uncured carbon fiber prepreg is done through uniaxial tensile testing.

A few studies have been done to investigate the tensile properties of uncured carbon fiber prepreg [12], [19], [20], [28]. In studying the variability of uncured carbon fiber epoxy prepreg, K. Potter et al. [20] investigated the tensile modulus of this material and how the waviness of the fibers should effect the tensile response. They believed that the fiber wrinkling and angle of misalignment in the prepreg would be reflected in the tensile response curve. They performed a uniaxial tensile test on a stack of 13 tows of unidirectional carbon fiber/ epoxy prepreg along the fiber direction and measured the stress/strain response using a 25 kN Instron test machine. The samples tested had a gauge length of 500 mm and were 40 mm wide. The displacement rate of the test machine was set to 1 mm/min. During the test setup, the ends of the test samples were rapidly cured using heater plates, and an extra layer of prepreg was cured to the ends of the

specimens. This was done in order to provide a non-viscous surface for which the grips of the tensile machine can clamp onto to prevent/minimize slippage in the grips during testing. During testing, failure was reported to occur at random locations along the width of the specimen in the form of fiber splitting and was observed to start at a load of about 8 kN. Additionally, testing was done over a range of temperatures, and it is important to note that at higher temperatures, failure in the samples occurred at a lower load. The study attributed the tensile response to fiber misalignment in the prepreg and a stress/strain plot was presented. The initial slope of the plot was characterized as a "lead-in" area of non-linearity followed by a linear region. This lead-in area was attributed to the resistance the fibers are experiencing as they move through the highly viscous resin. This region was found to be present up to approximately 0.17% strain in the samples.

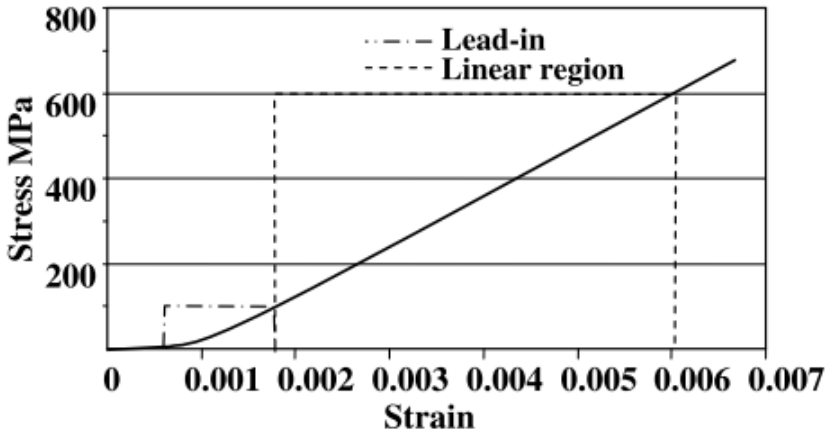

Figure 2.1: Stress vs. Strain Curve with Lead-In Region [20]

Researchers at North Western University, supported by a subcontract from the Ford Motor Company, published their findings on the mechanical response of woven composite prepreg during forming processes [19]. Focusing on the mechanical response and properties of the prepreg system, the uniaxial tension test was performed on uncured prepreg to obtain the tensile modulus. A Digital Image Correlation (DIC) setup was used to record the strain field on the surface of the samples and tests were conducted between a temperature range varying between 23 °C

and 80 °C. To prevent slippage from occurring in the grip, the ends of the specimens were partially cured, as seen in other works. Similar to the results observed by K. Potter [20], the stress/strain plots of the tensile response, over varying temperatures, all exhibited a region of non-linearity followed by a linear region as seen in Figure 2.2. This report studied the effects of temperature on the non-linear section of the plot and determined that as temperature increases, the area of non-linearity also increases. However, the phenomenon and the reasoning behind the non-linear region were not addressed, and the stiffness represented by the linear region of the plot was selected to describe the entire response of the uncured prepreg. While study of the lead-in region was not conducted by the author, it is most likely due to the same phenomenon discussed earlier, as the woven fabric has continuous fibers, the fibers must be drawn through the viscous resin and thus results in a reduced tensile modulus.

A similar test method was conducted by D. Sentis et al. [28] in their study of the tensile behaviour of uncured sheet moulding compounds. While working with chopped glass fibers in an ester-based resin instead of carbon fiber/ epoxy resin, their test method for determining the tensile response of the uncured prepreg is still applicable to our application, and follows the work of K. Potter [20]. Their test setup uses a uniaxial tensile machine with a 500 N load cell and samples were made with a gauge length of 300 mm. In order to minimize slipping and ensure a stable hold, the grips were wrapped in sandpaper to add an extra source of friction in holding the viscous sample. Prior to testing, samples were subjected to a small tensile stress to ensure stability of the sample and correct any misalignment. Additionally, a Digital Image Correlation (DIC) setup was used to record the stain field on the surface of the samples. A DIC setup prevents any slippage in the grip from affecting the results from the experiment as the strain is calculated based on the movement on the surface of the sample and is independent from the movement of the machine head. Furthermore, experimentation was also conducted under X-ray microtomography. This allows the recording of the microstructure of the prepreg sample and is able to make a more accurate link between the macro and micro scale movements in the prepreg samples. During testing, similar failure mechanics were observed to those seen in the work of K. Potter [20], which is failure occurring in the form of splitting along the vertical tensile direction. The resultant graphs differ greatly to the ones observed earlier [19], [20] primarily due to the

difference between how chopped fibers interact with the matrix as opposed to continuous fibers. Chopped fibers are free to move between each other and would result in a typical linear stress vs. strain curve while continuous fibers are restricted due to the fact they need to be drawn through the matrix. This can be seen in comparing the stress strain curves between both experiments.

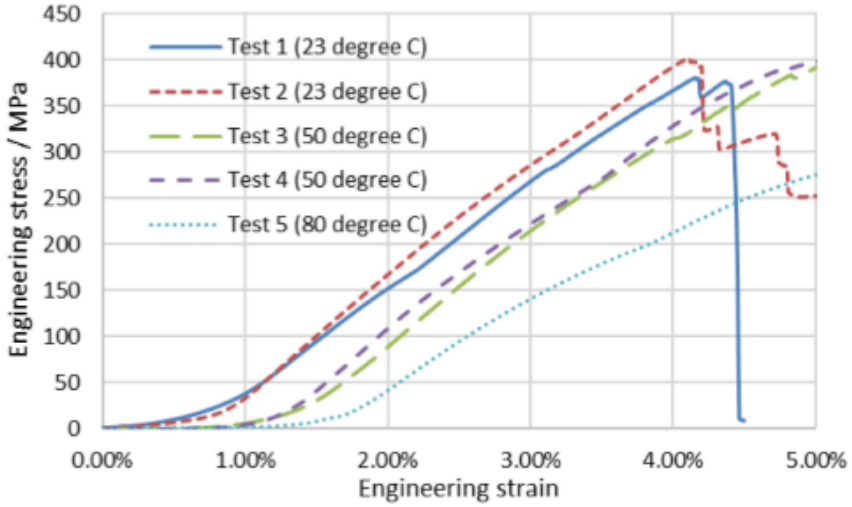

Figure 2.2: Effect of Temperature on the Tensile Response of Uncured Prepreg [19]

Dangora et al. proposed one more novel solution to overcoming the gripping difficulties in tensile testing uncured prepreg [12]. In her paper researching the temperature-dependent tensile and flexural rigidities of uncured thermoplastic prepreg, a similar tensile test was conducted as seen in the previously described works. Focusing on thermoplastic cross-ply prepreg oriented in a $(9/90)_2$ configuration, tensile testing was done in order to determine the apparent modulus and the effect of temperature on the tensile behavior of the material. To overcome the challenge of gripping the uncured prepreg, Dangora et al. proposed solution was to implement a modified gripping solution which incorporates two external pins, which the ends of the prepreg will be wrapped around. Once the prepreg has both its ends wrapped around the pins, the grip of the tensile testing machine will clamp down on the prepreg, leaving the pins to rest on the top surface of the grips. In this solution, the material is prevented from slipping in the

grips, as it is wrapped to an external pin resting outside of the grips. While testing was conducted on a thermoplastic cross-ply prepreg, a different material from the focus of this study, the gripping solution is still relevant and is applicable to any form of uncured AFP/ATL prepreg.

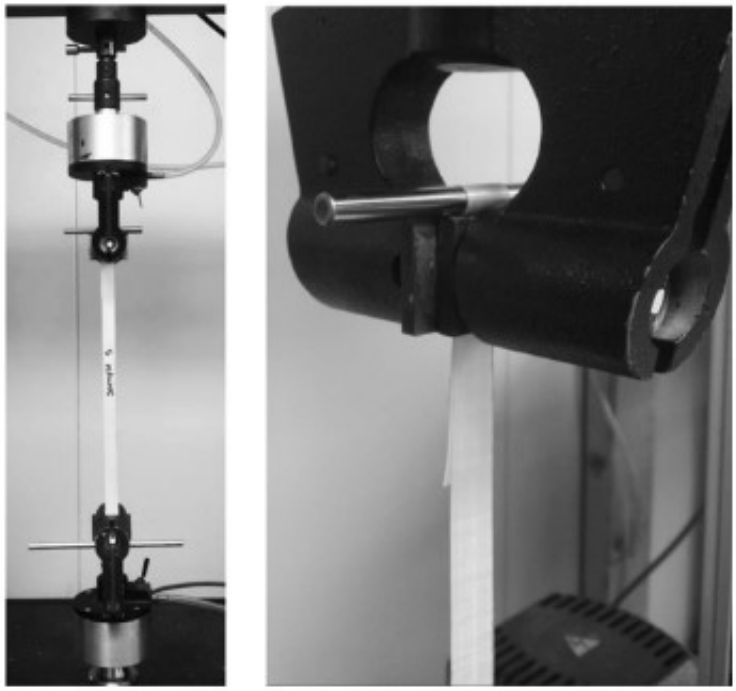

Figure 2.3: Proposed Gripping Solution Presented by Dangora et al. [12]

In addition to proposing a novel gripping solution, not seen in other works, Dangora et al. also investigated how temperature plays a role in affecting the mechanical behavior of prepreg in its uncured state. As discussed earlier, it is believed that the tensile behavior, up to approximately 0.2% strain, is dictated by the motion of the fibers as they are pulled through the viscous medium of the uncured resin. As a result, as temperature changes, the resin characteristics will change as well. As reported by Dangora et al., even in a thermoplastic cross-ply prepreg, temperature does influence the apparent tensile modulus of the material. It was reported that as temperature increases, the modulus lowers following a trend of a third-order polynomial. It is stated that this reduction in modulus was expected as the increase in temperature made the matrix more compliant to movement and facilitated the movement of the polymer chains resulting in reduced stiffness [12].

The uncured nature of the epoxy medium in carbon fiber prepreg, leads to the assumptions that the mechanical behaviour of the material is temperature dependant, considering that temperature of a liquid has an affect on the viscosity. Theoretically, as the temperature of a liquid increases, the viscosity would go down, resulting in an easier flow through the material. This can be expressed mathematically using the Andrade equation [29].

$$\mu = A * exp^{(-E/RT)} \quad (2.1)$$

Where μ represents viscosity, R is the gas constant, E is the activation energy of the viscous flow, A is the pre-exponential factor and T is temperature. Using this equation, the viscosity can be said to follow the function of temperature based on the exponential plot of the inverse temperature. Following this function, as temperature increases, the viscosity exponentially lowers. This equation can be applied in estimating the way the epoxy matrix will behave as temperature in the system increases. As the viscosity of the epoxy lowers with the rise of temperature, the carbon fibres theoretically should exhibit less impeded motion through the prepreg. In turn, the fibers will be able to rotate through the medium at a lower shear force compared to a medium of higher viscosity. As a result, it is expected that the mechanical behaviour of a heated uncured epoxy prepreg system to exhibit a lower stiffness than one that is at room temperature or that is cooled. This phenomenon is important to AFP/ATL manufacturing as the prepreg is heated during the process. As the head of the machine deposits the prepreg onto the tool, a point source of heat is introduced to the material. This heat is applied at a temperature below the curing activation temperature of the epoxy as the intention of applying heat is not to start curing, but to assist in the deposition, the tackiness and the placement of the fibers.

The resin matrix used to impregnate the prepreg tested in this study is CYCOM 977-2 epoxy resin. This epoxy cures at 177℃ and has service capability of 126℃ to 138℃ dry [30]. It is designed to be cured by autoclave and has an out of freezer shelf life of 10 days. Figure 2.4 represents the viscosity of this epoxy as a function of time and temperature.

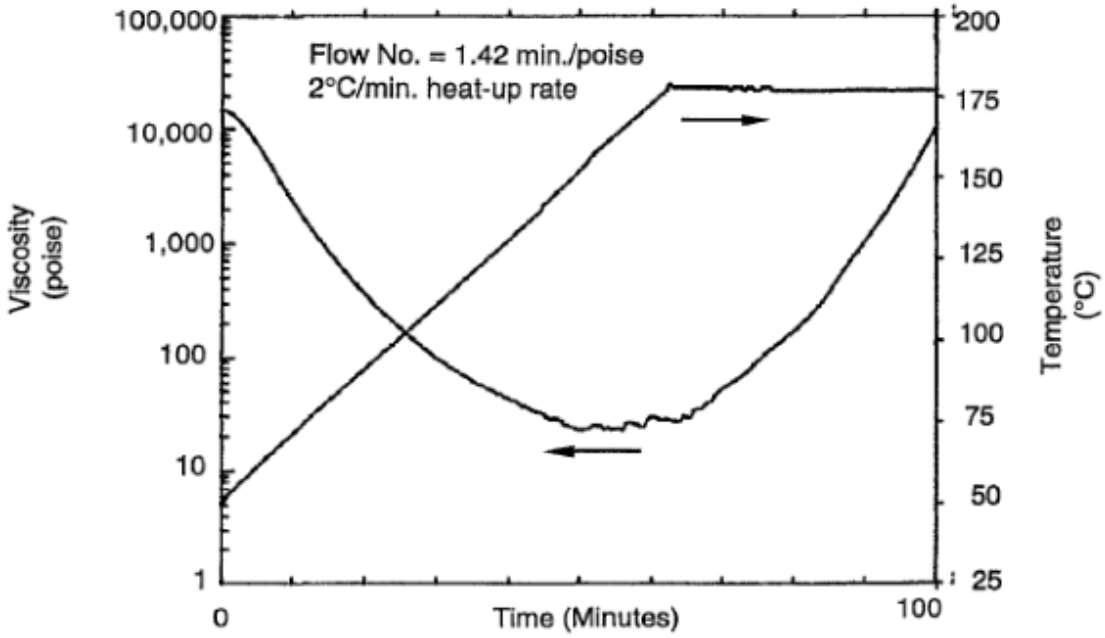

Figure 2.4: Viscosity Profile of CYCOM 977-2 [30]

As seen in this figure, starting at a temperature of approximately 50 ℃, the viscosity begins to decrease from a room temperature value of about 10,000 P. The resin system continues this downwards trend in viscosity as temperature increases until it reaches its lowest point at approximately 40-50 P at a temperature of 177 ℃ (cure temperature). As the system begins to cure, the viscosity increases once again until reaching a solid state. It is important to note the exponential decrease of viscosity that this epoxy can exhibit in a short amount of time. Being at a temperature between 50 ℃ to 75 ℃ for around 10 minutes can lower the viscosity of the system by an order of 10. Considering this large change of viscosity due to temperature effects, it is important to take this into consideration when performing tests on the mechanical behaviour of uncured laminate systems. As a result, many papers researching the mechanical behaviour of uncured carbon fiber prepreg included temperature effects as part of their study.

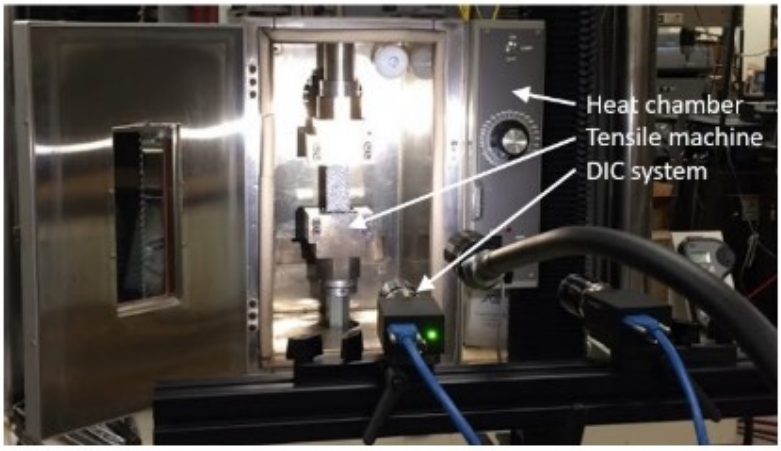

Figure 2.5: Experimental Setup for Uniaxial Tensile Test Performed by Zhang et al. [19]

In one such paper, Zhang et al. studied the effects of varying temperature on the tensile performance of uncured carbon fiber woven prepreg [19]. By performing the uniaxial tensile test inside of a heat chamber, as shown in Figure 2.5, each sample was exposed to uniform and continuous heating throughout the experimentation process. Performing tests at temperature increments of 23, 50 and 80 degrees Celsius, the resultant engineering stress vs strain curves can be seen in Figure 2.2. In analyzing the plots, it is noted that the stiffness of the material is reduced as temperature increases. Additionally, the lead-in area of non-linearity is increased as temperature is increased. There are several factors that can describe this phenomenon. Primarily, the rise in temperature increased the compliancy of the epoxy, therefore the stiffness was reduced. As the load increased, eventually the stiffness achieved a similar slope in the linear region, indicating that the fiber modulus became the dominant material property as the waviness was corrected. However, it is possible that some slippage was introduced into the system due to the decrease of viscosity which can result in the reduced stiffness and an increase in the lead-in region, at least until the system stabilised as the load increased. It is also important to note that Zhang et al. performed his tests on woven prepreg, while the focus of this study will be on UD material. While the two materials should behave in a similar fashion, the graphs presented in the research of Zhang et al. cannot be used as a baseline for unidirectional prepreg and our own conclusions must be made from experimental testing.

Dangora et Al. also performed a similar uniaxial tensile test on uncured prepreg material and included temperature into her experimentation process [12]. Using a ceramic heating plate on one face of the prepreg material, the laminate was subjected to uniform constant heating. Testing was conducted at varying increments of temperature between 20 and 120 degrees Celsius on cross-ply thermoplastic lamina. Figure 2.6 represents the apparent tensile modulus of the prepreg, calculated through tensile testing, as temperature was increased.

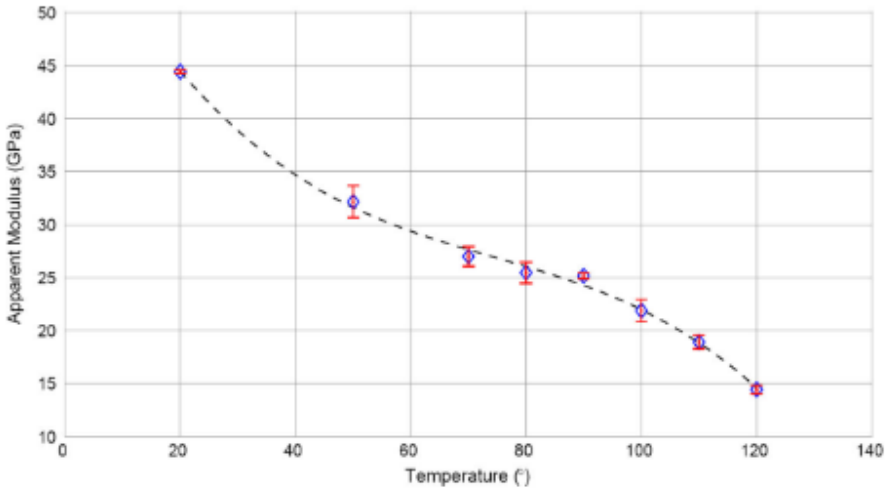

Figure 2.6: Apparent Tensile Modulus as a Function of Temperature [12]

As expected, the stiffness of the material was reduced as temperature was increased. Dangora et al. relates this reduction of modulus to the fact that the heat facilitated the motion of the polymer chains in the uncured thermoplastic, thus resulting in a reduced stiffness. However, once again, these experimental results are based on another material, in this case they were conducted on a cross-ply thermoplastic lamina, which can behave very differently than the UD carbon fiber epoxy system investigated in this study. Nonetheless, the findings of her report are still relevant to this study as both relate to the mechanical behaviors of an uncured viscous liquid exhibiting uniaxial tensile testing. While the tensile behavior of our material might not follow the same trend, the findings of Dangora et al. and Zhang et al. further supplement the assumptions made from equation 2.1, that a reduction in stiffness is expected in the uncured lamina as temperature is increased.

In addition to tensile behaviour of uncured prepreg, other mechanical properties such as compression and shear are just as important to the process modelling of AFP and ATL manufacturing and have been more widely researched [12], [13], [15], [16], [18], [21], [22], [25]. The bending behaviour during buckling caused by uniaxial compression has been studied by H. Alshahrani et al. and J. Wang et al. [16], [18] both conducted similar buckling tests in order to determine the compressive modulus of uncured prepreg. Tests consisted of securing a test sample, made from multiple plies of unidirectional uncured prepreg, into the clamps of a uniaxial tensile tester. As slippage is not a concern in buckling tests, no extra steps were taken to secure the clamping mechanism of the machine. Both researchers observed that the uncured prepreg has similar behaviour to a spring by having a linear buckling curve. Furthermore, the relaxation modulus was also determined using the same test method. By loading the sample to a specific load and holding is in that position, the change in force over time can be recorded. As the strain remains constant within the sample, the load will change over time as the material relaxes and thus the relaxation modulus can be determined. Figure 2.7 Represents the test setup as conducted by H. Alsharani et al. [16]

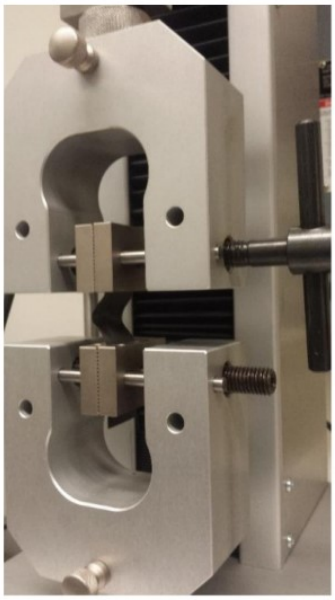

Figure 2.7: Buckling Test on Uncured Prepreg Sample as Prepared by H. Alsharani et al. [16]

Calculations of the compressive modulus and the relaxation modulus are important to the process modeling of AFP and ATL manufacturing, as the sample can be heated and formed at varying rates, which affects the bending behaviour of the material. Thus, knowledge of these properties are necessary to conduct accurate simulations. As a result, the compressive modulus, and the bending properties of uncured carbon fiber prepreg have been a focused topic of research in recent years and many researches have provided contributions into this field of study.

Fiber steering and the steering radius in AFP and ATL manufacturing is one potential source of defects during the manufacturing process of composite parts and is dictated by the shear behaviour of the uncured prepreg tape. Research has been done in studying the shear property by performing a 10° off-axis tensile test, as seen by the work done by Yi Wang et al. and K. Potter [23], [27] for studying the shear behaviour of unidirectional prepreg or by the picture frame method and bias-extension test for textile composites as seen in the work by P. Boisse et al. and Zhang w. et al. [19], [24]. While the shear property is similarly important in textile composites, due to the in-plane and out of plane movement of the fibers affecting the drapability of the prepreg, the same in-plane and out of plane behaviour influences the behaviour of unidirectional prepreg in automated manufacturing. Focussing on the off-axis test for unidirectional prepreg, the test consists of using a standard uniaxial tensile machine to tensile test a prepreg sample with the fibers at a 10-degree offset angle to the applied load as described in the work by F. Pierron. In the off-axis test conducted by Yi Wang et al. [27] samples were cut to a gauge length of 320 mm and a width of 40 mm and were gripped in the tensile test machine by roller jigs to minimize slipping. A DIC setup was used to measure the strain in the sample. It is important to note in their recorded data, that at loads exceeding 150-220 N, the sample began to buckle and wrinkle due to the compression in the sample in the transverse direction and Poisson's effect. Their work provided validity to the feasibility of this test method for uncured unidirectional prepreg and studied the shear behaviour of the material over a range of temperatures and test rates. Similar to research done on the compressive and buckling behaviour of unidirectional prepreg, test methods and research into the shear behaviour have been established in recent years [14], [19], [23], [24], [26], [27], while comparable work into the tensile modulus of this material is still lacking.

2.2 Review of Fiber Waviness in Unidirectional Prepreg

Fiber waviness is one aspect of uncured unidirectional prepreg that can greatly affect the material properties and the performance of the material. The fiber alignment in prepreg is a major source of variability between samples and needs to be addressed when studying the mechanical behavior of such materials. Fiber waviness is described as any angle of misalignment in the fibers along the fiber direction (1 direction) of the lamina. Due to the viscous matrix, the fibers are able to move between each other and disrupt their alignment. Many papers have been written concerning the effects that fiber waviness has on the material properties of the composite and how to measure the waviness in an uncured prepreg, and in a cured lamina [20], [31]–[38]. In 2018, A. Stewart [32] published his findings in studying the fibre alignment in aerospace grade unidirectional prepreg. It is important to study the waviness in the prepreg prior to and post manufacturing to get a clear idea of the mechanical behavior of the finished laminate. In his findings, it was assumed that the fibers follow a sinusoidal function, and they were able to estimate the degree of fiber misalignment using the arc length equation and the fibers radial position on a roll of prepreg. Additionally, A. Stewart proposes methodologies in measuring the angle of misalignment in cured prepreg. In cutting a cured sample at an angle of 5° in the 1-3 plane, then into 3 equal sections along the length, the cross section of the resultant wedge can be analyzed by microscopy. In studying the elliptical cross section of the fibers, the waviness can be determined. Using the equations of sin and the major and minor diameters of the ellipse, along the 3 sections of the sample, the fiber waviness can be determined. This methodology was derived by Yurgartis [31] and used by K. Potter et al. [20] The drawback of this methodology is that the samples must be cured before the waviness can be measured, and the effect on the material properties of the cured lamina were considered, instead of on the uncured prepreg.

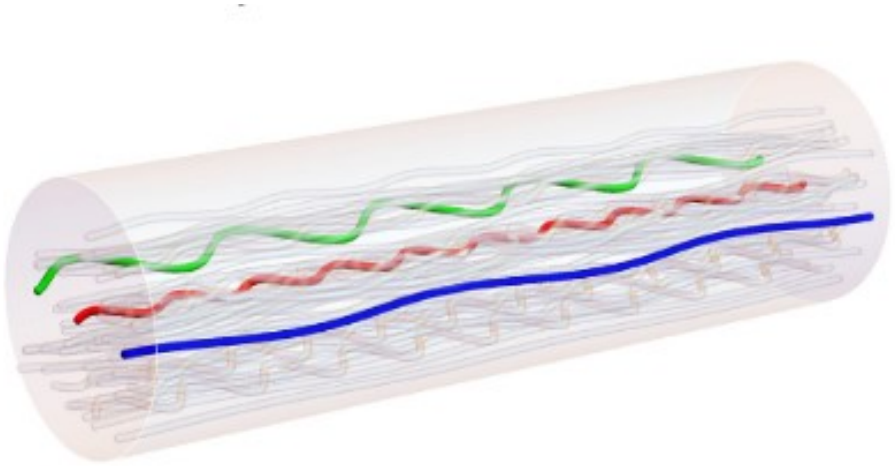

Figure 2.8: Assumed Sinusoidal Waveform of Carbon Fiber in an Uncured Prepreg [32]

Other methods for studying the waviness in prepreg and lamina have been developed by D. Wilhelmsson et al. [34]. Their methodology is based on studying the surface of the prepreg (1-3 plane) and using microscopy, identifying the individual fibers and studying their wavelength. This methodology has been seen before in work from P. Joyce [35], where the surface of a prepreg sample is analyzed and the amplitude and wavelength of an individual fiber is determined. With these measurements, the maximum misalignment angle of the fibers can be determined. One criticism P. Joyce [35] had about this method was how the results were extremely user dependent as the operator decided which fiber to analyze and selected the geometry. To overcome this disadvantage, D. Wilhelmsson [34] developed the HRMA method in which, using the same microscopic images of the surface of the prepreg, an algorithm based in MATLAB will identify the angle of individual fiber segments in lieu of a user. The software operates by first placing a grid of square cells over the microscopic image of the surface of the prepreg. With a small enough cell size, the curvature of the fibers will appear as linear slopes and allow the software to trace the individual fibers based on the color discrepancy between the white pixels of the fibers and black pixels of the resin. Using these tracing and regression formulas, the angles of each identified fiber in each cell can be determined and quantified into statistical data.

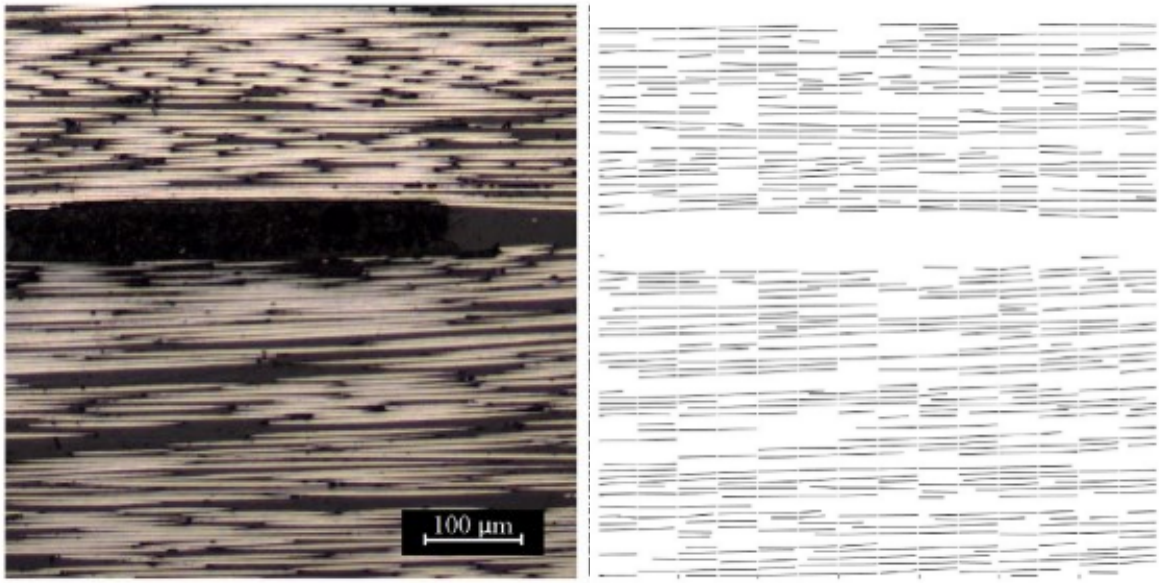

Figure 2.9: Close up of Fiber Micrography with Corresponding MATLAB Resultant Regression Lines [34]

This software is good at determining an overall idea of the waviness in the prepreg, however there are still limitations to it. The software is only able to identify the waviness on the surface fibers of the prepreg, therefore the waviness in the other planes are still unknown. Additionally, the samples must be prepared for microscopic imaging, and in doing so the fiber waviness may be affected. To prepare samples, they must first be polished as to clean the surface and to expose the fibers. In this polishing step, due to the circular motion of the polishing pad, and the viscous medium of the resin, movement of the fibers can still occur. Additionally, the software calculates the fiber misalignment angle based on the regression line of the fiber per its position in the square cell grid which can lead to a lower mean misalignment angle bias. If the fiber path is assumed to follow a sinusoidal function, there is only one location (at the tangent to the rising slope) where the misalignment angle is at its maximum. However, the software takes the misalignment angle along the entire sinusoidal path, resulting in the mean angle of misalignment for one fiber to be lower than the actual tangential angle of misalignment.

Chapter 3: Experimental Testing

The focus of this chapter will be on analyzing the tensile behavior of uncured carbon fiber prepreg through experimental testing. This chapter will describe the selected aerospace grade prepreg used along with the uniaxial tensile test setup. Two testing conditions will be explored, one standardized testing at room temperature to analyze the tensile behavior under normal circumstances, the other at elevated temperatures to study the heat effect on the tensile behavior. In addition, microscopic analysis on the waviness of the prepreg, prior to and after testing will also be explored in detail.

3.1 Materials and Equipment

The material used for analysis in this study was Solvay S.A., CYCOM 977-2. It is an aerospace grade carbon fiber & epoxy resin prepreg system, and the fibers used in this system are unidirectional (UD) 12K HTS-196 [39]. The relevancy of this material in aerospace manufacturing and its continued use is important in considering the finding from this report as it is applicable in current real-world applications. Table 3.1 summarizes the main material properties of this prepreg material per the datasheet from Solvay.

Table 3.1 Material properties of CYCOM 977-2 [39]

Fiber	12K HTS-196
Resin	CYCOM 977-2
Resin Content (%)	34
T_g (°C)	170
Tow width (mm)	6
Tow Thickness (mm)	0.01275
0^θ Tensile Modulus (GPa)	136

It is important to note that the prepreg used in AFP and ATL manufacturing are different than traditional prepreg as they are prepared as a several meter long and narrow wide continuous strip of material wound around a spool. This spool of prepreg is able to be fed through the delivery head of an AFP or ATL machine and deposited onto a tool. For experimental tensile testing, samples of this prepreg were cut from this spool to a length of 150 mm long. As only one ply of material was tested, the sample width and thickness stayed the same as to what is recorded in Table 3.1, a width of 6 mm and a thickness of 0.01275 mm.

The uniaxial tensile test was performed on a HOSKIN testing machine. This machine was equipped with a 1000 N load cell throughout the experimentations conducted in this study. As samples were not planned to be tested to failure, a higher rated load cell was not necessary. In addition, since the lead-in region of non-linear stiffness occurs at low force, at the beginning of the stress/ strain curve, in order to get an accurate reading of this area the use of a lower rated load cell is ideal. The HOSKIN testing machine is computer controlled; and with the included software, displacement rate, max load, and max displacement can be set. The resultant force vs displacement plot is recorded for each experiment.

The grips used by this testing machine are standard knurled grips as seen in Figure 3.1. Due to the viscous nature of the uncured prepreg, modifications to the standard gripping method had to be done, as discussed in literature [12], [19], [20], [28]. The solution developed in this study follows the solution presented by Dangora et al. Taking inspiration from her work, it was decided to make 4 rectangular bars in which the prepreg can be wrapped around and then place within the clamps of the HOSKIN machine. The steel rods were made from cutting standard steel key stock to a length of 40 mm. The cross section of the key stock is 5 mm by 5 mm. The ends of the prepreg sample was wound around one of the steel rods about 2 to 4 times, and then sandwiched against the other rod as shown in Figure 3.2 (a) & (c). The samples were first set up and clamped in the lower grip, then they were aligned and clamped in the upper grip. This was to ensure no misalignment in the sample setup and to ensure the tensile load was applied in the fiber direction. After being wound around the steel rods, the testing sample gauge length was 127 mm. This new assembly of prepreg and key stock was then placed in the grips of the HOSKIN machine and clamped down securely in place. The result being that the knurled clamps are now

applying the gripping force to the steel rods in lieu of the viscous prepregs as shown in Figure 3.2 (b).

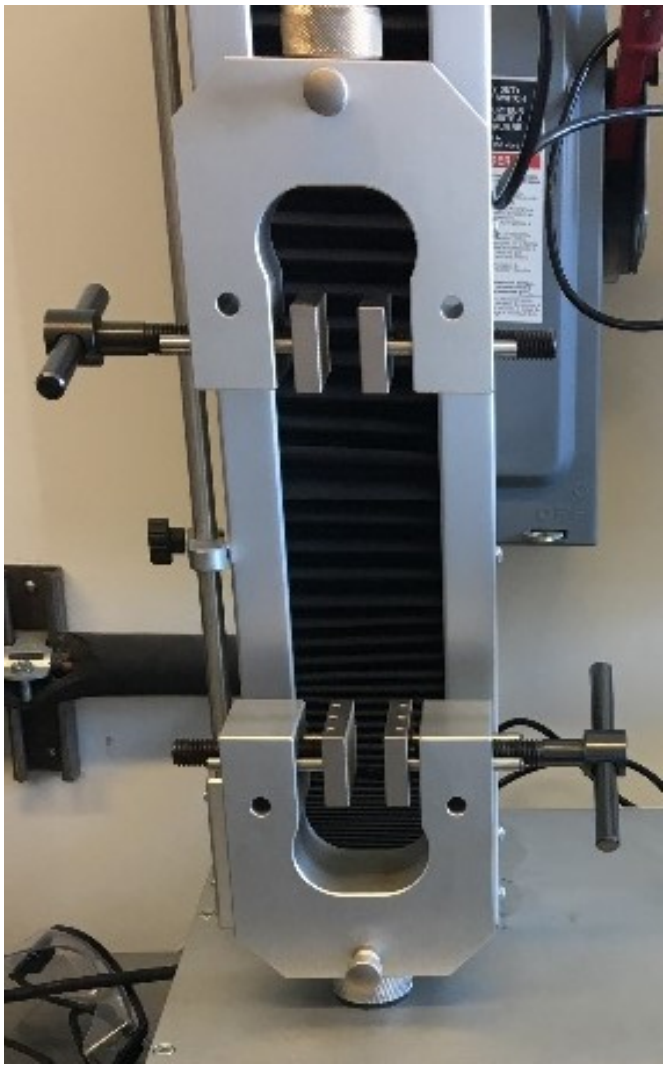

Figure 3.1: Grips of the HOSKIN Uniaxial Testing Machine used in Experimentation

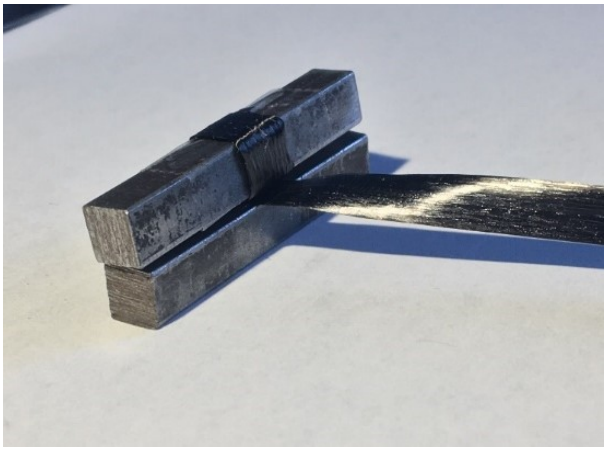

(a)

(b)

(c)

Figure 3.2: Test Sample for Uniaxial Tensile Testing Wrapped around Steel Blocks to Prevent Slippage

3.2 Uniaxial Tensile Testing of Uncured Prepreg

The primary method for calculating and plotting the tensile modulus of a material is to perform experimental uniaxial tensile testing. The basis of this type of testing consists of subjecting a sample to a force in one direction at one end, while having the other end fixed in place. Referring to Figure 3.1, the HOSKIN machine used in this study has the lower grips fixed to the machine, while the top grips move along the vertical axis. A load cell mounted above the top grips is used to record the force exerted during the experimentation. For our experimentation, it is important to have selected a load cell capable of recording a high force load due to the strong stiffness of carbon fibers, while still being rated low enough to accurately record the forces at the beginning of the experiment. Due to these criteria, a load cell rated at 1000 N was chosen for the experimentation.

3.2.1 Testing Parameters & Data Acquisition

In determining the testing parameters to use in this study, decisions were made based on initial testing observations and on the literature review. As there are no standards in performing tensile tests on uncured prepreg samples, variables such as the rate of displacement and the maximum load, as well as other testing parameters, must be based on the literature reviewed and on experimental observation. For this study, a displacement rate of 2 mm/min was chosen. This value was determined through initial testing and comparing the resultant plots at different displacement rates. A rate of 2 mm/min provided an accurate and clear plot of the lead-in region, which is critical to our study. It is also closely related to the speed chosen by Potter et al. in his experimental testing [20]. As mentioned earlier in this section, testing to failure is not the goal of this study; therefore, the value for maximum allowable force obtainable during testing was set to 500 N. To reiterate, across all experimentation, the displacement rate of experimentation was set to 2mm/min to a maximum load of 500 N, using a 1000 N load cell and a sample gauge length of 125 mm, width of 6 mm and thickness of 0.01275 mm. In addition, prior to testing, samples were removed from the freezer and left to sit at room temperature for 1 hour.

As for data acquisition for the stress/strain plot, the main method for recording the stress within the system during experimentation is to record the force through a load cell, and mathematically determine the engineering stress. As for recording the applied strain during testing, there are numerous different methods available to use. As seen in literature, one way of calculating the strain during experimentation is through the use of a DIC setup. DIC strain calculations are based around the theory of recording the displacements between dots of a speckle pattern sprayed onto the sample using a camera and analysis software. The camera used during video capture of an experiment must be sophisticated enough to resolve the speckle pattern; also, in literature, it was observed that the focal length and the aperture of the camera and lens assembly are important factors to address while using a DIC setup [40]. Once the camera captures the experiment, software such as ARAMIS must be used to calculate the strains. While researchers used a DIC setup to calculate the strain exhibited by the uncured prepreg during uniaxial tensile testing [19], [28]; however, a DIC setup was opted not to be used for this study. While DIC does provide accurate results of strain measurements on the sample, it is an extremely complex system to set-up and analysis. In addition, there is still a source of error present in the strain calculations while using this method, and variations in the speckle pattern between samples can lead to errors in the strain calculations [41].

Due to the complexity and the potential source of error, strain calculations during experimentation in this study will be mathematically calculated based on the observed displacement at the head of the HOSKIN machine during testing. This approach was used during testing by Potter et al [20], and Dangora et al [12]. In addition, in the research done by Sentis et al [28], the engineering strain was also calculated mathematically by measuring the displacement at the head of the tensile machine to calculate the mean strain in the 1 direction. In addition to the use of a DIC system to measure the local surface strain field as mentioned above, further justifying the use of calculating the strain based on displacement. Using the recorded force and displacement obtained during experimentation, the engineering stress and engineering strain values can be calculated based on the following equations:

$$\sigma_1 = {}^{F_1}/_{(w * t)} \tag{3.1}$$

$$\varepsilon_1 = {}^{\Delta L}/_{L} \tag{3.2}$$

Equation 3.1 was used to calculate the stress σ_1 in the 1 direction (along the fiber direction) in the prepreg. F_1 is recorded by the load cell used in conjunction with the HOSKIN machine and is the force exerted on the prepreg. The variables w & t are the width and thickness of the prepreg respectively. In calculating the stress, it was decided to only consider the cross-sectional area of the fibers within the prepreg instead of the cross-section of the entire sample. This decision was based on the assumption that the uncured epoxy has a negligible contribution to the tensile modulus, thus the entirety of the stress was exerted on the fibers. This assumption is founded on the equation of rule of mixtures equation (3.3) in determining the elastic modulus.

$$E_c = \left(V_f E_f + \left(1 - V_f\right) E_m\right) \tag{3.3}$$

From this equation, using V_f as the fiber volume fraction, E_f as the modulus of the fibers and E_m as the modulus of the resin, the combined elastic modulus E_c can be determined. Considering the order of magnitude between the modulus of the epoxy and the fibers, it is justifiable to assume a negligible contribution from the epoxy modulus towards the modulus of the laminate. Therefore, in calculating the stress within the sample, the width and the thickness of the samples were modified by the volume fraction of the fibers, present in table 3.1 to be 66%.

Equation 3.2 was used for calculating the strain ε_1 in the vertical direction (along the fiber direction). The variable L represents the gauge length of the sample, which was kept the same at 127 mm across all samples. The variable ΔL represents the change in length of the sample. This was experimentally determined and recorded as the displacement at the head grip of the HOSKIN machine.

3.2.2 Procedure for Evaluation of Test Method

As there are no standards for testing uncured prepreg, the accuracy and reliability of our test method was evaluated. Initial trials were done, prior to testing for the tensile behaviour, to evaluate if the proposed gripping solution was adequate in the prevention of grip slipping. To conduct this evaluation, test samples were set-up in the HOSKIN tensile machine using the four steel blocks as outlined earlier in this report, and were subjected to an initial load of 100 N. Once this load was reached, the samples were then released and the tensile force was returned to a predefined load, where it held the samples for a short time before they were tensile tested once more. The return loads chosen for each sample were 40 N, 30 N, 20 N and 10 N respectively. The theory behind this test is based on stress relaxation. As the samples are initially loaded to 100 N, a pre-load is applied to the system and any obvious slippage would have occurred at this point. Once the samples reached 100 N, the samples were then held at a lower load to investigate the stress relaxation before the machine applied a tensile force once more. During the stress relaxation event at the lower load, any slippage in the system not detected in the first load to 100 N would become apparent. If slippage occurred as the load is held, the force would drop, and it would become apparent in the plot. Additionally, after the stress relaxation period, the samples were being tensile tested once more for the final verification for slipping. The expected plots in the final tensile test are expected to be linear, as any non-linearity would indicate slippage.

3.2.3 Procedure for Studying Tensile Behavior

Once the evaluation of the gripping solution is deemed acceptable, testing to record and study the full tensile behaviour of the uncured prepreg will be conducted. Testing of the samples were separated into two distinct testing runs per sample. The purpose of the first run is to bring the system to stability, verify the gripping, and to apply a pre-load to the sample. This first run consisted or performing a standard tensile test up to a maximum load of 100 N. As discussed in the previous section, this verifies that the sample was secured properly in the grips of the machine. In addition, any bends, twists or warping in the sample are corrected during this initial

tensile test run. These deformations have been observed to occur during hand manipulations of the uncured sample. An initial run to equilibrate the samples was also observed to be done in literature [28].

After the first run was completed, samples were returned to their initial position, and the load was removed. Once the sample was reset, the second run was conducted, following the parameters outlined in the previous section.

3.2.4 Procedure for Studying Temperature Effects

As the focus of the experimentation was to determine the effect of temperature on the non-linear portion of the stress/strain curve, forces in excess of 250 N are not necessary to the findings. The displacement of the head was set to 2 mm/min. As the rate of motion is an aspect that affects the viscosity, the displacement value was kept constant to testing performed at room temperature. Samples were heated by using a heat gun which applied a direct point source of heating as expected during AFP and ATL manufacturing, and a FLIR camera was used to measure and observe the changes in temperature of the prepreg. The heat gun was set-up on a stand and the nozzle of the heat gun was 254 mm away from the prepreg. The target temperature for the two tests are as follows; one at approximately 60 ℃ and the other at approximately 80 ℃.

In the initial tensile tests performed on the uncured prepreg, each sample was tested twice. The first test was to set the system to equilibrium in order to remove any sources of slippage and to ensure that the samples were gripped tightly. Additionally, in the first run, any misalignment of the sample was corrected as the initial force acted as a preload to the sample. The same philosophy was conducted when performing the tensile tests under temperature. Each sample was heated with the heat gun continuously as the sample were put under a preload. Heat was then removed as the sample was returned to its initial position. Following this, heat was applied once again until the sample reached a uniform temperature as observed through the FLIR camera and the second tensile test was conducted. These values obtained during the second test will be the values that will be taken for comparison. Four samples were tested at each temperature range. Once again, due to the assumption that the percent of the tensile modulus of the laminate

contributed by the epoxy is very small (based on rule of mixture theory) the engineering stress was calculated using the cross section of the prepreg and the volume fraction of the fibers, which is 66%. Figure 3.3 shows the setup used for testing.

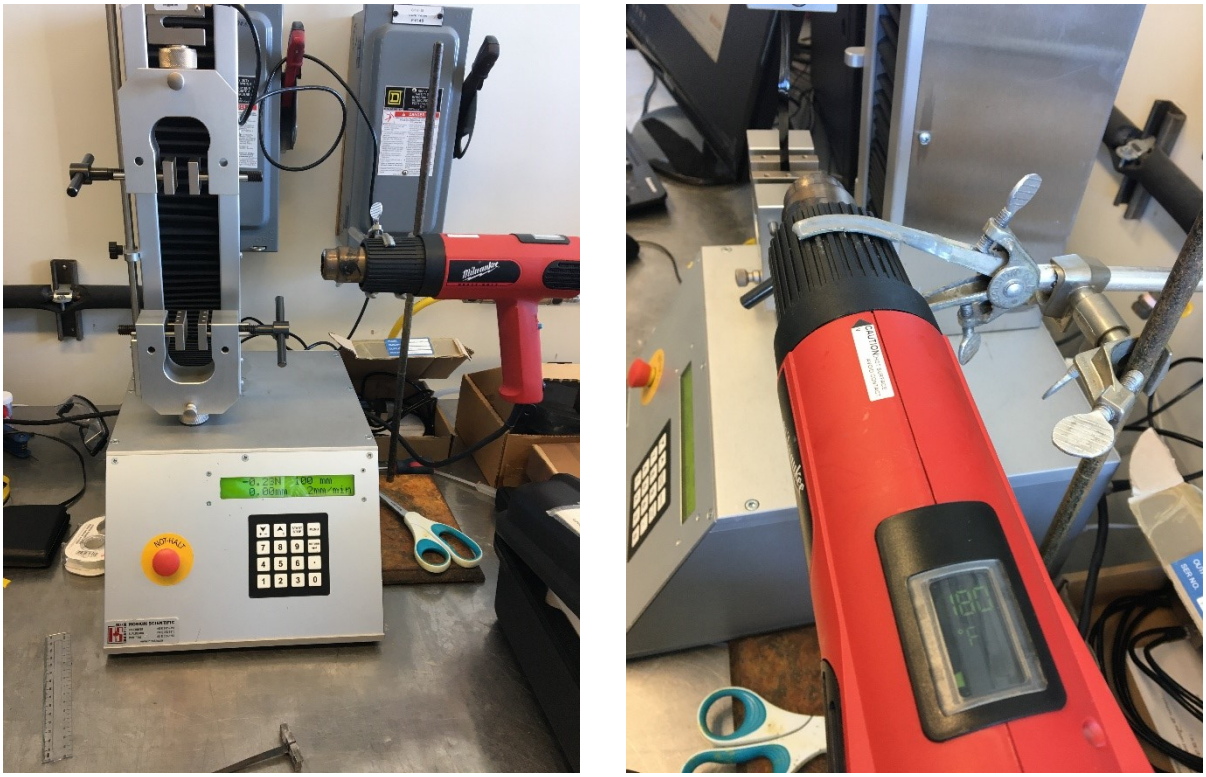

Figure 3.3: Setup for Tensile Testing under the Effects of Temperature

Note that the temperature recorded in the prepreg by the FLIR camera was different than the temperature of the heat gun. This is due to the convection forces and the heat transfer between the heat gun air and the samples. It was recorded that at a heat gun temperature of 140 °F, the prepreg achieved a temperature averaging 35 °C and at a heat gun temperature of 180 °F, the prepreg achieved a temperature averaging 40 °C.

3.3 Microscopic Analysis of Fiber Waviness of the Uncured Prepreg

To study the effect of fiber waviness and fiber misalignment, microscopic images and analysis were performed on the prepreg samples prior to and post tensile testing. D. Whilhelmsson and L.E. Asp at the Chalmers University of Technology developed a MATLAB code for characterizing the degree of fiber misalignment in microscopic images [34]. Using this software, the change in misalignment, and in turn the change in waviness before and after testing can be studied. Samples were prepared by embedding them in an epoxy resin puck, then polishing them until the sample was exposed on one end. The PRESI polishing machine used is shown in Figure 3.4. Once the samples were polished, microscopic images were taken at 10x magnification and analyzed with the MATLAB code. Additionally, ImageJ software was used to manually analyse the fiber waviness for comparative purposes to the code developed by D. Whilhelmsson et al.

Figure 3.4: PRESI Polishing Machine Used to Prepare Samples for Microscopic Analysis

Chapter 4: Results and Discussion

4.1 Tensile Test Results

The results of this study will be separated between studying and developing an idea about the tensile behavior of uncured carbon fiber prepreg and then a focus will be made on the effects of temperature. During testing, an emphasis will be made on analyzing the non-linear region of the stress/strain plot, as the tensile behavior at these low loads are most applicable to AFP and ATL manufacturing; also, there is a lack of knowledge as to what phenomenon is responsible for causing this non-linearity in the modulus. As stated in the literature review, it is believed that the initial fiber waviness (following an assumed sinusoidal function) and that the motion of the fibers being pulled taught through the viscous epoxy matrix that are the cause of the non-linear tensile behavior. Through tensile testing, the primary objectives will be to quantify this theory concerning the cause of non-linearity, to propose a standard test method for performing tensile tests on uncured prepreg, and to quantify data on the tensile modulus to compare to FEA and provided a basis for a mathematical model.

4.1.1 Evaluation of Test Method

As outlined in section 3.2.2, the first tests conducted in this study were based around evaluating the gripping solution proposed to limit/prevent slippage on the uncured samples. Following the testing procedure outlined in that section, a total of 4 samples were tested using the new gripping solution. Samples consisted of a single tow of prepreg, with a width of 6 mm and a thickness of 0.01275 mm. After wrapping both ends of the sample around the steel blocks, the final gauge length of each sample was 127 mm. The force and displacement recorded at any given time using the equations 3.1 and 3.2. and a 1000 N load cell was used. Figure 4.1 shows the initial setup used for evaluating the gripping solution. Sample (a) shows the areas of the sample which have twisted due to manual manipulation. Sample (b) shows bending that

occurred. To eliminate these twists, bends and folds in the prepreg, an initial load must be applied prior to testing. In the context of this study, the preload force was decided to be set at a 100 N.

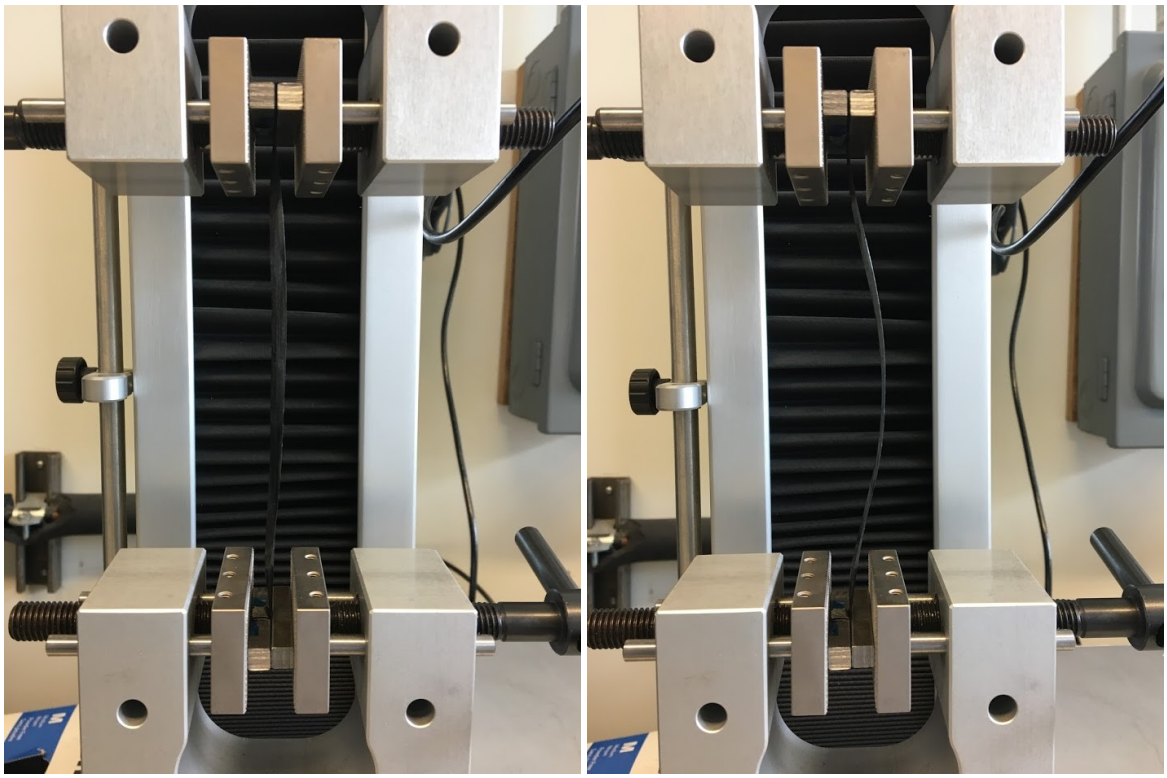

(a) (b)

Figure 4.1: Initial Setup for Evaluation of Gripping Solution

In continuing our evaluation, once the test samples were set up using the steel blocks and were subjected to an initial load of 100 N, samples were then released, and the tensile force was returned to a predefined load. The samples were held at this load for a short time before they were tensile tested once more. The return loads chosen for each sample were 40 N, 30 N, 20 N and 10 N respectively. Figure 4.2 shows the resultant plot for all 4 samples.

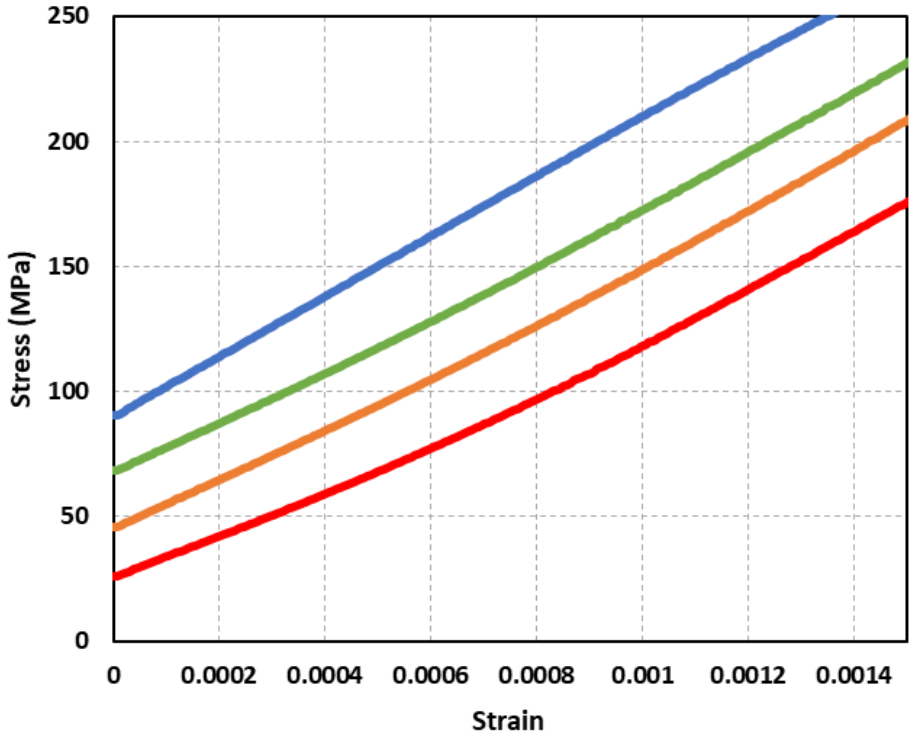

Figure 4.2: Experimental Results for Identification of Slippage in the Grips

Table 4.1 Tensile Modulus Recorded in Linear Section of Stress Vs. Strain Plot

Sample #	**Young's Modulus (GPa)**	**Sample #**	**Young's Modulus (GPa)**
1	113.78	3	113.69
2	115.54	4	112.99
Mean Tensile Modulus (GPA)	114	**Standard Deviation**	1.085

As shown in Figure 4.2 and Table 4.1, all samples tested exhibit a linear modulus with similar slope of approximately 114 GPa. The similarities in the slope indicate good repeatability of our test method. Comparing this value to the recorded tensile modulus of a cured laminate, found in Table 3.1 to be 136 GPa, we can see that they both follow a comparable modulus. This is expected, as between both cured and uncured states, the primary influence on the tensile modulus of the laminate stems from the tensile modulus of the fibers, as seen by the rule of mixtures equation 3.3. Variation between the modulus of a cured and uncured sample is expected, nonetheless. A cured sample undergoes effects of pressure and temperature which are able to correct waviness in the prepreg to a certain extent, this waviness is not able to be corrected during uncured tensile testing. Therefore, as the two values should not be compared in the context of accuracy in our test method, it is still comparable as a justification towards the calculations of stress in uncured testing. The values also defends the assumption to only consider the fibers contribution towards the uncured laminates elastic modulus.

In evaluating the gripping solution, it was determined that the proposed use of steel blocks provides an adequate platform for securing the sample within the test grips. As seen in Figure 4.2, the resultant plots across all 4 samples follow a linear trend. If there were any slippage within the grips, we would have seen some non-linearity or larger variations between the recorded tensile modulus. The small standard deviation between the samples is a strong indication that slippage is not occurring. Moreover, having held the samples at an elevated load prior to performing the tensile test provides further confirmation of the success of this gripping solution. If any slippage were to occur, it would happen under load (during this stress relaxation area prior to testing) and be expressed as a lower or non-linear stiffness in the resulting tensile stress plot.

In summary, the evaluation of the proposed test method indicated good repeatability between test samples. The proposed gripping solution was deemed feasible in preventing slipping of the samples and testing for the tensile modulus will follow the procedure used during this evaluation.

4.1.2 Tensile Behavior of Uncured Carbon Fiber Prepreg

Following the testing procedure derived from evaluating the test method, a total of eight samples were tested from two distinct batches of material. Both batches were manufactured by Solvay and share the same date of manufacturing. Testing of each sample occurred over two runs of tensile testing. As determined in the previous section, samples were first loaded to a load of 100 N to eliminate any twisting, bending or folding that may have been imposed on the sample. In addition, the pre-load provided stability to the system and served as a basis to ensure that the sample was aligned properly and that the grips were effectively set up. The second tensile load applied to the sample was imposed a few seconds after the sample returned to its initial position from the first run. The tensile behavior study will take the results from the second tensile test run.

The results indicate that the tensile response of an uncured carbon fiber can be characterized as a non-linear behavior at the beginning of the test followed by a linear region. The same behavior has been reported in literature where the non-linear region described as a lead-in region of the reduced modulus [12], [19], [20], [28]. From experimental observations, the lead-in (non-linear) region of the stress strain curve for our prepreg material was observed up until 0.2% strain where it then followed by a linear trend. Figure 4.3 represents the resultant stress vs. strain plot observed in one test sample. At an approximate strain value of 0.2%, the transition between a non-liner to linear stiffness can be seen.

Additionally, it is important to note that across all samples, at a tensile force of approximately 200 N, failure in the prepreg started to occur. Failure was observed to propagate in the form of fiber splitting and tearing, as observed in the research of K. Potter et al. as well [20]. This failure can be seen in Figure 4.3 to begin to occur at a strain rate of 0.6%, represented as a decrease in stiffness. This type of failure was detected across most samples as the strain reached values around 0.5%-0.6%. Considering that the focus of this study is based on the tensile response and the stiffness of the prepreg, failure conditions will be considered, and the plots will

be analysed up to a maximum value of 0.6% strain. Figure 4.4, provides a visual for the fiber splitting observed to occur at a force of 200 N.

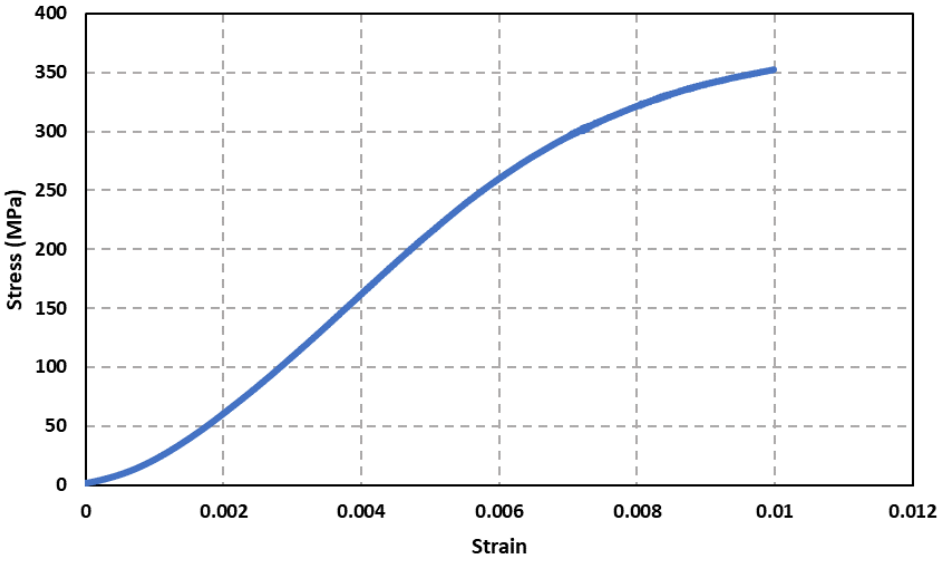

Figure 4.3 : Tensile Response Curve of an Uncured Prepreg Sample

Figure 4.4: Observed Fiber Failure

Using the recorded data taken from experimentation, plots were generated, taking the average stress and strain across all the samples. From this average, conclusions can be made on the non-linear stiffness and on the final linear stiffness experienced in the prepreg. Figure 4.5 represents the resultant plot of the average stress vs. strain curve of all experiments.

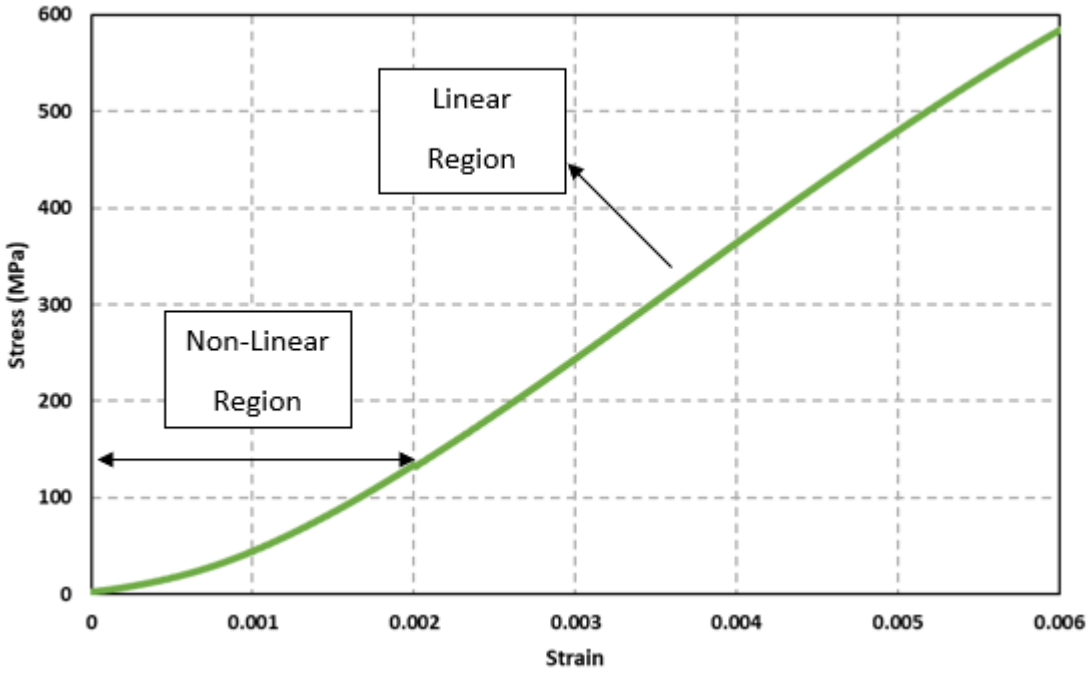

Figure 4.5: Average Experimental Results of the Tensile Behavior of Uncured Prepreg

As mentioned earlier, the non-linear region, on an average appears to occur between 0–0.2% strain. Succeeding this non-linear region, the stiffness follows a linear plot. Fitting a linear trendline to the strain region (0.2% - 0.6% strain) on the average plot results in a slope of 113.41 translating to an average linear modulus of 113.41 GPa. This again is comparable to the linear modulus observed in Section 4.1.1, recorded to be 114 GPa. This repeatability in the linear modulus indicates that on average the test method is repeatable. However, there is still a large standard deviation between the samples. The experimentally derived values for the linear tensile modulus of each sample is represented in Table 4.2.

Table 4.2: Linear Tensile Modulus of each Sample

Sample #	Linear Tensile Modulus (GPa)
Sample 1	127.35
Sample 2	132.71
Sample 3	124.89
Sample 4	108.56
Sample 5	86.74
Sample 6	117.98
Sample 7	95.63
Sample 8	113.42
Mean Tensile Modulus (GPa) 113.4127	Standard Deviation 15.9

Considering the large standard deviation, it is important to take a statistical approach to analyzing the data collected during experimentation. From Table 4.2, samples 5 and 7 have been omitted from the statistical analysis as they are considered outliers to our data pool. Figure 4.6 represents the normalized distribution of this data.

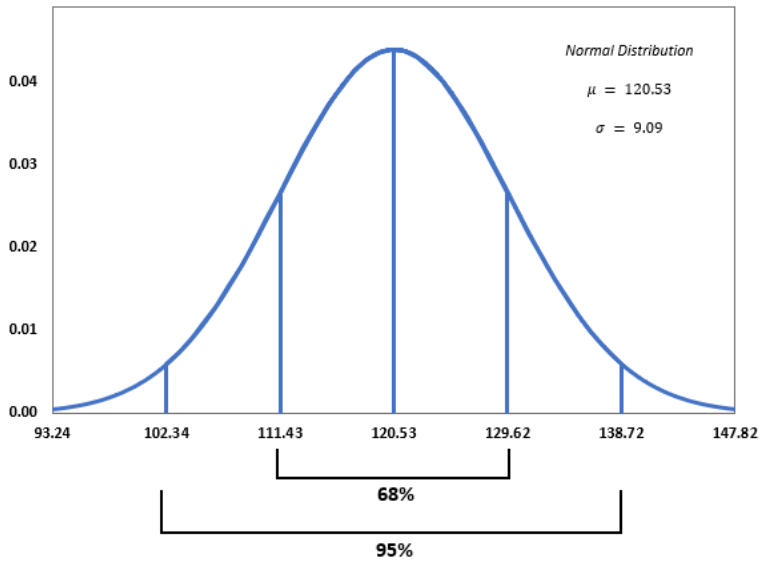

Figure 4.6: Normal Distribution of Linear Tensile Modulus (GPa) Values

Looking at the collected data, following the normal distribution, 68% of the samples will have a linear tensile modulus between 111.43.41 GPa and 129.62 GPa, while 95% of the sample will have a linear tensile modulus between 102.34 GPa and 138.72 GPa. While there does appear to be a large delta between these values, it is understandable due to the nature of the uncured material. As demonstrated through studying the failure mechanism of the material, it is apparent that the uncured matrix does not provide adequate resistance to prevent fiber splitting to occur. At a strain rating of approximately 0.5% - 0.6%, fiber splitting occurs and leads to failure in the sample. Due to splitting of the fibers, and the inability of the matrix to transfer the load from one fiber to another through the laminate, a large standard deviation is expected as premature failure of the fibers can occur. As a result, the trendline was generated between 0.2% strain to 0.5% strain. If premature failure occurred, a resultant dip in stiffness will skew the linear trendline and thus result in a lower slope hence the reason to stop the trendline at 0.5% strain. Figure 4.7 represents one such sample. As shown in the plot, this sample experiences a drop-in stiffness prior to reaching 0.6% strain. Thus, the variations in the mechanical behavior of the uncured prepreg samples, leads to a large statistical standard deviation in terms of experimentally calculated modulus.

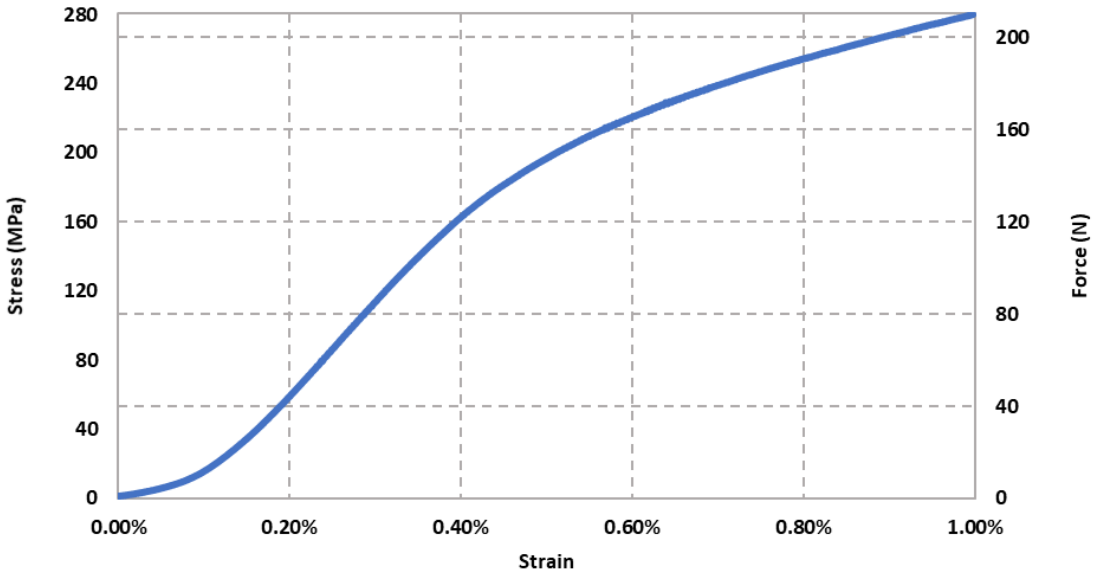

Figure 4.7 : Sample Experiencing a Premature Drop in Stiffness Due to Failure

This variation in the linear modulus can be observed even over the two different batches of identical material, where there is a standard deviation between results. Figure 4.8 shows the tensile response between two batches of identical Solvay prepreg. While both plots exhibit the same characteristic lead-in area followed by an area of linear response, the two plots have their own distinct behaviour.

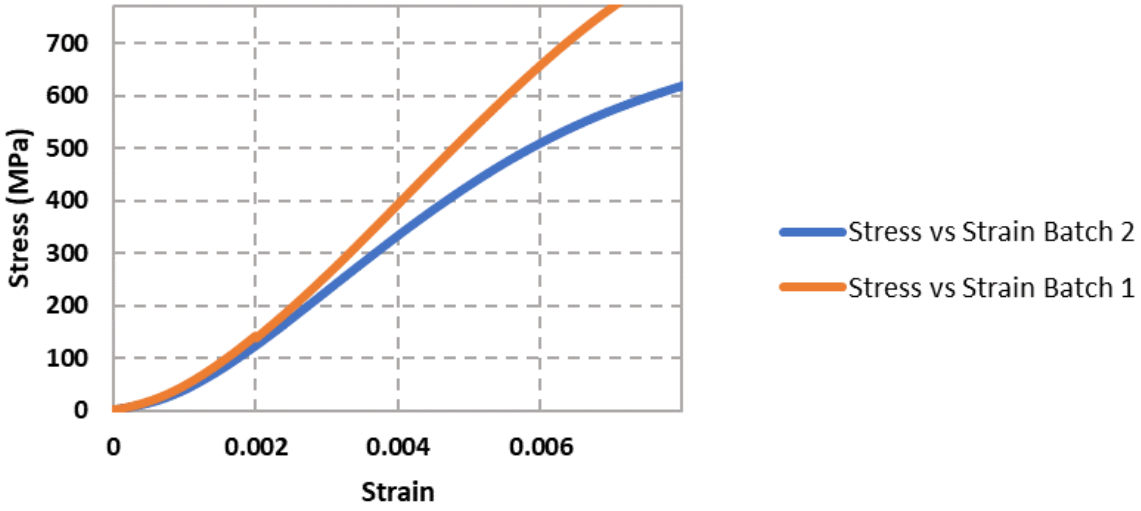

Figure 4.8 Difference in Average Tensile Response Between Two Different Spools of Towpreg Materials.

As a result, it is important to compare samples together as a statistical whole, and at the individual level. In terms of comparing the experimental plots derived from room temperature experimentation to those at elevated temperatures and to the mathematical model, it is essential to keep this statistical deviation in mind. In summary, the linear tensile modulus of the uncured carbon fiber prepreg tested in this study averages around 113-114 GPa. This value holds true as an average; however, at the individual sample level the majority of the samples linear tensile modulus is expected to be between 111 GPa and 129 GPa.

Shifting from the analysis of the linear stiffness region, the non-linear region of the plots must also be addressed. This region of non-linearity is observed between 0% - 0.2% strain and ends at a load of approximately 50 N. This region is most important to AFP and ATL manufacturing, as the expected loads exhibited on the prepreg during this process fall within this

region of non-linear stiffness. In AFP and ATL manufacturing, tensile loads are expected to be close to 25 N. It is, however, difficult to measure exactly what the applied loads are during this process. Nonetheless, the tensile modulus of the uncured prepreg is expected to be in the non-linear region of its response and thus modeling of the manufacturing process must consider the waviness, misalignment and the changing modulus in this region.

Following the same approach as with studying the linear region, curve fitting methods were used to determine the tensile modulus in this non-linear region. Firstly, taking the average plot across all samples, a 2nd order polynomial was used to fit a trendline to the region between 0-0.2% strain. The following trendline can be seen on Figure 4.9. Using the second order polynomial present on the figure, the slope can be derived by taking the first derivative of the equation. This slope represents the average tensile modulus exhibited by the uncured prepreg at a specific point in this non-linear region. Equations 4.1 and 4.2 represent the second order polynomial and it's first derivative.

$$y = ax^2 + bx + c \tag{4.1}$$

$$\frac{dy}{dx} = 2ax + b \tag{4.2}$$

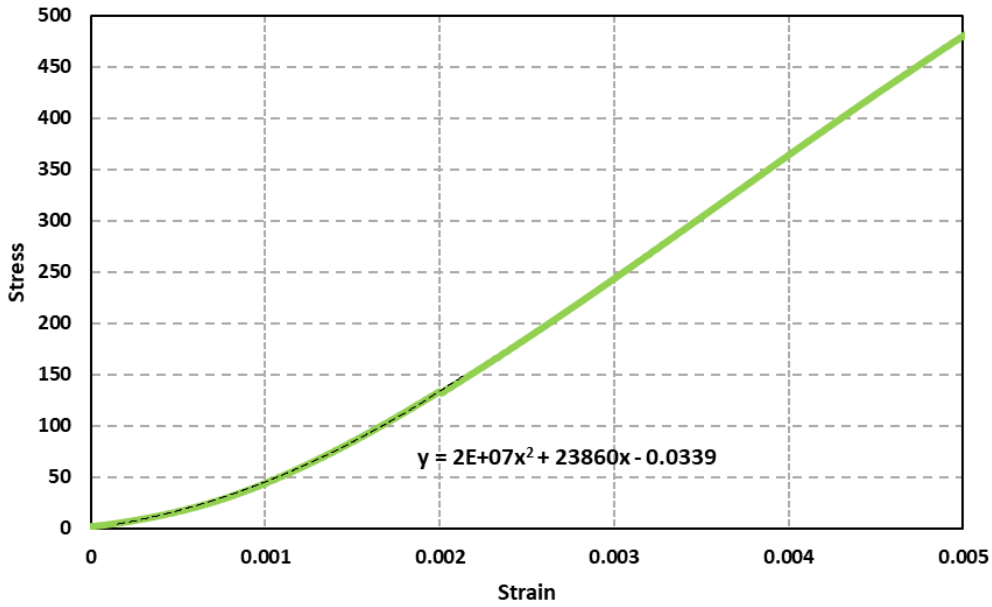

Figure 4.9: Trendline Fit to Non-Linear Region

It is important to note that the trend-line was fitted at a starting strain value of 0.0002, as to remove any initial noise or possible testing error that can occur at the start of the experimentation. The trendline and resulting equations will be able to predict the initial stress and strain points and the expected modulus of the uncured prepreg at 0 N. Converting the stress into a function of force, equation 4.1 can be modified as follows:

$$\left({}^{1}/_{A} * f\right) = ax^2 + bx + c \tag{4.3}$$

Using equation 4.3 and the quadratic equation (4.4) a value for the variable *x* can be determined. This value can be reintroduced into equation 4.2. The resultant formula is the first derivative of the second order polynomial in terms of force (equation 4.5)

$$x = \frac{-b \pm \sqrt{b^2 - 4a\left[c - \left({}^{1}/_{A} * f\right)\right]}}{2a} \tag{4.4}$$

$$\frac{dy}{dx} = 2a\left(\frac{-b \pm \sqrt{b^2 - 4a\left[c - \left({}^{1}/_{A} * f\right)\right]}}{2a}\right) + b \tag{4.5}$$

Equation 4.5 can be further reduced as follows:

$$\frac{dy}{dx} = \left(-b \pm \sqrt{b^2 - 4a\left[c - \left({}^{1}/_{A} * f\right)\right]}\right) + b \tag{4.6}$$

$$\frac{dy}{dx} = \left(\pm\sqrt{b^2 - 4a\left[c - \left({}^{1}/_{A} * f\right)\right]}\right) \tag{4.7}$$

$$\frac{dy}{dx} = \left|\sqrt{b^2 - 4a\left[c - \left({}^{1}/_{A} * f\right)\right]}\right| \tag{4.8}$$

The resultant equation 4.8 represents the first derivate of the best fit line in terms of force, where a and b are derived from Figure 4.9, and A represents the cross section of the fibers only. That is to say, the cross section is calculated by taking the fiber volume fraction percentage (66%) of the total cross section of the prepreg (thickness multiplied by the width). Applying these values to equation 4.8 results in the following equation:

$$E^{eff} = \left|\sqrt{23860^2 - 4(2 * 10^7)(-0.0339 - 2.02f\ )}\right| \text{ (MPa)} \tag{4.9}$$

Equation 4.9 can be used to calculate the effective tensile modulus of the uncured prepreg based on the experimentally derived plots in terms of force *f* in Newtons. This equation is valid only between strain values of 0-0.2% and is only applicable for the material used in our experimentation. Applying Equation 4.9 to AFP or ATL manufacturing, where the expected applied tensile load is approximately 25 N, the resultant Young's modulus is calculated to be approximately 66 GPa. At 0 N, the modulus is approximately 17.8 GPa. While this equation is useful for calculating an effective Young's modulus based on the average plots across all samples, there is still potential to gain a more accurate representation of what is occurring at this non-linear region.

In order to gain a clear idea of the tensile response in this region, the plots were broken down into increments of 0.033% strain. The resultant non-linear region was separated into the following sections outlined in Figure 4.10.

Figure 4.10 represents the non-linear section from the average stiffness plot across all samples broken down into six linear trendlines. The equations for each trendline is visible on the plot as well. Similar to the analysis done for the linear portion of the plots, the slope of the trendline represents the tensile modulus of the uncured prepreg system. Applying these trendlines to each test sample, the average tensile modulus per strain zone can be determined.

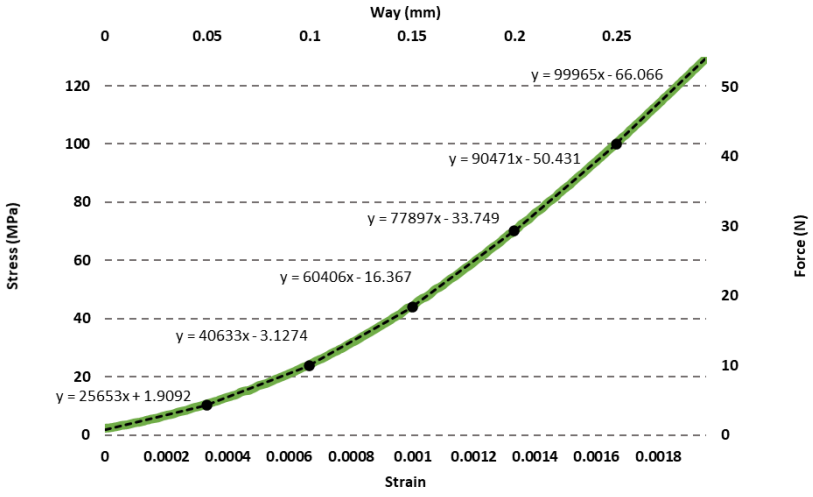

Figure 4.10: Linear Trendline Fit to Non-Linear Region

Observable in this figure, the non-linearity of the tensile modulus becomes most apparent. To tabulate this data, as mentioned above, taking the average tensile modulus per strain zone across all samples, the resultant values are shown in Table 4.3.

Table 4.3: Tensile Moduli in Non-Linear Region

Strain Section #	Tensile Range (N)	Average Tensile Modulus (GPa)	Standard Deviation
1	1.025 – 3.15	25.6	5.78
2	3.15 – 6.27	40.63	10.67
3	6.27 – 10.59	60.41	15.48
4	10.59 – 15.57	77.89	14.25
5	15.57 – 21.99	90.47	14.29
6	21.99 – 30.12	99.56	13.73

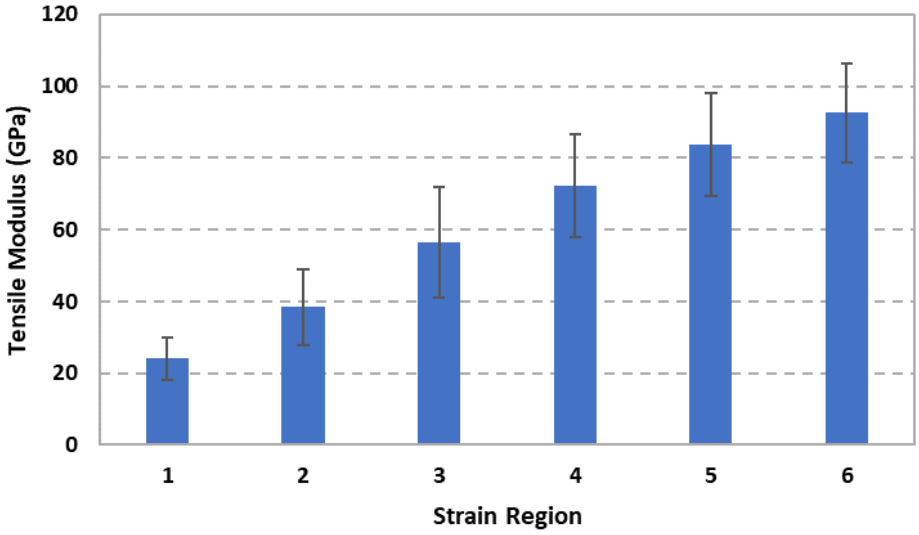

Figure 4.11: Graph of Tensile Moduli in Non-Linear Region

Once again, coinciding to what was observed in the linear region, there is a large standard deviation between samples, as evidenced in Figure 4.11. It is possible that the variations in tensile modulus are attributed to the differences in waviness between the samples. As the waviness in uncured prepreg can change due to the ease of fiber movement within the uncured viscous epoxy, the angle of misalignment will then vary per sample, and in turn introduce a source of variability in values for the tensile response. This can be further supported when comparing the tensile response of each sample individually. The tensile response between samples, even those within the same batch of material, have a high standard deviation between each other. Each sample was cut from the same roll of AFP prepreg and theoretically should have the exact same properties. However, as recorded experimentally, each sample exhibits a different tensile response due to the varying waviness and misalignment of the fibers between each sample caused by the movement of the fibers in the viscous epoxy matrix. One aspect of the tensile response curve that stays constant between all samples are the lead-in and linear regions caused by the re-aligning of the misaligned fibers. As all samples experience a certain degree of misalignment, they in turn all display a non-linear gain in modulus as the fibers align themselves along the direction of the applied load.

4.1.3 Effects of Temperature on the Tensile Behavior

Due to the viscous nature of the uncured epoxy matrix, temperature is expected to have a large contribution to the mechanical performance of the prepreg. As observed in Figure 2.4, as the temperature increases, the viscosity of the matrix is expected to decrease. In relation to the observations found at room temperature testing, it becomes evident how a decrease in viscosity can affect the non-linear region of the tensile response curve. It was determined that the cause of the non-linear region was based on the waviness of the carbon fibers being strung through the viscous matrix during uniaxial tensile testing. As the motion of the fibers are being impeded by the viscosity of the resin, a non-linear tensile response is observed. With testing at higher temperatures, the stiffness in this non-linear region is expected to drop. Considering that the viscosity of the epoxy will be reduced, there will be less resistance against the motion of the fibers. In relation to the linear region of the tensile plot, the stiffness is expected to stay constant at elevated temperatures. As the dominant aspect dictating the response in this region are the aligned fibers, the epoxy matrix is expected to have less effect on the mechanical performance in this region.

As outlined in section 3.2.4, the tensile tests performed at elevated temperatures used the same gripping solution used in testing at room temperature. Samples were left out of the freezer and placed at room temperature for one hour prior to testing. The same testing procedure of applying a first run tensile load to a maximum of 100 N, followed by a return to the initial condition and a second tensile test was followed when testing at elevated temperatures. The following plots represents the recorded results at a heat gun temperature of 140°F and 180°F. The relative prepreg surface at these temperatures are represented on the plots and were recorded by FLIR camera to be at a temperature of 35°C and 40°C respectively.

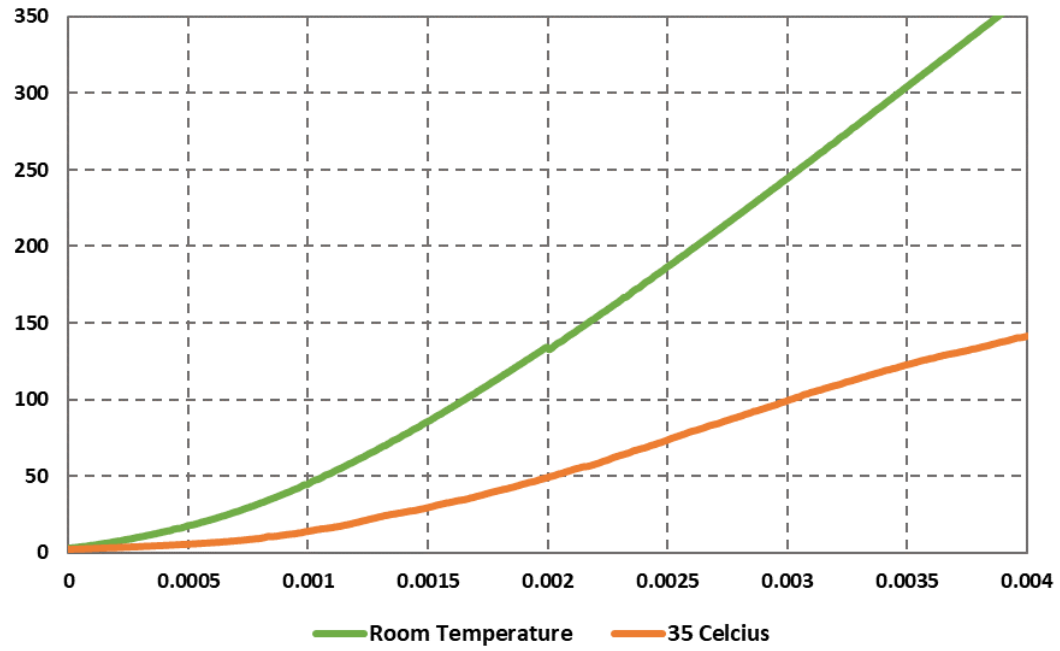

Figure 4.12: Average Tensile Plot at Room Temperature vs. Average Tensile Plot at 35℃

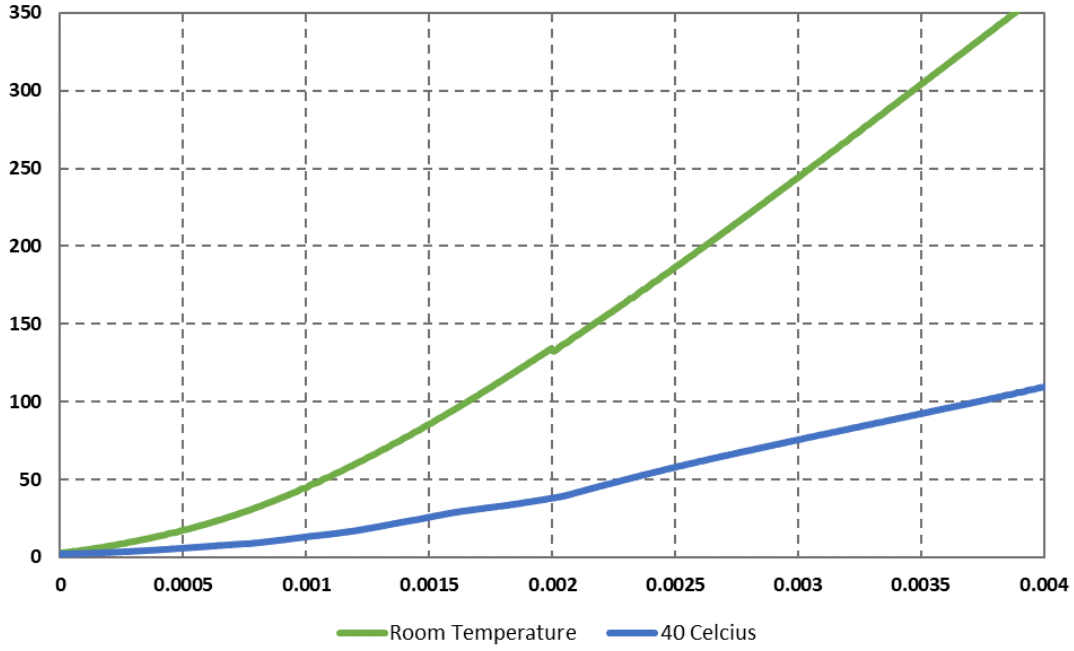

Figure 4.13: Average Tensile Plot at Room Temperature vs. Average Tensile Plot at 40℃

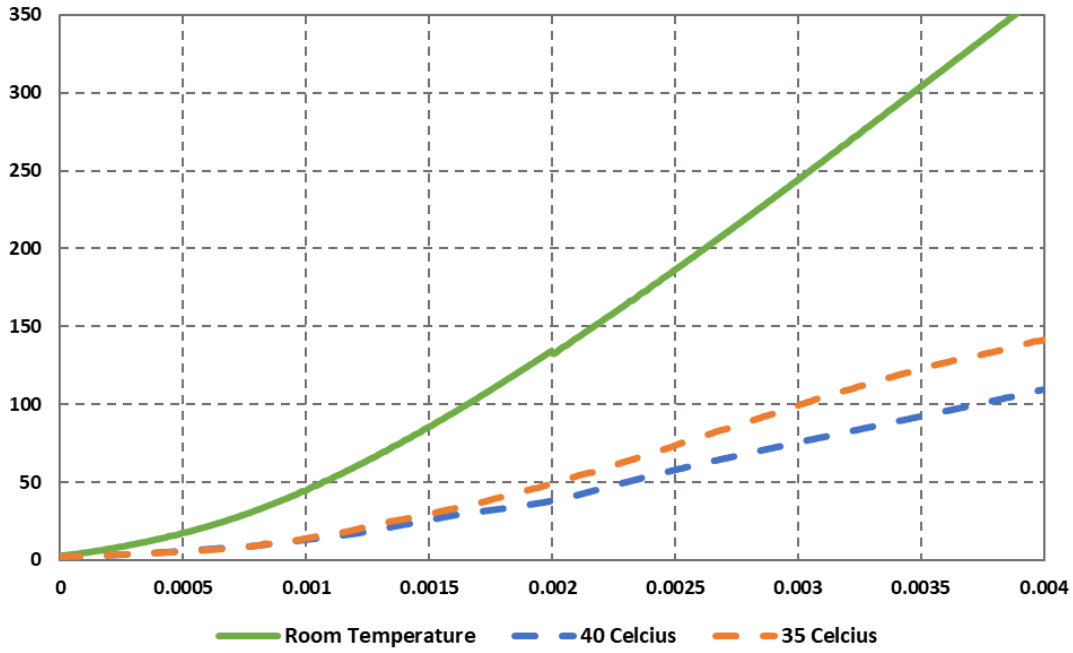

Figure 4.14: Comparison Between Tensile Plot at Varying Temperatures.

At elevated temperatures, the stiffness of the prepreg sample is recorded to be lower than that at room temperature. This is expected based on the mathematical theory discussed in literature and reviewed above. As the temperature increases, the viscosity of the epoxy matrix decreases, thus there is less resistance to the movement of the prepreg. Considering that, on average, the fibers still need to travel the same distance to correct the waviness within the sample (straighten up), having less resistance to this movement will shift the stiffness plot down, as seen in the results.

It is also important to note that sample size influences the plots as well. As discussed earlier, there is a large standard deviation between samples, and this is the same case when testing at elevated temperatures. Looking at the comparisons of the average plots, Figure 4.14, it appears at first that the stiffness in the non-linear region is reduced at elevated temperatures. However, this is not the case when analysing the tensile response of individual samples.

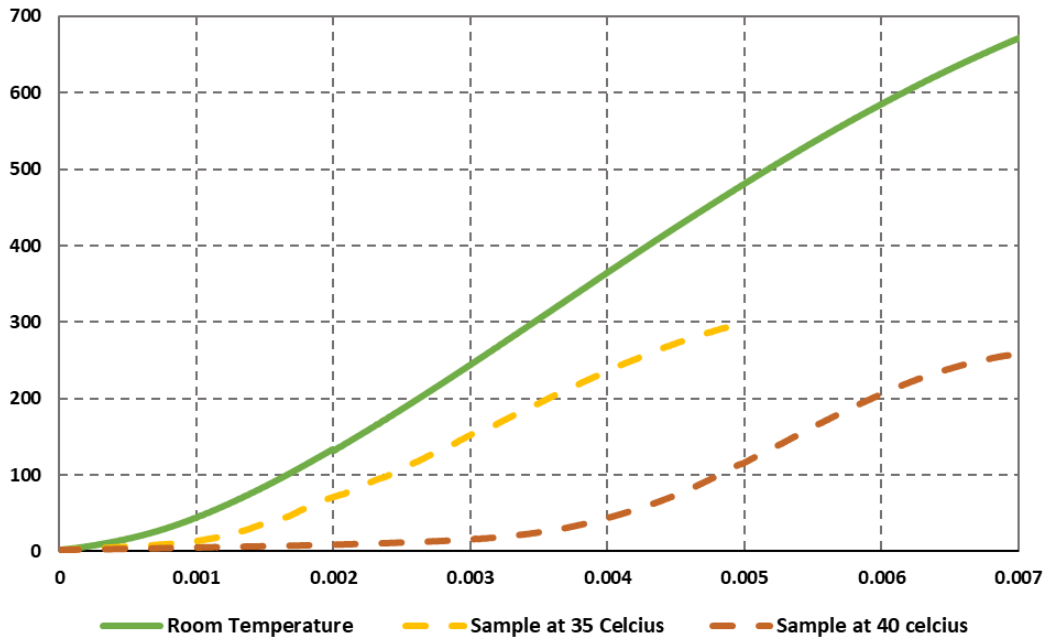

Figure 4.15: Average Tensile Plot at Room Temperature vs Individual Sample Plot at Elevated Temperatures

In Figure 4.15, the two different samples are recorded to share a similar linear stiffness as to the average calculated at room temperature. However, there still resides a large standard deviation between the area of samples non-linear region, and in the exact behavior of the prepreg. Potential causes for this are premature failure in the form of fiber splitting which can be induced when cutting and setting up the samples. This can be seen during experimentation as gaps propagating within the prepreg. Additionally, as only surface temperature was observable with the FLIR camera, there is a potential source of discrepancy between testing. Additionally, due to the nature of fiber waviness in this uncured state, large variabilities can be seen between one sample to another.

In conclusion, due to the changes in behaviour of the prepreg once elevated temperatures are introduced into the system, it is no longer feasible to take a total sample average for comparative purposes. Comparing individual samples tested at higher temperature to the baseline produces better observations. This is seen in the work done by Zhang et al. as well [19]. In the work presented, only individual samples are compared at elevated temperature, not whole

averages. At the individual level, the results are as expected to the theory of viscosity and seen in literature.

4.2 Waviness Analysis

Through experimental testing, it was determined that the main factor affecting the mechanical behaviour of the uncured prepreg system is the waviness of the fibers. The mechanism driving the stiffness to follow a non-linear plot was related to the effects of fiber straightening as they were being pulled through the viscous matrix. The resistance imposed on the movement of the fibers by the resin resulted in a non-linear stiffness. Furthermore, as the angle of the fibers changed with the amplitude of the geometric waveform, the stiffness of the fibers changed as well following the equations of classical lamination theory.

Studying classical lamination theory, it is known that the modulus of composites is directly related to the angle of the fibers. This theory is important in addressing the initial non-linearity of the uncured prepreg system, as it is believed that this region is caused by the misalignment in the fibers. As discussed in literature, the initial waviness of the fibers presents a reduced stiffness modulus in the prepreg. As a uniaxial tensile load is applied on the material, the fibers are able to align themselves in the direction of the load due to the viscous nature of the uncured epoxy matrix. As the load and displacement increases, the alignment of the fibers coincides more with the 0 degree (direction of the applied load) resulting in a higher modulus. Eventually, as the load and displacement reach a critical point, most of the fibers will have their misalignment corrected and the resulting tensile response will be linear. This can be seen in the mathematical equations governed by classical lamination theory. The relationship between stress and strain in classical lamination theory is described in the compliance matrix shown in equations 4.10 – 4.12 and Figure 4.16 [7].

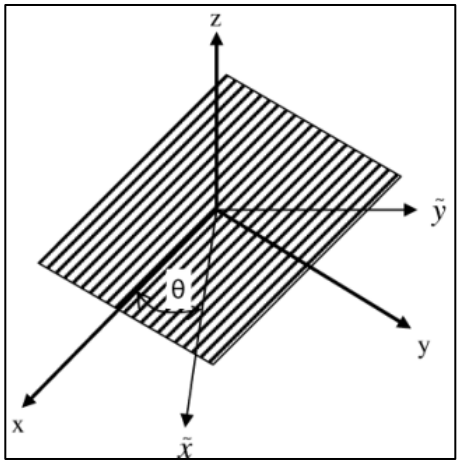

Figure 4.16: Off-Axis Coordinate System for Compliance Matrix Transformation [7]

$$\begin{Bmatrix} \varepsilon_x \\ \varepsilon_y \\ \varepsilon_z \\ \gamma_{yz} \\ \gamma_{xz} \\ \gamma_{xy} \end{Bmatrix} = \begin{bmatrix} S_{11} & S_{12} & S_{13} & 0 & 0 & S_{16} \\ S_{12} & S_{12} & S_{23} & 0 & 0 & S_{26} \\ S_{13} & S_{23} & S_{33} & 0 & 0 & S_{36} \\ 0 & 0 & 0 & S_{44} & S_{45} & 0 \\ 0 & 0 & 0 & S_{45} & S_{55} & 0 \\ S_{16} & S_{26} & S_{36} & 0 & 0 & S_{66} \end{bmatrix} * \begin{Bmatrix} \sigma_x \\ \sigma_y \\ \sigma_z \\ \tau_{yz} \\ \tau_{xz} \\ \tau_{xy} \end{Bmatrix} \tag{4.10}$$

$$\begin{aligned}
S_{11} &= S_{11}^0\cos^4\theta + (2S_{12}^0 + S_{66}^0)\sin^2\theta\cos^2\theta + S_{22}^0\sin^4\theta \\
S_{12} &= (S_{11}^0 + S_{22}^0 - S_{66}^0)\sin^2\theta\cos^2\theta + S_{12}^0(\sin^4\theta + \cos^4\theta) \\
S_{13} &= S_{13}^0\cos^2\theta + S_{23}^0\sin^2\theta \\
S_{22} &= S_{11}^0\sin^4\theta + (2S_{12}^0 + S_{66}^0)\sin^2\theta\cos^2\theta + S_{22}^0\cos^4\theta \\
S_{23} &= S_{13}^0\sin^2\theta + S_{23}^0\cos^2\theta \\
S_{33} &= S_{33}^0 \\
S_{16} &= 2S_{11}^0\cos^3\theta sin\theta - 2S_{22}^0 cos\theta\sin^3\theta + (2S_{22}^0 + S_{66}^0)(\cos\theta\sin^3\theta - \cos^3\theta\sin\theta) \\
S_{26} &= 2S_{11}^0 cos\theta\sin^3\theta - 2S_{22}^0\cos^3\theta sin\theta + (2S_{22}^0 + S_{66}^0)(\cos^3\theta\sin\theta - \cos\theta\sin^3\theta) \\
S_{36} &= 2(S_{13}^0 - S_{23}^0)cos\theta sin\theta \\
S_{44} &= S_{55}^0\sin^2\theta + S_{44}^0\cos^2\theta \\
S_{45} &= \left(S_{55}^0 - S_{44}^0\right)cos\theta sin\theta \\
S_{55} &= S_{55}^0\cos^2\theta + S_{44}^0\sin^2\theta \\
S_{66} &= 4(S_{11}^0 + S_{22}^0 - 2S_{12}^0)\sin^2\theta\cos^2\theta + S_{66}^0(\sin^4\theta + \cos^4\theta - 2\sin^2\theta\cos^2\theta)
\end{aligned} \tag{4.11}$$

$$
\begin{aligned}
S_{11}^{0} &= {}^{1}/_{E_{11}} \\
S_{12}^{0} &= -{}^{\nu_{12}}/_{E_{11}} \\
S_{13}^{0} &= -{}^{\nu_{13}}/_{E_{11}} \\
S_{22}^{0} &= {}^{1}/_{E_{22}} \\
S_{23}^{0} &= -{}^{\nu_{23}}/_{E_{22}} \\
S_{33}^{0} &= {}^{1}/_{E_{33}} \\
S_{44}^{0} &= {}^{1}/_{G_{23}} \\
S_{55}^{0} &= {}^{1}/_{G_{13}} \\
S_{66}^{0} &= {}^{1}/_{G_{12}}
\end{aligned}
\tag{4.12}
$$

As seen in equation 4.10, the calculations for the compliance matrix is directly related to the angle at which the fibers are orientated. This shows how the young's modulus, E, of the laminate is reliant on the angles of the fibers. Applying this principle to waviness in the prepreg, the degree of misalignment in the fibers presents itself as a source of reduced stiffness in the material. Furthermore, it is evident how the stiffness modulus, and the stress/strain plot can exhibit a non-linear slope as the fiber's misalignment is corrected and the modulus approaches its maximum value. Once the majority of the fibers are aligned to the 0 degree, then the modulus linearizes and reaches its maximum value.

Using classical lamination theory in conjunction with the waviness of the fibers, the non-linear region of the stress vs. strain plot is clearly defined by the geometry of the fibers. In order to prove this theory and to capture the effect of fiber waviness and misalignment in the prepreg, microscopic analysis was done on the prepreg samples prior to, and post tensile testing. Figure 4.17 represents microscopic images of one sample at 10x magnification. Visually, the waviness is shown to have changed after the sample was tested in uniaxial tension. The waviness appears to have diminished along the fiber direction and the overall misalignment of the fibers has been reduced. To further support the visual observations, the photos were processed using the MATLAB software developed by D. Whilhelmsson as described in the literature review [34].

Sample Prior to Testing **Sample After Testing**

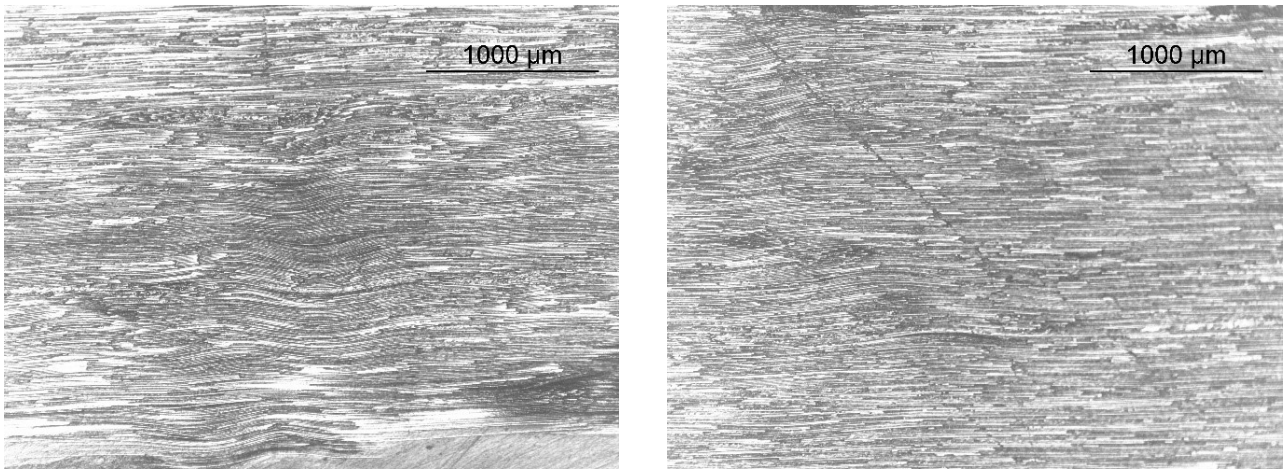

Figure 4.17: Microscopic Images of an Uncured Carbon Fiber Prepreg Before and After Uniaxial Tensile Testing

The results of the MATLAB analysis shown in Table 3.1 support the visual findings of the microscopic images. The overall mean misalignment angle, the maximum misalignment angle and the standard deviation of angles have all been reduced after uniaxial tensile testing. Following classical lamination theory, this means that the theoretical tensile modulus of the same prepreg sample after testing is higher than the modulus prior to testing. In addition, Figure 4.17 justifies the assumption that there is an event of fiber re-alignment during the tensile testing experiment and that the lead-in area of the tensile response plot is attributed to this movement of fibers. This exercise in microscopy was conducted on two distinct samples and the results can be seen in Figure 4.18. The samples support the findings discussed already; the waviness and the angle of misalignment have been reduced due to the movement exhibited by the fibers during uniaxial tensile testing.

Table 4.4 Results of Fiber Misalignment Before and After Uniaxial Tensile Testing

	Sample Prior to Testing	Sample After Testing
Successfully Measured Area	89.1%	93.4%
Mean Angle (Deg)	1.750	1.170
Mean Misalignment Angle (Deg)	3.722	2.773
Maximum Misalignment Angle (Deg)	15.500	11.904
Standard Deviation of Angles (Deg)	4.696	3.575

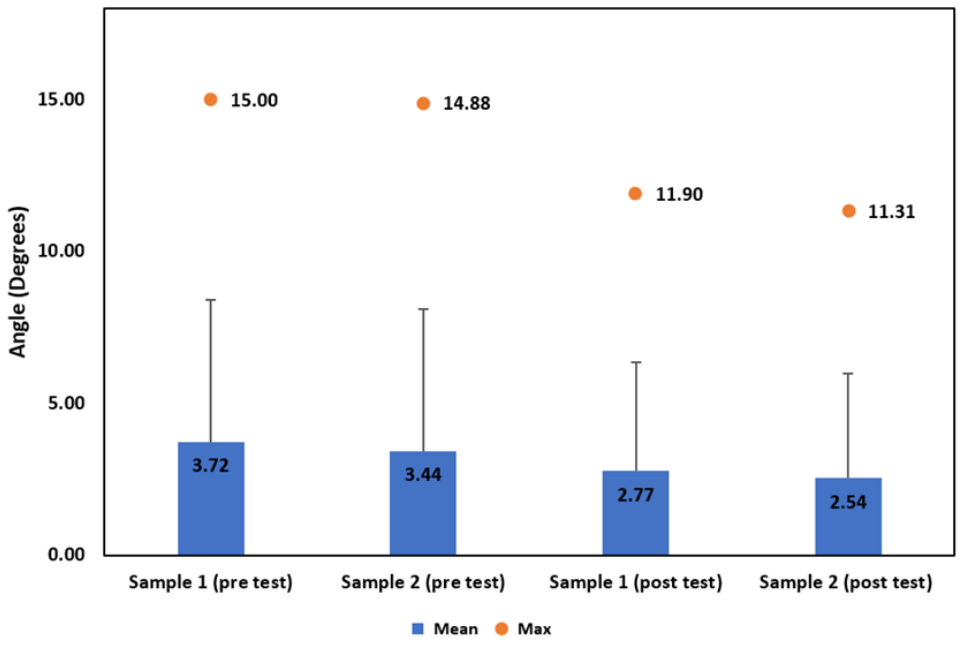

Figure 4.18: Results on The Angle of Misalignment of Two Samples Before and After Uniaxial Tensile Testing

It is important to take note of some limitations on the software used in studying the waviness of these microscopic images. As described in the work of D. Whilhelmsson [34], the MATLAB software works by first placing a predefined grid over the photo, then through binarization and fiber identification , the code is able to trace the fiber path in each individual grid square. The limitation is that this process results in an underestimation of the mean fiber waviness. In calculating the angle of fiber misalignment at every point along the fiber path, the mean angle calculated will be significantly smaller than the true angle of misalignment, which is calculated at the maximum tangential point of the sine wave also known as the crest of the slope. This underestimation of the mean if observable in Figure 4.18, when looking at the maximum observed angle of misalignment to the mean, and in the large standard deviation.

To overcome this challenge, the same images were analyzed in ImageJ and the angle of misalignment was manually measured through pixel measurements. The angle taken was calculated at the crest of the slope for each fiber. A total of 30 measurements were taken per sample. Table 4.5 represents the resultant mean angle of misalignment that was manually determined. In comparing these results to those calculated by the MATLAB code in Table 4.4, there is a difference between the observed mean angle of misalignment.

Table 4.5: Manually Measured Mean Angle of Misalignment

Sample 1 (pre test)	Sample 2 (pre test)	Sample 1 (post test)	Sample 2 (post test)
Mean: 9.986433	Mean: 10.3263	Mean: 6.416733	Mean: 3.994667

The manually calculated results reports a larger delta between pre tested and post tested samples and also reported a larger mean angle. This confirms the problematic measurement procedure when using the MATLAB code, however the data still corelates a drop in mean angle of misalignment after uniaxial tensile testing. The results prove that there is a large of movement happening within the prepreg with the application of a uniaxial tensile load. Relating this movement and the change in fiber angle to classical lamination theory, it becomes clear how the non-linear stiffness is directly influenced by the initial fiber waviness.

Chapter 5: Finite Element Model

5.1 Literature Review on Finite Element Methods

To support the claims made from experimental testing, a Finite Element (FE) simulation of the uniaxial tensile test was developed. Creating a simulation to quantify the effects that waviness has on the prepreg at the micro and meso scale, and comparing the results to experimentation will provide further evidence to the claim that initial waviness in the fiber is responsible for the non-linear to linear stiffness behavior of the material. In literature, some investigations have been done in simulating this effect of waviness on a laminate [37], [38], [42]. In their work titled *Effect of micromechanical parameters of composites with wavy fibers on their effective response under large deformations* by Dmytro D. Kuksenko et al. a microscale and meso scale FE model was created in order to investigate how the initial waviness affects the stiffness response under uniaxial load. In their study, three different fiber arrangements were studied (Figure 5.1).

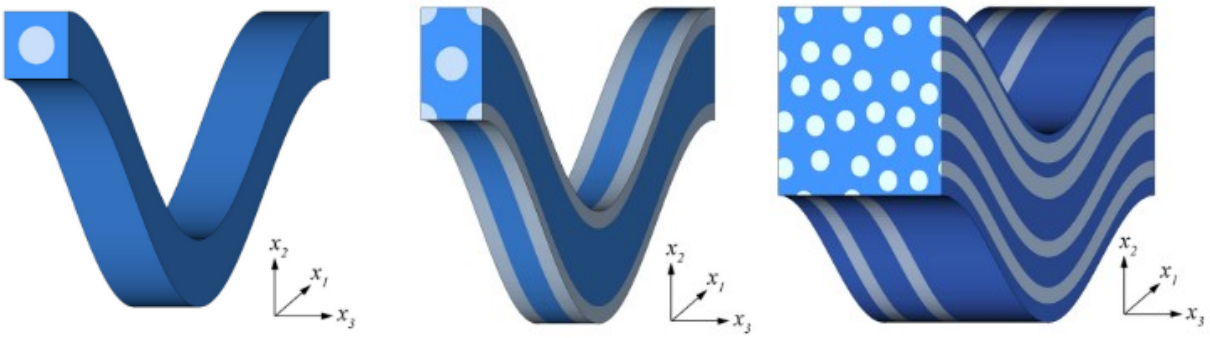

(a) (b) (c)

Figure 5.1: Three types of Fiber Arrangements under Investigation: (a) Square; (b) Hexagonal; (c) Random Periodic [37]

For the simulation, the boundary conditions restricted motion in all directions other than in the direction of the applied load, X_1. The elastic material properties used in this study are 0.1 GPa for the epoxy matrix, and 100 GPa for what they designated as high contrast fiber. A crimp ratio of 0.05, 0.10 and 0.15 was used. The crimp ration being defined as the ratio between the straight length of the fiber before weaving and the length of fiber after. Therefore, having a lower crimp ratio reflects in having a lower fiber waviness. Figure 5.2 represents the results observed in the study.

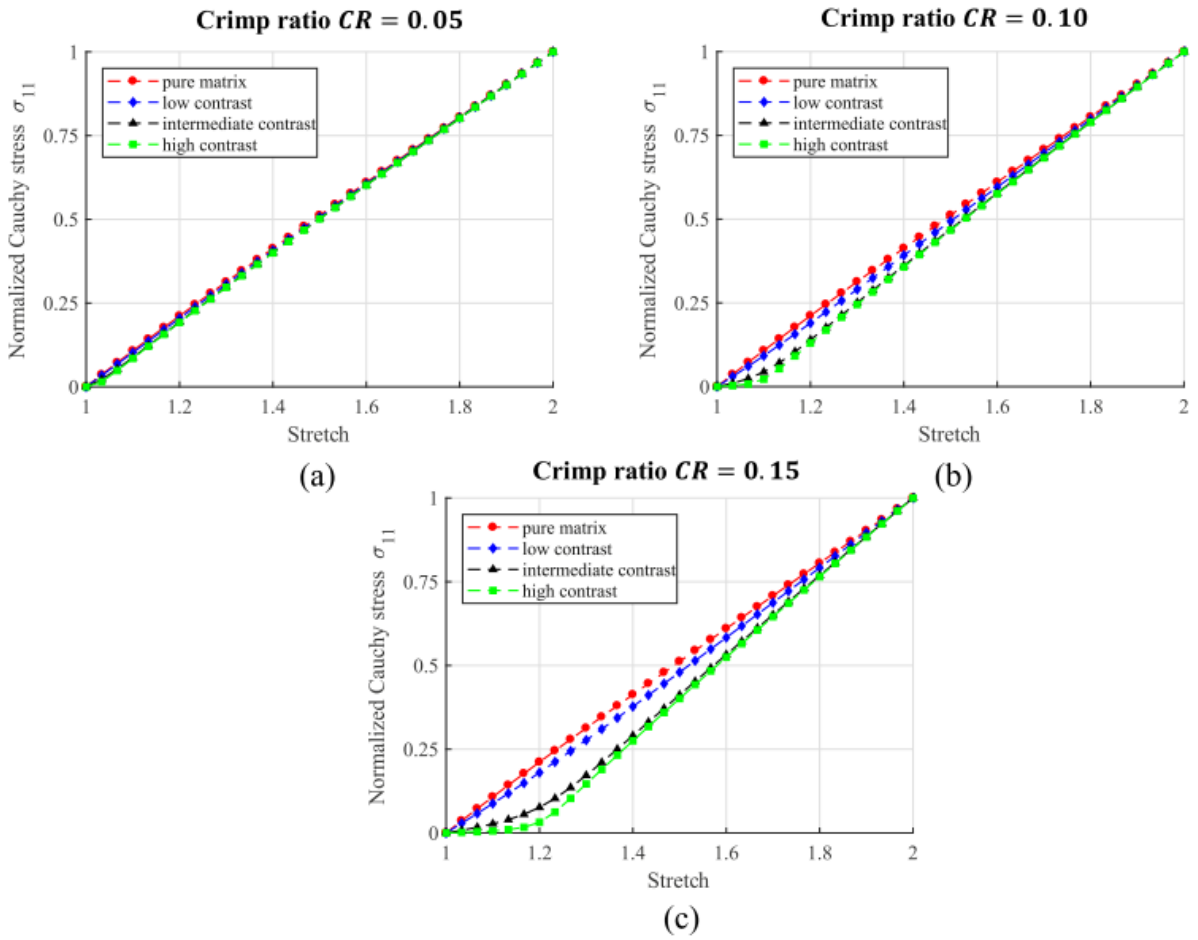

Figure 5.2: Effect of Crimp Ratio on the Homogenized Mechanical Response of the Composite under Elongation in the x1 Direction [37]

Analyzing these results, it is seen how having a lower crimp ratio (lower waviness) results in a purely linear stiffness response, while at a higher crimp ration, a non-linear region (similar to what was recorded in our experimentations) is visible. In addition, lowering the material properties of the fibers, expressed in Figure 2.1 as a low and intermediate contrast ratio, results in a change in the stiffness behavior.

Referencing the work done by M. Garnich et al. in investigating the stiffness and strength of wavy fiber composites, a hexagonal mesoscale FE analysis of a composite laminate was modeled and simulated [38]. In their work, similar to D. Kuksenko et al., a hexagonal fiber arrangement was investigated. The focus of this study was to determine how the wavelength affects the stress components across the length of the wavy fiber. To conduct this simulation, boundary conditions were set to prevent rotation and displacement in all but the fiber direction. The simulation was force controlled, and two equal and opposite axial forces in the fiber direction were applied to the end faces of the model. The elastic material properties used in the study was applied to the fiber and the epoxy. The fiber was set to have an E_1 value of 207.5 GPa, E_2 & E_3 values of 25 GPa respectively. The epoxy was set to have an elastic modulus of 4.5 GPa. After performing the simulation, the stress components and the Tsai-Wu failure criteria were applied to the study. Figure 5.3 represents the resultant S_{11} stress reported from the simulation.

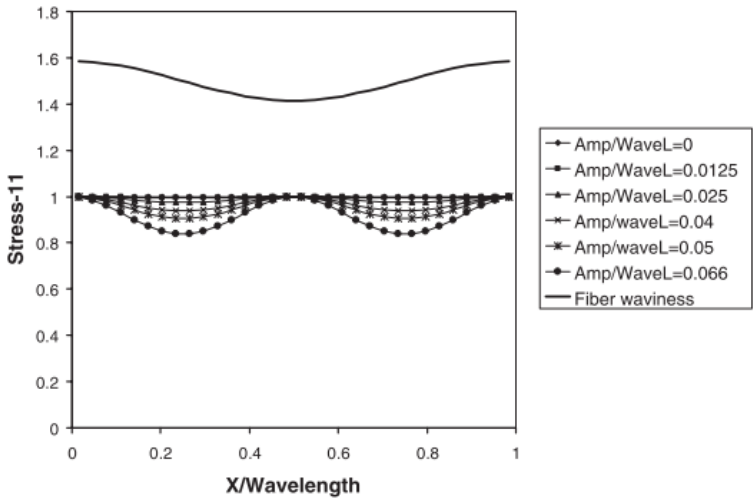

Figure 5.3: The Distribution of Average Normal Stress along the Length of the Unit Cell [38]

The resultant plot indicates that the highest stress concentrations occur at the center point and the two end faces of the fiber. At the maximum misalignment point of the fiber, the lowest S_{11} stress was observed. Additionally, as the waviness was increased, the variations between the maximum and minimum observed stress were also increased, with a waviness of 0 reporting a perfectly linear stress distribution. These results can be translated into quantifying the non-linear region of stiffness observed in our experimental results. The larger the angle of misalignment was within the waviness of the fiber resulted in a lower observed S_{11} stress. In the report, similar observations were made in the remaining stress components and in studying the Tsai-Wu failure of the wavy composite. The results recorded in this study confirm that the waviness has an impact on the stiffness and mechanical behavior of the system.

Taking the lessons learned from literature, simulating a FE model for this study into the tensile behavior of uncured prepreg will strengthen the assumptions that the initial waviness in the prepreg is responsible for the non-linear tensile behavior. For this study, ABAQUS 2016 will be used to develop and simulate the FE model. The main limitations of this study will be in modelling the viscous epoxy resin. As standard FE models are based on the elastic properties of the material and the solver uses the continuum components of stress and strain at nodal points of each cell, modelling of the epoxy will have to use elastic properties. Modelling the displacement of a truly viscous epoxy requires computational fluid dynamics (CFD) to be taken into consideration. If this approach is taken, then the elastic properties of the fibers will not be taken into consideration. It is difficult to simulate CFD and FE in the same analysis and requires much more extensive work. For the purpose of this study, the epoxy matrix will be assigned elastic material properties and the study will be solely done in FE modelling. Following the assumptions made in experimental testing, it is believed that the viscous epoxy does not contribute to the overall modulus of the laminate, the major contribution being the fibers. In the FE model, applying a significantly lower stiffness to the epoxy in comparison to the fibers is assumed to be sufficient for this level of study. The purpose of the simulation is to investigate the effects of fiber waviness on the system and compare the response curve to that of experiments.

5.2 Micro Scale Model

To start the FE model and to verify the feasibility of the analysis, a micro scale model was developed to investigate the behavior of a single fiber in resin. The basic dimensions of the model were derived from the microscopic images measured in ImageJ. From the same photo in Figure 4.17 (a), a fiber with amplitude of 0.0366 mm and a wavelength of 0.47514 mm was chosen to be modelled. The fiber diameter was taken from the technical data sheet, being 7 um [43]. Based on the resin fiber content found in Table 3.1 to be 34%, the resin system surrounding the fiber was modeled with the same volume percentage.

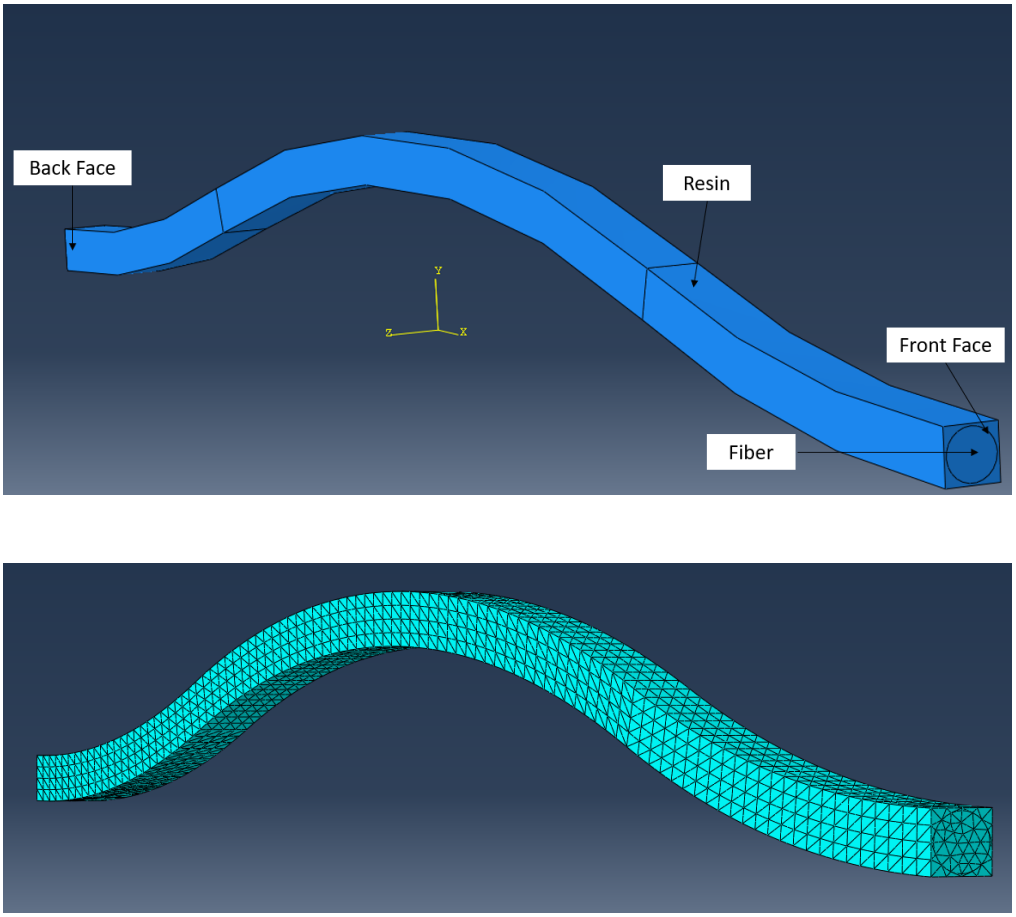

Figure 5.4: Micro Scale Model

The material property of the fiber was taken from the same technical data sheet mentioned earlier and the elastic modulus was set to a value of 237 GPa and a Poisson's Ratio of 0.3. The fiber was treated as an isotropic elastic material, and only the Young's modulus and the Poisson's Ratio was assigned. Additionally, failure mechanics will not be investigated in this simulation. Therefore, properties attributing to fracture mechanics such as yield strength are not necessary to the model. As stated in the previous section, the epoxy was modeled as an isotropic elastic material. The Young's modulus was assigned to a value of 3.5 GPa. This value is that of a cured epoxy system, and is similar to the values used by Granich et al. [38]. Similar to how the models were simulated in literature, the structure was made by separating sections and assigning each section to a specific material. This method assumes that the entire laminate is of one solid structure made up of two distinct material properties. This assumption was based on the limitations of the unknown bond strength between the uncured epoxy resin and the fiber. Considering that the chemical bonding is an unknown parameter, it was opted instead to have the fiber and the resin joined as the same part and have the two systems move as one. As the purpose of the simulations is to verify that the behavior is based on initial fiber waviness, a factor of error between experimental and simulated results is expected and allowable.

The microscale model was set to output the primary stress components at the front face of the model. In terms of boundary conditions, the parameters were set to mimic that of experimentation as closely as possible. The entire back face of the laminate was bound as follows:

$$U1 = U2 = U3 = UR1 = UR2 = UR3 = 0$$

During the simulation, the front face of the model was displaced in U1 by 0.02 mm. It was determined that the implicit numerical computation of the model benefitted from displacement based solving in lieu of an applied force. This was decided based on the idea that implicit displacement-based solutions are preferred in simulating problems with slow/moderate increments over time, which we have in this situation. Full Newton direct equation method was assigned with the non-linear geometry over a single time increment. The mesh for this system followed a free tetrahedral shape with a 0.005 mm global size as seen in Figure 5.4.

The results from the microscale simulations reflect the same tensile behavior seen in experimentation. Shown in Figure 5.5, the microscale results follow the same trend of having a non-linear stiffness up until a strain value approximately equal to 0.2%. Following this non-linear region, a region of linear stiffness occurs until the end of the plot.

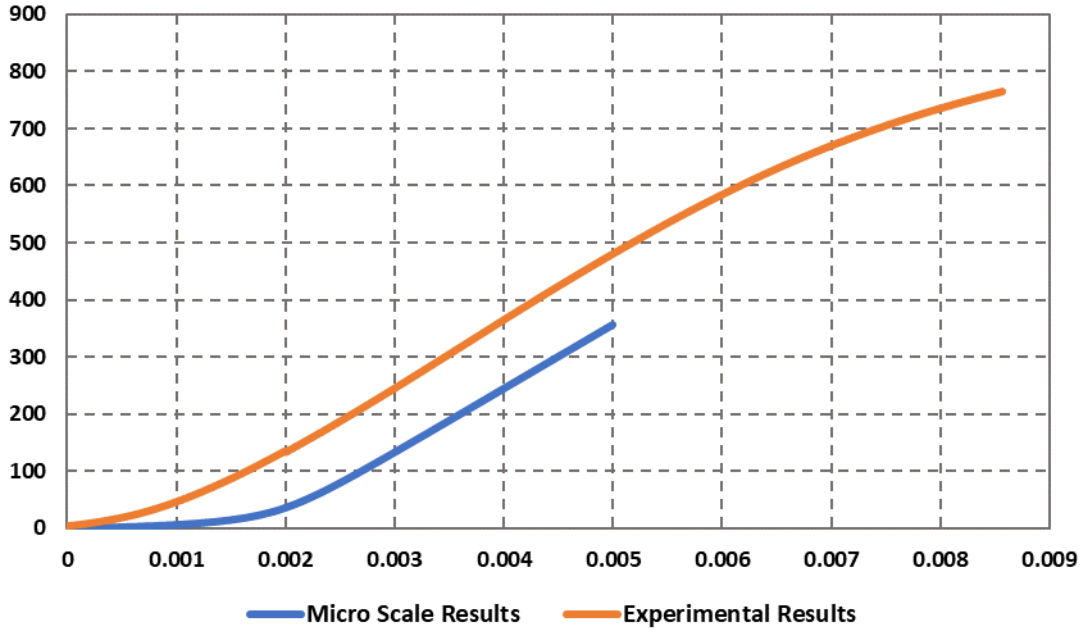

Figure 5.5: Micro Scale Result Compared to Experimental Results

Observing the linear portion of the plot, it is evident that the simulation shares the same stiffness value as recorded in experimentation. This indicates that the elastic properties and the assumptions made in modeling the laminate are accurate to what was observed in the experiment. This confirms that modelling the system as one part with different properties is viable for this simulation. Additionally, the properties used for modelling at this scale will be carried over to the meso scale model.

Looking at the non-linear region of Figure 5.5, there are noticeable deviations to the experimental result. In the case of the micro scale results, the lead-in region starts to increase in slope much later when compared to the experimental results, at around 0.13%. This can be attributed to the initial wavelength chosen to model the system. Figure 5.6 compares the

stiffness plot between two micro scale simulations, modelled using the same parameters, with different starting waviness. In the figure, the green plot was modeled with a 21% reduction of initial amplitude compared to the blue plot. As seen in the figure, the increase in slope in the non-linear region starts earlier with the decrease of wavelength. In addition, the linear area shares the same stiffness showing the repeatability of the model.

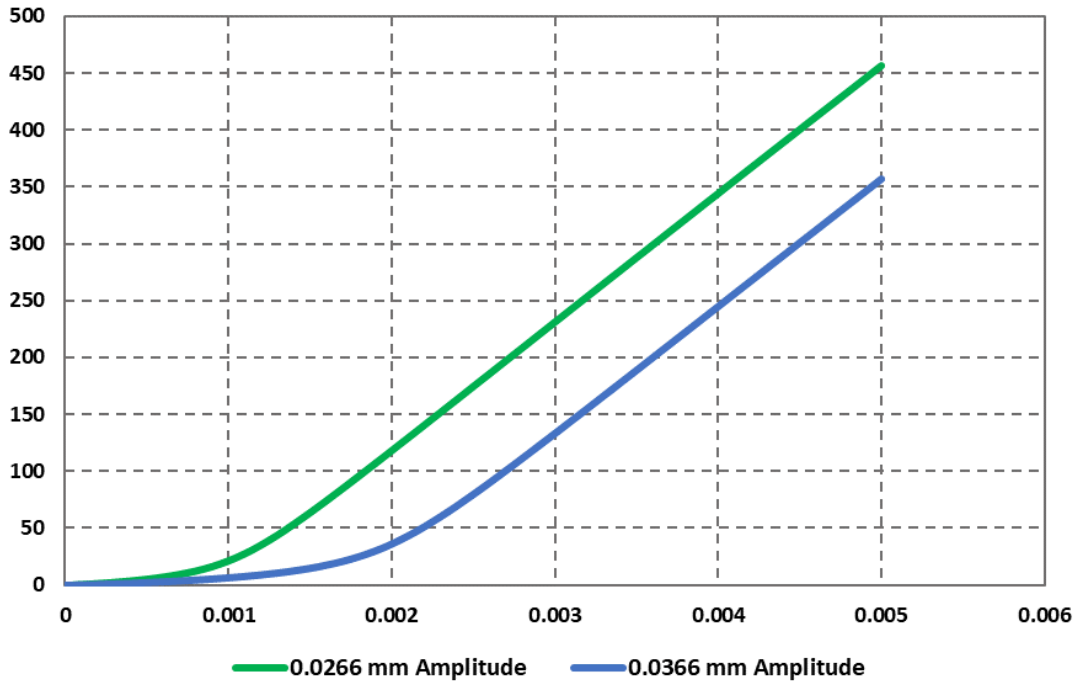

Figure 5.6 : Comparison Between Micro Scale Models of Different Amplitudes

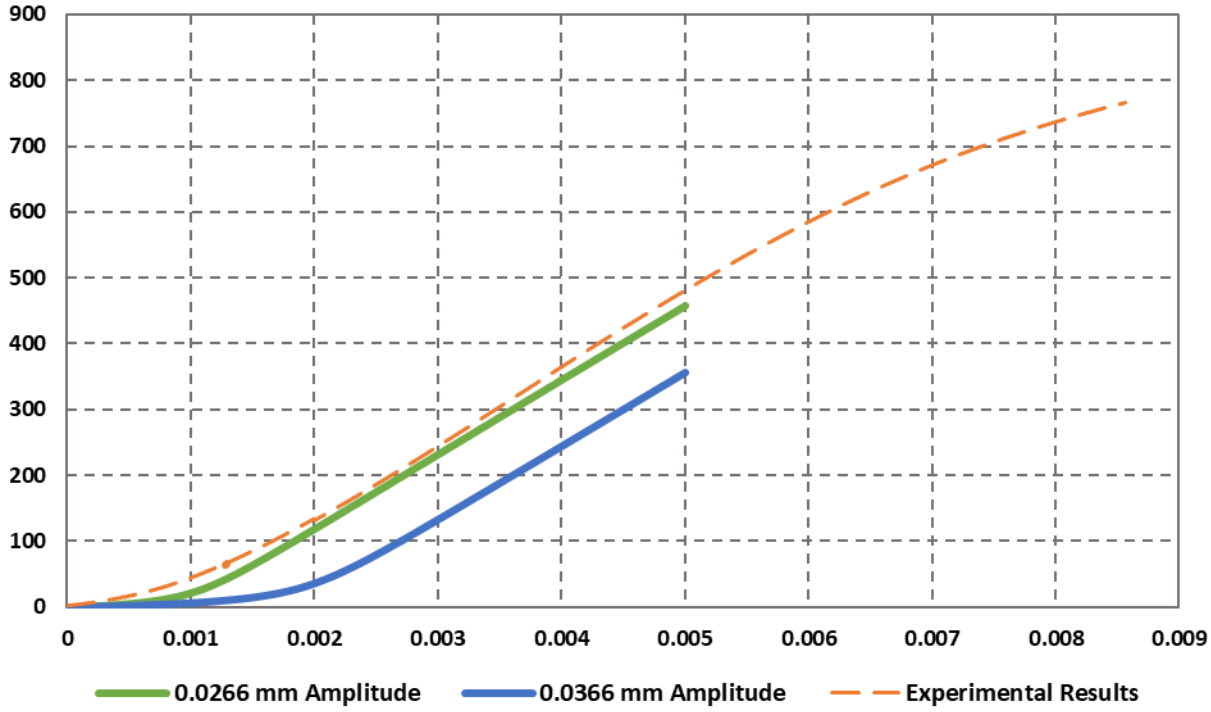

Figure 5.7: Comparing Micro Scale Results to Experimentation

Comparing the results of the simulation with initial fiber waviness of 0.0266 mm to the stiffness plot recorded through experimentation (Figure 5.7) it can be seen that the new waviness parameter matches that of experimentation more closely. These results from the simulation indicate that initial fiber waviness does have a direct impact on the uniaxial tensile behavior of the prepreg.

5.3 Meso Scale Model

While the micro scale model was sufficient in preliminary observations on how the model behaves and the repeatability and the accuracy of simulation, a meso scale model is necessary in investigating fiber interactions. A key aspect into analyzing the non-linear region is to study the intra-fiber interactions as the fibers move through the resin system. The meso scale model will use the same elastic parameters as the micro scale, and the model will be made following the same philosophy of separating the single part into distinct fiber and resin sections. For the meso scale model, a hexagonal fiber orientation based on the model of D. Kuksenko et al. [37] was developed. Figure 5.8 shows the fiber area in red, and the resin area highlighted in green. This model follows the same fiber volume fraction present in the micro scale, being a fiber volume fraction of 66%. Once again, the elastic modulus of the fiber was set to 237 GPa with a Poisson ratio of 0.3. The resin was assigned a Poisson ratio of 3.5 GPa and a Poisson ratio of 0.3 as well. Considering the close relation between experimental and micro scale models, the meso scale model was developed in the same way of separating the part into resin and fiber sections and assigning each section its distinct properties. As for dimensions, the wavelength used was 0.47514 mm with an amplitude of 0.0266 mm, as determined in the microscale model. The fiber diameter was set to 0.007 mm.

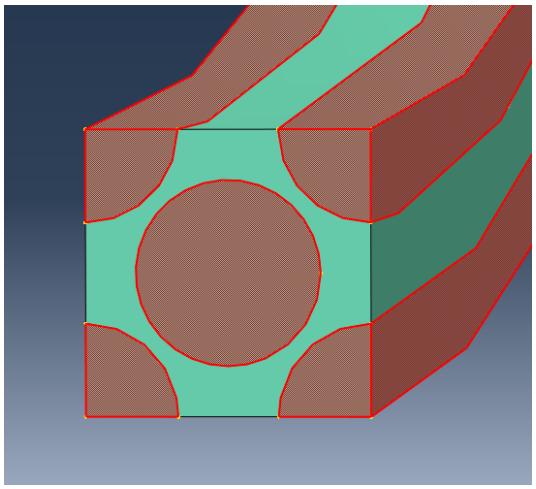

Figure 5.8: Hexagonal Fiber Orientation for Meso Scale Simulations

The boundary conditions of the model followed the same conditions set in the micro scale model. The back face of the model was fixed with zero displacement in U1, U2 and U3, as well as zero rotation in UR1, UR2, and UR3. The entire front face, as shown in Figure 5.9, was set to a U1 displacement of 0.02 mm. The front face U2, U3, UR1, UR2 and UR3 displacements and rotations were not fixed. For the simulation, the fixed back face was set as an initial condition, and the front face displacement was applied at the first and only step. Data output was set to record the S stress on the front face of the model at 100 evenly spaced time intervals. This history output will be primarily used to compare to experimental testing, as the stress in both cases are recorded at the tip of the model.

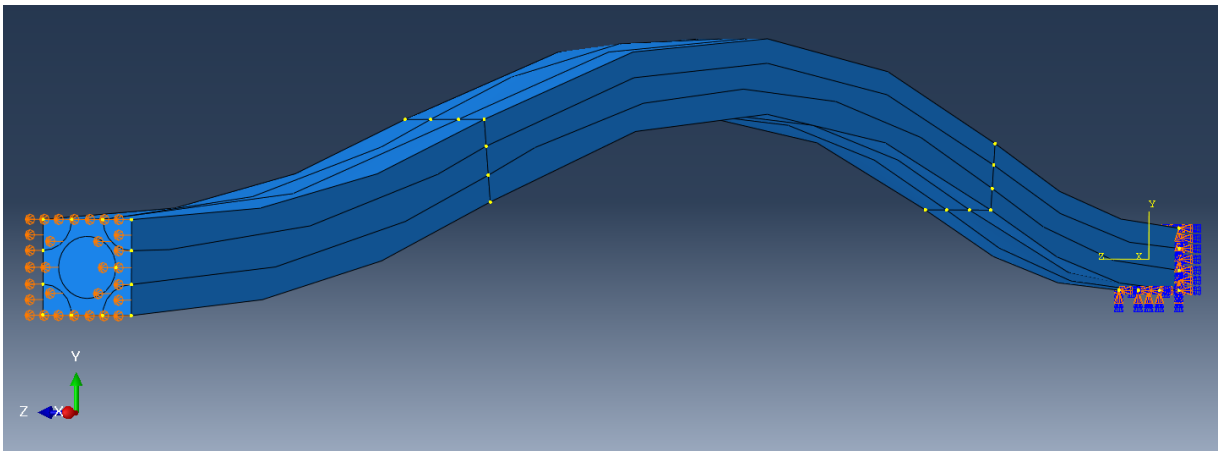

Figure 5.9: Meso Scale Model Boundary Conditions

Meshing the meso scale model was done following free tetrahedral element shape. The fiber cross-section was meshed under number control to a set value of 12 elements. The resin was meshed under size control to an approximate global mesh size of 0.012 mm with curvature control allowable to a maximum deviation factor of 0.1. As the fibers are the primary load carrying system, it is important to have them under a finer mesh in comparison to the resin. In addition, the coarser resin mesh was allowable due to optimization of computational times. Figure 5.10 is a visual representation of the mesh used for the meso scale model.

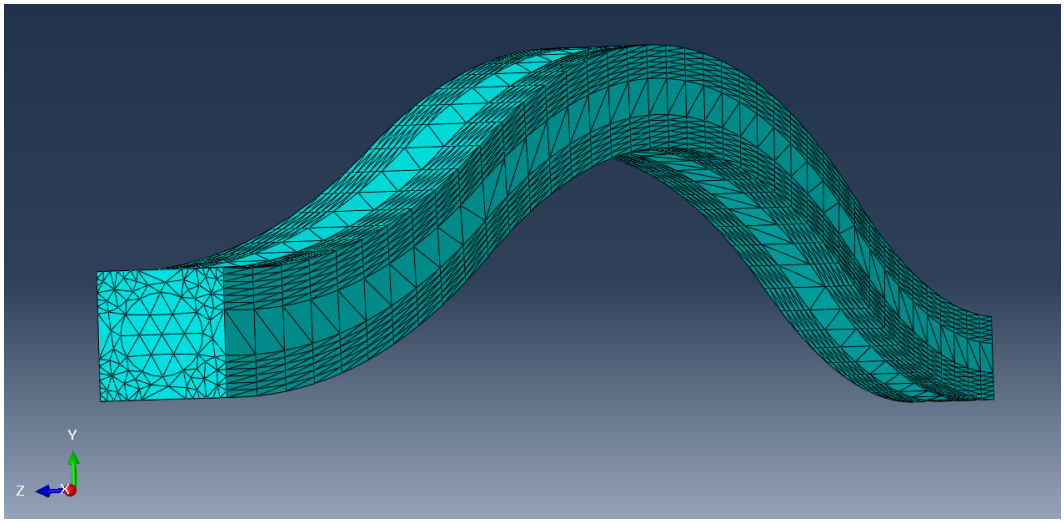

Figure 5.10: Meso Scale Model Mesh

From the simulation results, the S_{11} stress distribution shown in Figure 5.11 coincides with that of a tensile load straightening the fibers, similar to the results observed by M. Garnich et al. [38]. Pockets of high stress can be seen at the points with the lowest angle of misalignment to the U1 direction (fiber direction), as they are zones experiencing the lowest degree of displacement. Additionally, it is clear how the fibers are the primary stress carrying system of the model, and the resin contributes a negligible amount to the overall stiffness.

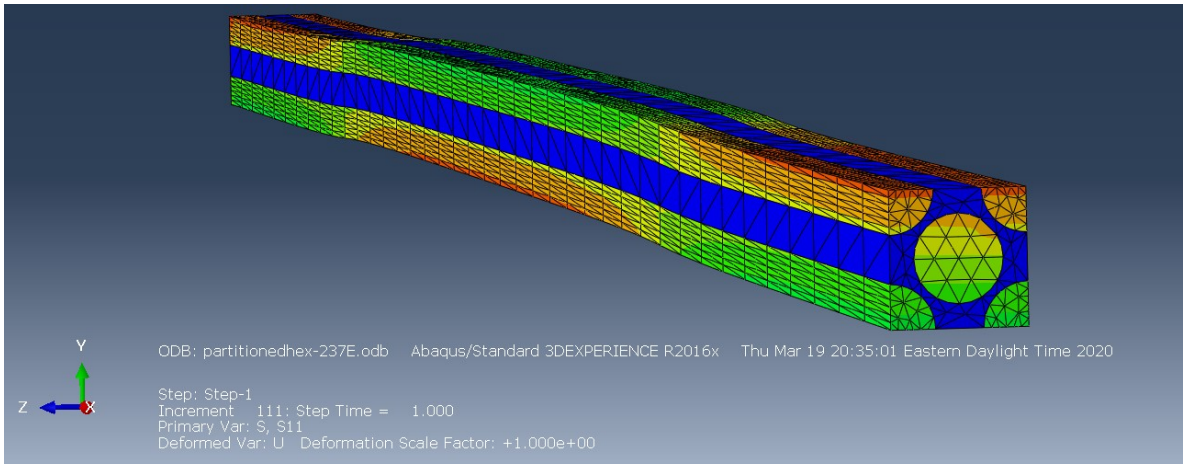

Figure 5.11: S_{11} Stress Distribution in FEA

From the resultant output, the S_{11} stresses recorded at the front face of the model will be used for comparison with the micro scale simulation and the experimental results. Figure 5.12 & Figure 5.13 are the resultant plots from the Abaqus simulation.

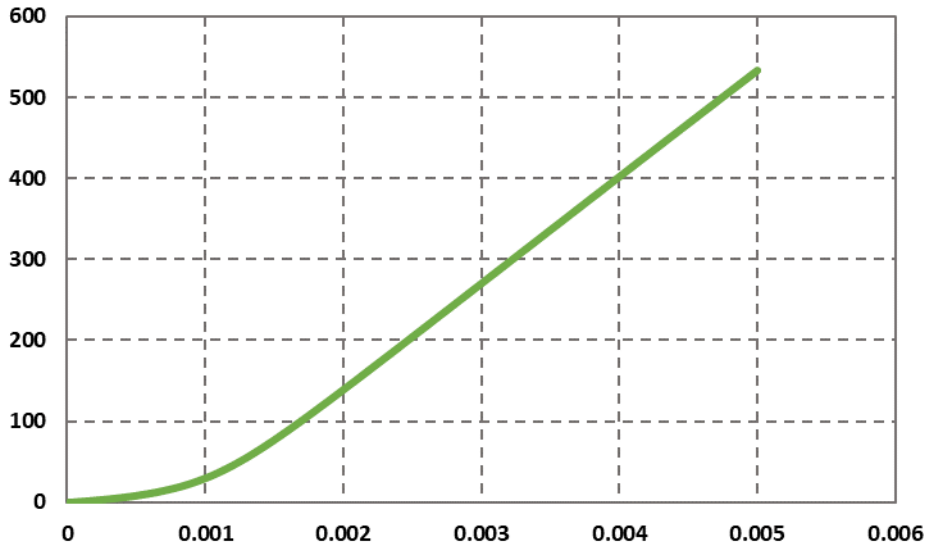

Figure 5.12 : S_{11} Stress on the Front Face of the Meso Scale Model

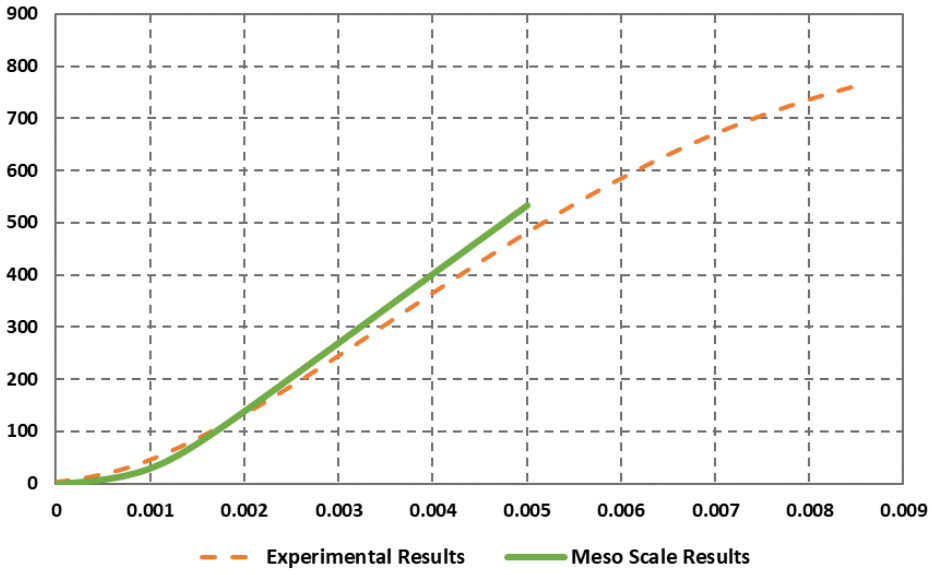

Figure 5.13: Meso Scale Model Compared to Experimentation

From these two plots, a correlation between the experimental results and the Abaqus simulation can be seen. Both stiffness plots follow a non-linear trend up to a value of approximately 0.2% strain, leading into a linear stiffness plot. Focusing in on the non-linear portion of the plot, the simulated response reflects a smoother increase in stiffness when compared to experimentation. This is potentially due to the have a single set waviness that was used for the FE model, while in a full prepreg, each individual fiber can have their own degree of waviness, and the experimental stiffness plot represents a full average. However, it can be assumed that if the fibers in the experimentally tested prepreg follow a sinusoidal function, and based on these results, the average fiber within the prepreg has a wavelength of 0.47514 mm and an amplitude of 0.0266 mm, resultant in a waviness value w of 0.056 where $w = A/L$. Shifting focus to the linear region of the stiffness plot, in both experimental testing and the FEA the system has approximately the same final stiffness. Being based on the rule of mixtures equation and the initial elastic properties set in Abaqus, the similar stiffness shows a correct assumption in the FE model parameters and model construction.

Comparing the stiffness plots between the micro scale and the meso scale simulations, very small variations can be seen (Figure 5.14). Between the two samples, variations are seen between the transition point among the non-linear to linear stiffness trends. The meso scale FE model exhibits a steeper and earlier exit from the non-linear region of stiffness. This is attributed to the quarter fibers on the lower half of the model. As these two quarter fibers have less travel before aligning to the U1 direction, they are able to enter the linear portion of their stiffness response earlier and shift the average S_{11} stress higher. The increase in stiffness from these lower fibers outweigh the reduced stiffness in the upper fibers caused by the increased travel path. This is displayed to in Figure 5.15, showing how even a small change in initial amplitude can greatly affect the stiffness response.

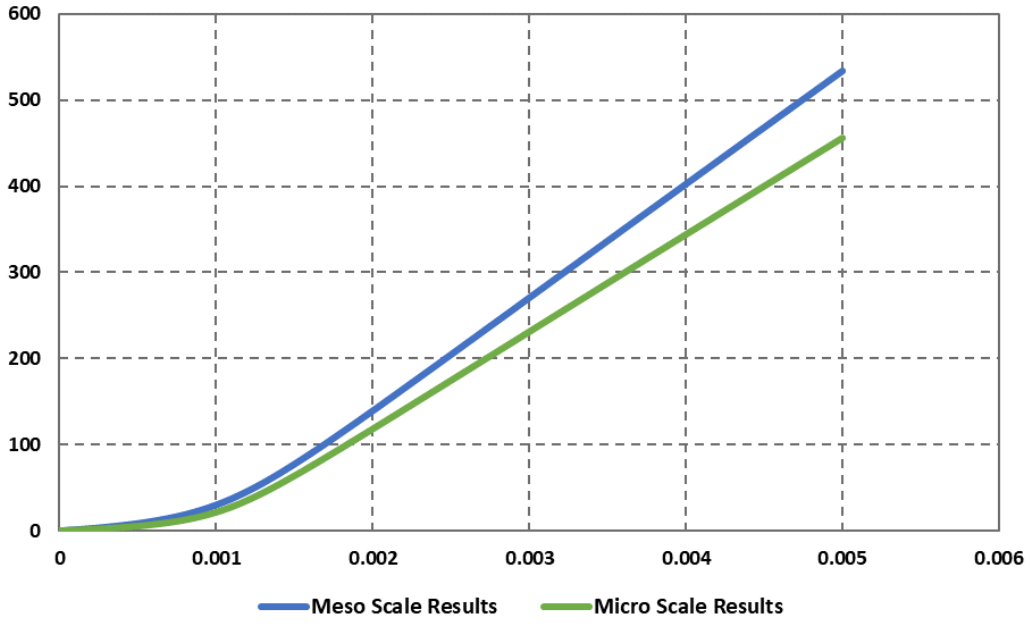

Figure 5.14: Meso Scale vs. Micro Scale Results

To study the effects that initial fiber geometry has on the model, the meso model was simulated under three distinct amplitudes. Amplitude values of 0.0366 mm, 0.0266 mm, and 0.0166 mm were used in each model respectively to study how the stiffness plot is affected by initial waviness. Looking at Figure 5.15, it is determined that the initial fiber waviness does have an immediate effect on the non-linear region of the stiffness plot. As nothing other than the geometry of the models were changed, any differences in the tensile response are completely attributed to the changes in dimension. Between the three simulations, it is shown how increasing the initial amplitude by a value of 0.01 mm effectively changes the tensile behavior between 0 to 0.25% strain. As the fiber has a shorter path to travel before being aligned to the primary direction of displacement (U1), the non-linear region of the plot is reduced in length. These results are critical in explaining the large standard deviation experienced in experimental testing as a change as small as 0.01 mm are shown to dramatically change the tensile behavior of the system.

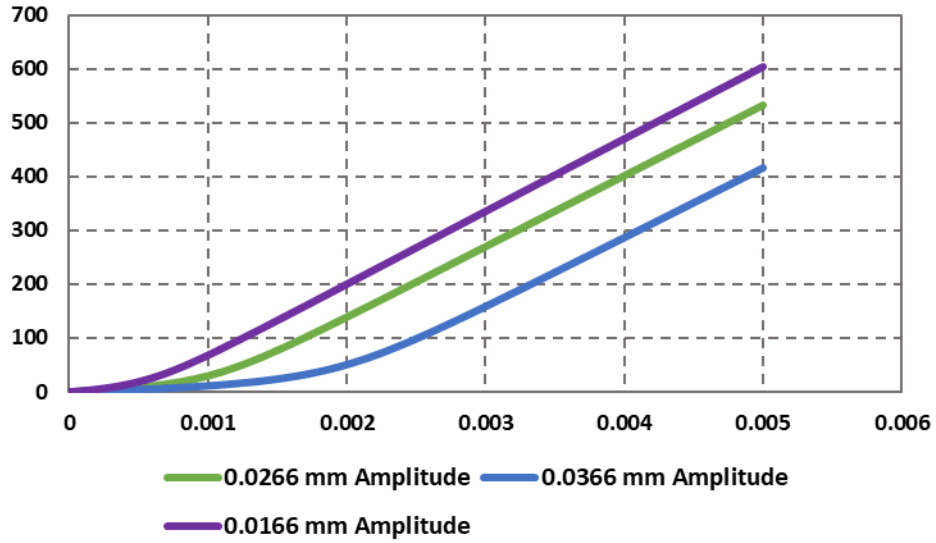

Figure 5.15: Meso Scale S_{11} Results Under Different Initial Waviness

The goal of conducting FEA on uncured prepreg was to verify if the initial assumptions based on the fibers following a sinusoidal function within the prepreg as the main source affecting the stiffness of the system hold true. As shown through simulations, the stiffness response of an uncured prepreg system is dependent on the initial waviness parameters of the fibers. These simulations correlate to what was observed in experimental testing and provides support for the results.

Chapter 6: Mathematical Model

The objective of this report is to provide an applicable model based on experimental observations to accurately simulate the tensile response of uncured prepreg. In Chapter 5, a FE model was simulated to validate the effect fiber waviness has on the stiffness of the system. However, it is impractical and extremely time consuming to rebuild meso scale simulations in order to determine the stiffness of an uncured prepreg. In this chapter, a mathematical model will be proposed, based on the fiber geometry, that can be used to determine the stiffness of an uncured prepreg at any given fiber waviness.

Studying the geometry of a single fiber, a mathematical model was also developed to predict the force based on the amplitude and period of the waveform. The fiber was modelled with the assumption that waviness follows a sinusoidal function with a period (*k*), and amplitude (*a*) as seen in Figure 6.1 (a).

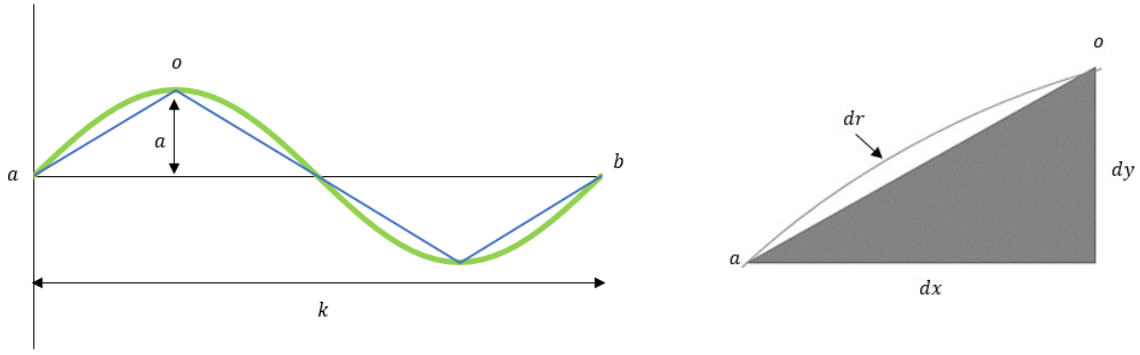

(a) (b)

Figure 6.1: Generalized Sinusoidal Waveform of a Single Fiber

To find the true length of the fiber, an integration will be used. Figure 6.1 (b) represents a zoomed in portion of the sinusoidal plot between the points *a* and *o*. Using Pythagoras' theorem, the length *ao* can be determined with the sides *dx* and *dy* resulting in equation 6.1.

$$dr \cong ao = \sqrt{dx^2 + dy^2} \tag{6.1}$$

To get an exact solution of the curved length *dr*, an integration must be used with Pythagoras' theorem. The resultant equation is shown in equation 6.2.

$$dr = \int_a^b \sqrt{dx^2 + dy^2} \tag{6.2}$$

Rearranging this equation, into a usable formula to apply the derivative of the sine function to, equation 6.3 was determined.

$$L = \int_a^b \sqrt{1 + \left(\frac{dy}{dx}\right)^2}\, dx \tag{6.3}$$

This equation can be used over the period of the wavelength (point *a* to *b*) to determine the total length of the fiber *L*. Using the same fiber dimensions measured through microscopic observation in ImageJ, used in Chapter 5, the following equations are applied to equation 6.3 to determine the true fiber length.

$$y = a * sin[k(x)] \tag{6.4}$$

$$\left(\frac{dy}{dx}\right) = k * a * \cos[k(x)] \tag{6.5}$$

$$L = \int_a^b \sqrt{1 + (k * a * \cos[k(x)])^2}\, dx \tag{6.6}$$

$$\int_0^{950} \sqrt{1 + \left(\left({}^{2\pi}/_{950}\right) * 36.8871 * \cos\left[\left({}^{2\pi}/_{950}\right)(x)\right]\right)^2}\, dx = 963.982\ \mu m \tag{6.7}$$

The resultant fiber length from this example is 963.98 nanometers long. Using Equation 6.6 to calculate the true length of the sinusoidal graph, the rate of change of the amplitude *a* as the length *b* can be numerically determined using Equation 6.8. MATLAB was used to numerically solve for the change in amplitude by equating the integral in Equation 6.8 to the arc length that was solved for in Equation 6.7. Figure 6.2 represents the resultant values between the change in amplitude to the change in period.

$$L = \int_{a}^{b+\Delta b} \sqrt{1 + \left((k+\Delta k) * (a+\Delta a) * \cos[(k+\Delta)(x)]\right)^2}\, dx \tag{6.8}$$

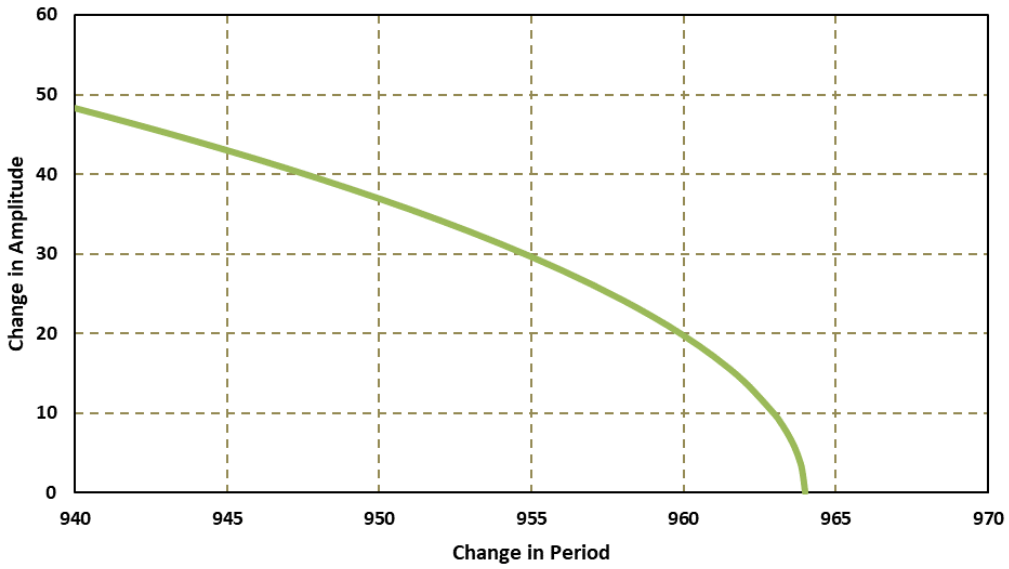

Figure 6.2: Ratio Between the Change in Amplitude & the Change in Period

Based on the graphical results in Figure 6.2, the ratio between the change in amplitude vs wavelength follows a non-linear trend. The sharp drop in amplitude as the period approaches the arc length is attributed to the values approaching the node of the periodic function. With this plot, the change in waviness can be geometrically determined through the entire movement of the fiber under tensile load. To mathematically calculate the forces in relation to the change in waviness, the stiffness equations developed by P. Cartraud et al, an equation based on the

geometric wave of a single fiber, can be developed to solve for the axial force and the bending moment exerted on the system [44]. While there are several papers studying the force analysis of period functions [44]–[47], the work done by P. Cartraud et al. is easily applicable for the purposes of this study. In their research, a free body diagram model was developed for a periodic beam structure as seen in Figure 6.3.

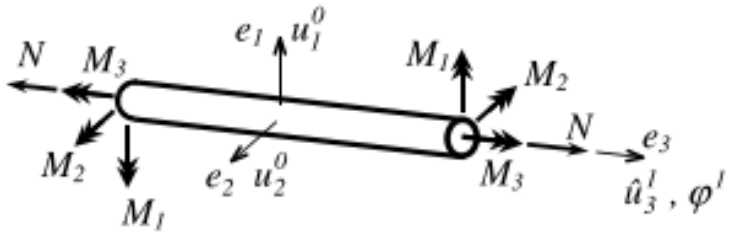

Figure 6.3: Loading and Displacements of a 3-axis Beam Structure [44]

Using this free body diagram as the basis for their equations, P. Cartraud et al. expand the linear cell problem into a functional equation for solving the normal force and the moment exerted on the system at the macroscopic level. The problem is solved using finite element method in taking account of the periodicity of the linear relationships between the degrees of freedom of two nodes on opposite sides of the beam in the beam axis direction. Their solution works by imposing only one component of the macroscopic strain to be equal to one, and the two others to zero. Applying these conditions, the effective properties are applied to the solved homogenized constitutive equation [44]. The following equations were derived from P. Cartraud et al. and will be used in our applications in this study.

$$\begin{Bmatrix} N \\ M_1 \\ M_2 \\ M_3 \end{Bmatrix} = [a^{hom}] \begin{Bmatrix} E^E \\ E^{C_1} \\ E^{C_2} \\ E^T \end{Bmatrix} \tag{6.9}$$

Modified equation for stiffness in periodic beam

$$\begin{Bmatrix} N \\ M_2 \end{Bmatrix} = \begin{bmatrix} a_{11}^{hom} & a_{13}^{hom} \\ a_{31}^{hom} & a_{33}^{hom} \end{bmatrix} \begin{Bmatrix} E^E \\ E^{C_1} \end{Bmatrix} \tag{6.10}$$

$$\begin{cases} a_{11}^{hom} = \dfrac{E(cos\theta)}{\dfrac{(cos^2\theta)}{A} + \dfrac{(X_1^2)}{I}} \\ a_{33}^{hom} = EI(cos\theta) \\ a_{13}^{hom} = a_{31}^{hom} = 0 \end{cases} \tag{6.11}$$

Where $(\ldots.)$ represents an average operator, X_1^2 represents the amplitude, I is the second moment of inertia, E is the Young's Modulus and θ is the inclination angle (as shown in Figure 6.4.

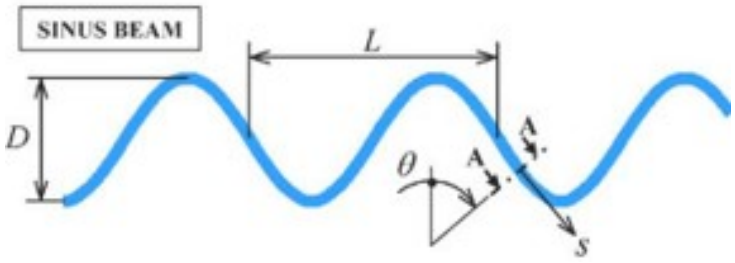

Figure 6.4: Periodic Function as Described by P. Cartraud et al. [44]

As mentioned earlier, for the equations to work, all but one macroscopic strain parameter must be set to zero. For the case of uniaxial tensile loading, the sole strain parameter measured will be the E^E parameter. Therefore, for our loading case the following strain parameters will be used.

$$E^{E} = X;\ E^{C_1} = 0 \tag{6.12}$$

Using these equations, combined with the relationship of amplitude to period determined in Figure 6.2, the normal force and the moment in the fiber can be determined at any initial wavelength and throughout the fibers movement path. At each step of the fibers movement, the angle of inclination and the wavelength will change, resulting in a change in forces. Applying equation 6.12 to 6.11, the resultant equation for solving the normal force in the fiber is as follows;

$$\{N\} = \left(\frac{E(cos\theta)}{\frac{(cos^2\theta)}{A} + \frac{(X_1^2)}{I}} \right) * E^{E} \tag{6.13}$$

To solve for the angle of inclination, the maximum tangential angle of the sinusoidal plot will be used. The solution for solving the angle is based on the solution to the derivative of the sine function when $x = \left({}^{1}/_{2}\right)b$. As the amplitude and the wavelength changes due to the application of the normal force, so too will the angle of inclination. For the application of these equations, the same dimensions studied earlier in this section will be used. Equation 6.14 represents the general solution for the maximum angle of inclination at any wavelength *b* and amplitude *a*.

$$\theta = \tan^{-1}\left|\left({}^{2\pi}/_{b}\right) * a * \cos\left[\left({}^{2\pi}/_{b}\right)\left(\left({}^{1}/_{2}\right)b\right)\right]\right| \tag{6.14}$$

In equation 6.13, a value of 237 GPa will be used for the variable *E* as the Young's Modulus of the fibers. The cross-sectional area *A* will be calculated with a fiber diameter of 7 microns. The second moment of inertia *I* is calculated about the e_2 axis in Figure 6.3 and is calculated by equation 6.15.

$$I = \frac{\pi}{2} r^4 \tag{6.15}$$

The following table represents the initial parameters for the calculations:

Table 6.1: Variable Values for Equation 6.13

E (Pa)	2.37E+11
A (m^2)	3.84845E-11
r (m)	0.0000035
I (m^4)	2.35718E-22

At each increment of amplitude, equation 6.13 was applied to solve the normal force exerted on the cross section of the periodic beam. For equation 6.13, the engineering strain at each increment was used for the variable E^E. With the normal force know, the stress in the beam was calculated using the area shown in Table 6.1. Using the calculated stress and the engineering strain, the effective Young's modulus at every increment was solved. The resultant equation for determining the effective Young's modulus at any given waviness is as follows, where a is the amplitude, E is the Young's modulus of the fiber, A is the cross sectional area of the fiber, *I* is the second moment of inertia, *e* is the Cauchy strain of the fiber, Δa is the change in amplitude, v_f is the volume fraction of fiber and θ is the angle of inclination of the fiber.

$$E^{eff} = \frac{\left\{\left(\frac{E(cos\theta)}{\frac{(cos^2\theta)}{A} + \frac{(a^2)}{I}}\right) e \cdot a\right\} \cdot {}^{1}/_{v_f}}{A\,\Delta a} \tag{6.16}$$

The resultant plot of Effective Young's modulus against waviness, waviness being the amplitude over the wavelength, can be seen in Figure 6.5. As a result from applying equation 6.13 to the fiber geometry observed in Figure 6.2, the steep slope present in representing the change in amplitude is reflective in the calculations for determining the effective modulus of the fibers. The effective modulus remains close to zero until a waviness parameter of approximately 0.023, representing a wavelength of 959 microns and an amplitude of approximately 22 microns. After this point, the effective modulus quickly rises to a maximum value of 156 GPa. This value being 66% of the initial fiber modulus of 237 GPa, as shown in Table 6.1. As the fibers only make

up 66% of the volume fraction of the laminate, and the assumption of 0% contribution from the epoxy towards the rule of mixtures equation, this final value of 156 GPa holds true.

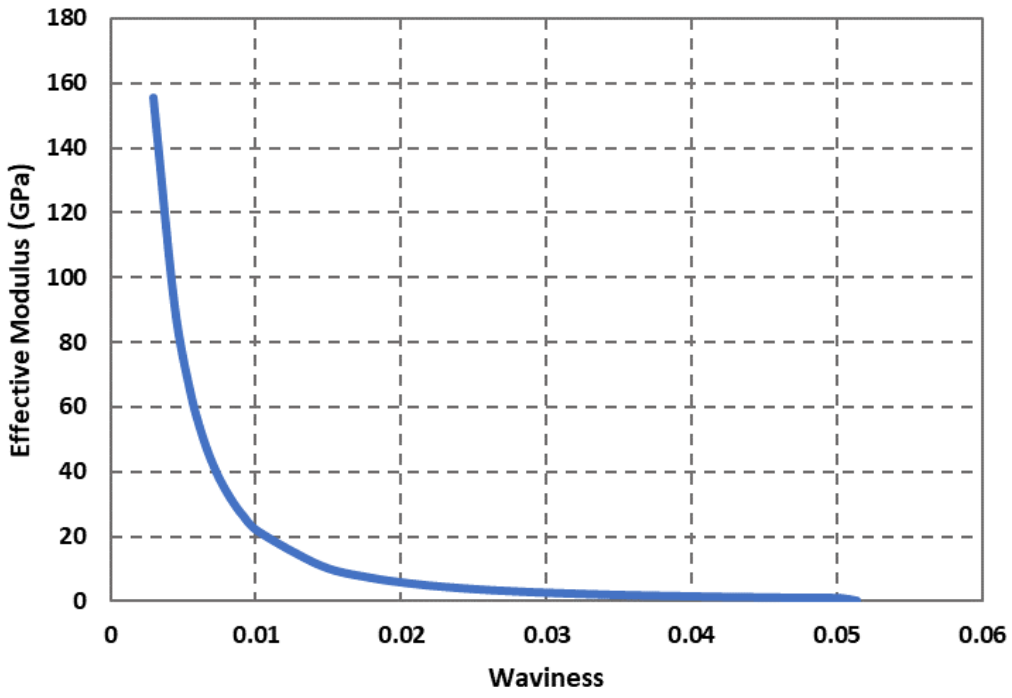

Figure 6.5: Effective Property of Carbon Fiber Based on Waviness

As the waviness increases (from left to right on Figure 6.5) the modulus reduces and reaches an asymptote to zero. This curve in effective Young's modulus is the source of non-linearity seen in experimental and simulated uniaxial tensile testing of uncured carbon fiber prepreg. Due to each fiber in the prepreg having its own initial waviness parameters, the stiffness response does not present a slope as steep as the one shown in Figure 6.5. As some fibers reach their maximum effective modulus earlier or later than others, as an average, the resultant stiffness follows a less abrupt slope.

Relating to the experimental results observed in Chapter 4.1.2, the effective modulus calculated by equation 6.16 can be compared to the effective modulus obtained through uniaxial tensile testing. Overlaying the Figure 4.11 and Figure 6.5, the resulting effective modulus observed can be compared between the two sources. From the mathematically calculated

effective tensile modulus, only the last 6 points will be compared to the effective modulus calculated within the six strain zones as described in Chapter 4.1.2. The resultant Figure 6.6 shows the bar graph comparison between the two results.

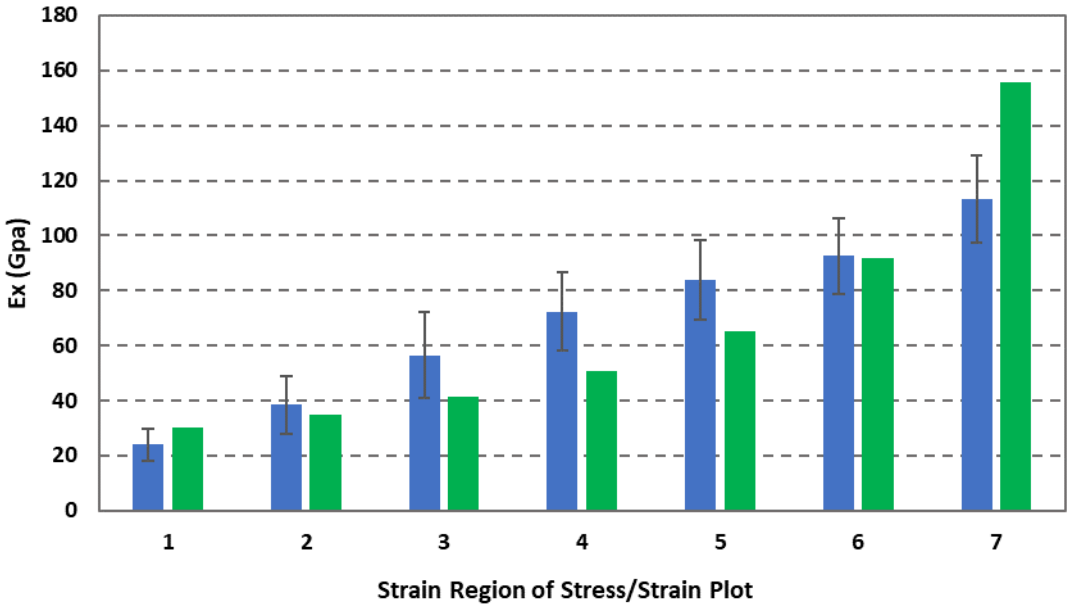

Figure 6.6: Comparison Between Experimental and Calculated Effective Modulus

Comparing the two results, there are evident similarities between the experimentally determined, and the mathematically determined effective modulus of elasticity. Excluding the last point on the plot, the calculated effective modulus lies within or close to the standard deviation of the experimentally determined values. As the values we have are based on the mean across all samples, if a larger sample size was used, potentially the experimental values will align themselves closer to the mathematically determined values. The final point calculated mathematically resulted in an effective young's modulus of approximately 156 GPa. This final mathematically determined modulus is much higher than the maximum observed through experimentation (approximately 114 GPa). Potential sources for this delta can be based on the fiber failure observed in some samples during the area of linear stiffness. This failure during experimental testing presents the possibility of lowering the overall final linear stiffness.

Nonetheless, the effective stiffness values between the numerical model and the experimental model are comparable and follow the same non-linear to linear trend.

To compare and verify the accuracy of the mathematical model, calculations based on the classical lamination theory (CLT) of composites were done using material properties based on the rule of mixture equations. As discussed in section 4.2, CLT is able to predict the effective properties of a lamina based on fiber orientation and the initial mechanical properties. The following table represents the distinct fiber and resin material properties that will be used in conjunction with rule of mixtures equations to determine the laminas initial properties.

Table 6.2 Material Properties of Resin and Fiber

Resin		**Fiber**	
E (Mpa)	1.00	E (Mpa)	237000.00
G (Mpa)	0.30	G (Mpa)	27300
V	0.47	V	0.30

The mechanical properties for the resin were unavailable for CYCOM 977-2, however similar values were taken from that of silicon rubber [48], [49]. The properties of the carbon fibers were also taken from datasheets of similar fibers to the one used in the by SOLVAY in the prepreg [50]. The following equations are based on the rule of mixtures equations and were used in solving for the lamina properties.

$$E_1 = E^f V^f + E^m(1 - V^f) \tag{6.17}$$

$$v_{12} = v^f V^f + v^m(1 - V^f) \tag{6.18}$$

$$\frac{1}{E_2} = \frac{V^f}{E^f} + \frac{(1 - V^f)}{E^m} \tag{6.19}$$

$$\frac{1}{G_{12}} = \frac{V^f}{G^f} + \frac{(1 - V^f)}{G^m} \tag{6.20}$$

$$v_{21} = \frac{v_{12}}{E_1} \cdot E_2 \tag{6.21}$$

In these equations, the parameters with subscripts 1 & 2 represent the material properties of the lamina in 1 (the fiber direction) and 2 (Perpendicular to the fiber direction). Additionally, in this model, the lamina is assumed to be very thin and thus the parameters in the 3rd direction are assumed negligible. The parameters with superscript m, represents the properties of the matrix resin, and superscript f represents the properties of the fiber. V^f is the volume fraction of the fibers and was assigned to be 66%. Using these equations, the following table represents the calculated initial mechanical properties of the lamina.

Table 6.3 Lamina Material Properties for CLT Model

E_1 (Pa)	1.56E+11
E_2 (Pa)	2.94E+06
v_{12}	0.3578
v_{21}	6.73E-06
G_{12} (Pa)	882334.12

Following classical lamination theory, and the plane-stress assumption for on-axis orthotropic materials, the following equations represent the solution to the Q-matrix which relates the on-axis stress to strain components of the lamina.

$$Q_{11} = {E_1}/{1 - v_{12}v_{21}} \tag{6.22}$$

$$Q_{12} = Q_{21} = {v_{12}E_2}/{1 - v_{12}v_{21}} \tag{6.23}$$

$$Q_{22} = {E_2}/{1 - v_{12}v_{21}} \tag{6.24}$$

$$Q_{66} = G_{12} \tag{6.25}$$

Applying the off-axis transformation theory to the Q-matrix, the $\bar{Q}$-matrix can be developed to relate the off-axis stress to strain components of the lamina. Figure 6.7 shows how the off-axis angle is determined for $\bar{Q}$-matrix calculations.

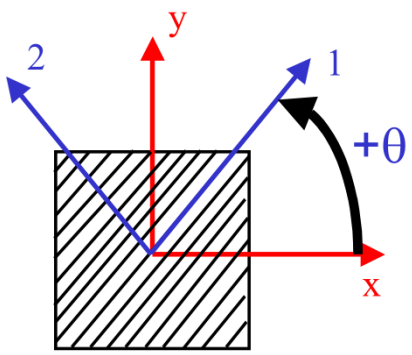

S

Figure 6.7 Off-Axis Transformation for CLT Model

The following equations represent the solution to the $\bar{Q}$-matrix and its application in solving off-axis stress & strain relations.

$$\begin{Bmatrix} \sigma_x \\ \sigma_y \\ \tau_{xy} \end{Bmatrix} = \begin{bmatrix} \bar{Q}_{11} & \bar{Q}_{12} & \bar{Q}_{16} \\ \bar{Q}_{21} & \bar{Q}_{22} & \bar{Q}_{26} \\ \bar{Q}_{61} & \bar{Q}_{62} & \bar{Q}_{66} \end{bmatrix} \begin{Bmatrix} \varepsilon_x \\ \varepsilon_y \\ \gamma_{xy} \end{Bmatrix} \tag{6.26}$$

$$\bar{Q}_{11} = U_{1Q} + cos2\theta \cdot U_{2Q} + cos4\theta \cdot U_{3Q}$$

$$\bar{Q}_{22} = U_{1Q} - cos2\theta \cdot U_{2Q} + cos4\theta \cdot U_{3Q}$$

$$\bar{Q}_{12} = U_{4Q} - cos4\theta \cdot U_{3Q}$$

$$\bar{Q}_{66} = U_{5Q} - cos4\theta \cdot U_{3Q} \qquad (6.27)$$

$$\bar{Q}_{16} = \frac{1}{2} sin2\theta \cdot U_{2Q} + sin4\theta \cdot U_{3Q}$$

$$\bar{Q}_{26} = \frac{1}{2} sin2\theta \cdot U_{2Q} - sin4\theta \cdot U_{3Q}$$

$$U_{1Q} = \tfrac{1}{8}(3Q_{11} + 3Q_{22} + 2Q_{12} + 4Q_{66})$$

$$U_{2Q} = \frac{1}{2}(Q_{11} - Q_{22})$$

$$U_{3Q} = \frac{1}{8}(Q_{11} + Q_{22} - 2Q_{12} - 4Q_{66}) \qquad (6.28)$$

$$U_{4Q} = \frac{1}{8}(Q_{11} + Q_{22} + 6Q_{12} - 4Q_{66})$$

$$U_{5Q} = \frac{1}{8}(Q_{11} + Q_{22} - 2Q_{12} + 4Q_{66})$$

With the result $\bar{Q}$-matrix shown in equation 6.26, the lamina stiffness matrix [ABD] can be determined. For determining the effective off-axis tensile modulus, only the A portion of the stiffness matrix is necessary to solve for. The following equation represents the solution for solving the A portion of this stiffness matrix.

$$A_{ij} = \sum_{k=1}^{N} \bar{Q}_{ij} \cdot t_k \quad where\ i,j = 1,2,6 \tag{6.29}$$

In equation 6.29, the parameter k represents the layer number in the lamina, and t is the thickness of the layer. For our model, only 1 layer will be taken into consideration since only one ply of prepreg material is being modelled. The thickness t_k is therefore equal to the thickness of the single ply of prepreg, which is 0.01275 mm. With the resultant A portion of the stiffness matrix, the effective Young's modulus in the uniaxial loading direction can be mathematically determined. The equation for solving $\bar{E}_x$ is shown below.

$$\bar{E}_x = \frac{1}{H}\left[A_{11} - \frac{A_{12}^2}{A_{22}}\right] \tag{6.30}$$

In equation 6.30, H represents the total thickness of the entire lamina. For this model, since the lamina is comprised of the single layer of prepreg, H and t_k both share the same value of 0.01275 mm. In order to relate these equations, 6.26 to 6.30, to our model of varying waviness through uni-axial loading, the $\bar{Q}$-matrix was solved for every change in angle across the fiber's path. Using the data from Figure 6.2, the angle at every step of the fiber's path was already determined and can be applied to solving the $\bar{Q}$-matrix. Code was developed to compute the resultant A stiffness matrix for each possible angle and then solve the resultant effective young's modulus. Figure 6.8 represents the resultant plot of effective modulus in the loading direction to fiber waviness within the prepreg.

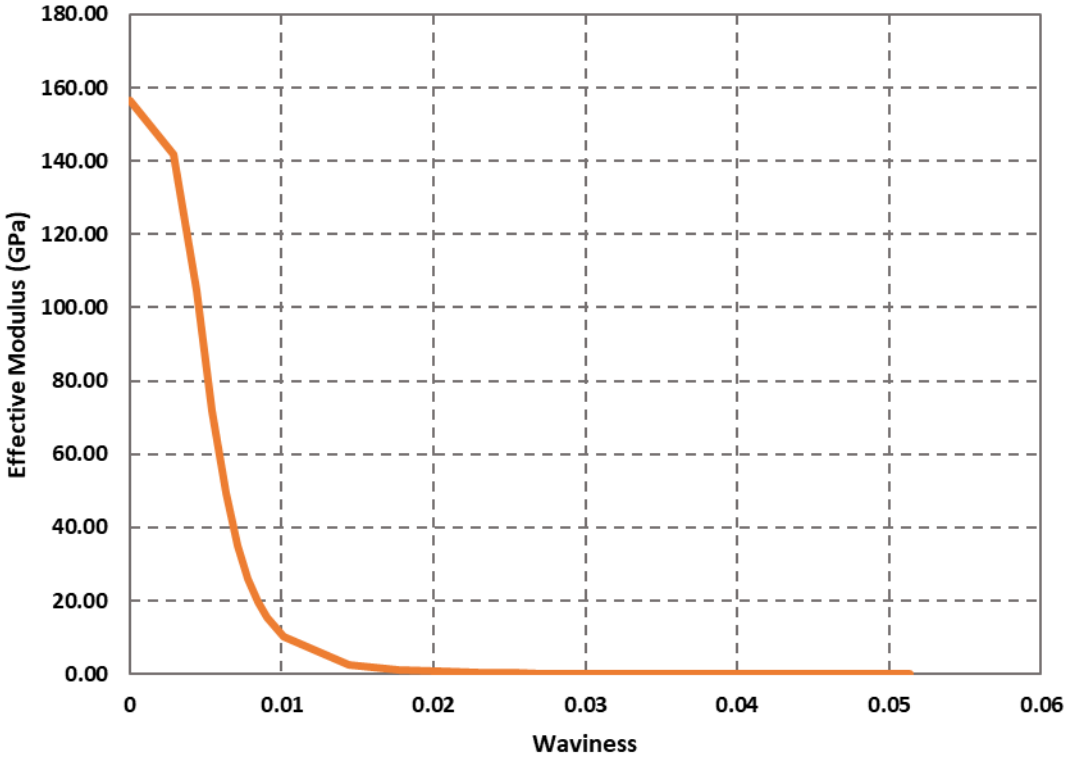

Figure 6.8: Effective Tensile Modulus Based on CLT Model

The resultant plot indicates a sharp increase in effective modulus around a waviness parameter of 0.01 and an effective modulus of approximately 15 GPa. The modulus then rises to a maximum value of 156.42 GPa once the waviness reaches 0. This maximum modulus corresponds to the calculated lamina on-axis property shown in Table 6.3, which is a good indication that the CLT model is accurately solving for the correct modulus. Comparing the plot calculated through the CLT model to the effective modulus plot calculated using the free body diagram method discussed early, both plots are shown to follow a similar trend.

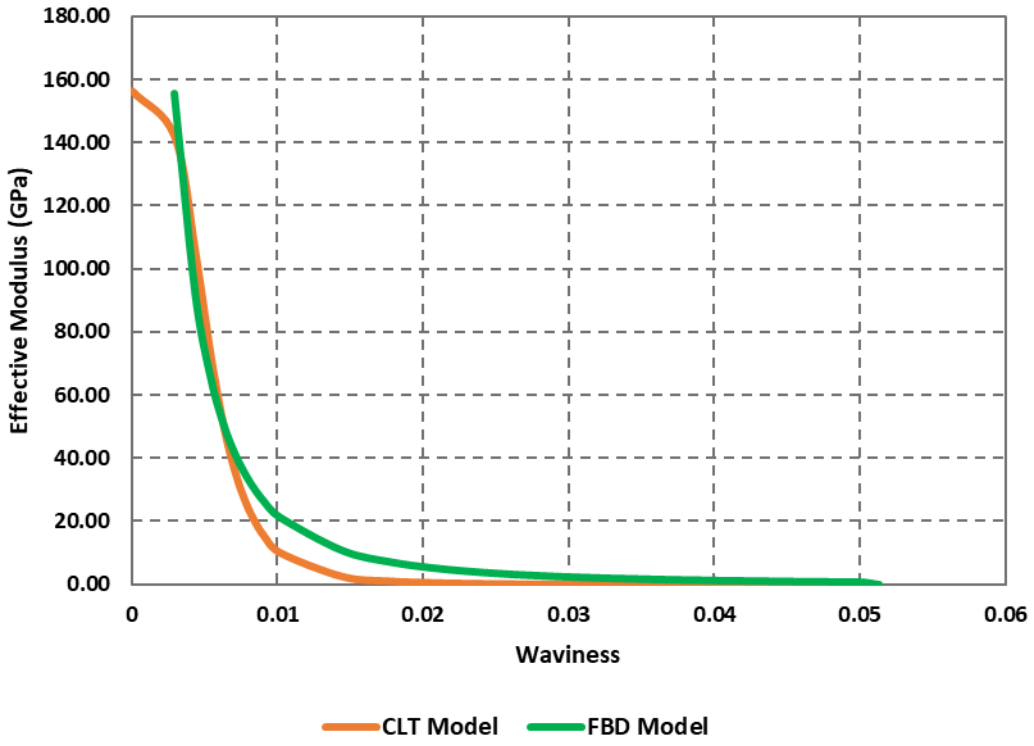

Figure 6.9: Effective Tensile Modulus Based on CLT Model

Modeling the mechanical behaviour of the prepreg as the waviness parameter changes under load through CLT allowed for comparison and validation to our new math model based on free body diagram modelling. With both mathematical models following a similar trend, it is reasonable to say that the free body diagram model is accurate in predicting the effective modulus of an uncured carbon fiber prepreg.

Chapter 7: Conclusion & Contribution

The tensile modulus of uncured carbon fiber prepreg follows an initial non-linear stiffness behavior followed by a region of linear stiffness due to the initial fiber waviness found in the uncured prepreg. Through experimental testing, it was determined that the modulus of the composite system exhibits characteristics of non-linear tensile modulus up to a strain value of 0.002. Focusing in on this region, on a per sample basis, a large standard deviation in stiffness values were observed. The cause of this non-linear stiffness behavior was determined to be due to the initial fiber waviness present in the uncured system. Based on the assumption that the epoxy has a negligible contribution to the overall elastic modulus of the system through the theory of rule of mixtures, the fiber Young's modulus (multiplied by the volume fraction of the fibers) was equal to the total Young's modulus of the system. By applying a uniaxial tensile load to the fiber direction of the unidirectional prepreg, the waviness of the fibers is reduced as they exhibit movement through the viscous epoxy, and the effective Young's modulus of the system is increased up to its maximum stiffness once the majority of the fibers are aligned to the primary fiber direction. At this stage of the uniaxial tensile testing, the stiffness of the aligned fibers is represented by a linear plot.

Temperature was also observed to have an effect on the tensile response of the uncured prepreg system. As the temperature of the system is elevated, the overall viscosity of the epoxy matrix is reduced. This reduction in viscosity was observed to result in an elongated stress vs. strain curve during uniaxial tensile testing. As the resin at elevated temperatures provides less resistance to the movement of the fibers, the overall stress is reduced. During experimentation, with an increase of temperature by 15 degrees Celsius, the non-linear region of the stiffness plot was almost doubled in length, and the linear region of the stiffness plot was only observed to begin at a strain of 0.004. The linear region of stiffness was comparable to the stiffness observed at room temperature, indicating that temperature does not affect the mechanical performance of the system once the fibers are aligned to the direction of the force.

To quantify the effect of fiber waviness, microscopic imaging was performed on samples prior to, and after applying a uniaxial tensile load. Through MATLAB software, the mean angle of misalignment was computed and compared. The results showed that there is a decrease in the mean angle of misalignment in the carbon fibers after they were subjected to a tensile load. These results validate the theory that the waviness within the fibers is reduced during the application of uniaxial force as the fibers move through the viscous matrix.

To supplement the experimental observations and to simulate the fiber and resin interactions at the micro and meso scale of the laminate, a FE Model was developed using ABAQUS software. The goal of the model was to simulate a fiber with a set initial waviness undergoing a uniaxial displacement and recording the stress vs. strain curve to plot the stiffness response. These simulated results were compared to the plots obtained through experimental testing to verify if the same tensile behavior can be obtained through application of the finite element method. The results from both the micro scale and the meso scale FE models closely correspond with the stiffness plots observed during experimental testing, with the stiffness response of the meso scale model being the closest to experimentation. This is due to the fiber interactions introduced at the mesoscale. Having the FE results line up with the observed experimental results proves that the initial fiber waviness within the prepreg is the driving force behind the non-linear tensile modulus seen in the stiffness response curve of the uncured prepreg when a uniaxial force is applied.

Answering the main goal of this thesis, a mathematical model was developed to accurately predict the effective Young's modulus of the uncured prepreg system based on the initial waviness of the fibers. The model was created on the assumption that the fibers within the prepreg follow a sinusoidal periodic function. Based on this geometry and the relationship between the change in amplitude and the change in wavelength, two distinct mathematical equations were proposed to solve for the corresponding axial force and the Youngs modulus of the carbon fiber. The first equation, being based on the free body diagram analysis of a fiber moving through the resin, and the second being based on classical lamination theory analysis. Both mathematical models were able to accurately predict the effective Young's modulus of the

carbon fiber prepreg though uniaxial tensile load. The equations provide a short hand method to calculate the stiffness of the uncured prepreg based solely on the initial material properties and waviness of the composite system. Results from the mathematical model line up closely to the stiffness plots observed during experimentation and provide an accurate model to quantify the effects of waviness on the stiffness parameter of the uncured prepreg system.

The results of this study can be applied to AFP and ATL process modelling as well as other simulations relating to the modelling of uncured carbon fiber prepreg tape. Using the mathematical model proposed in this study and to initial set waviness for the fibers, the tape can be modeled with variable Young's modulus based on the applied tensile load during the simulation. This type of simulation can be applied to any simulation where uncured tape is being manipulated either through AFP or by any other means. The resultant simulations using the new material properties are believed to be more accurate than using linear properties and will have a better representation of what will happen during experimentation. Additionally, future research in modelling of uncured prepreg can benefit from these advanced material property equations. Research into AFP fiber steering can use the non-linear Young's modulus equations to obtain better simulations of what happens during manufacturing. As steering introduces additional loads to the uncured tape, the inclusion of more detailed and precise material properties is believed to yield more accurate simulations. In conclusion, the knowledge of the non-linear stiffness properties of uncured carbon fiber prepreg can be applied to both industrial applications such as AFP process modeling, and to research applications such as models for fiber steering.

Chapter 8: Future Work

In the completion of this thesis, there are still areas of study that can be expanded on through future research. One aspect in particular would be focused on expanding the FE model of the prepreg system. One of the limitations in the model described in this thesis is that it assumes elastic properties for the resin system. Future work can improve on the model by coupling the ABAQUS explicit solver with ABAQUS CFD. Modeling the resin as a true viscous member has the potential to yield more accurate results, in addition to being able to model temperature changes on the system. In order to do this, experimental testing on the rheology on the epoxy will also need to be performed to obtain the viscous parameters of the resin. Once all the initial parameters are known in relation to the vicious behavior of the epoxy, fluid and elastic analysis will have to be done in unison to study the effects of the model.

One other area of future work is in relation to the application of obtaining the initial fiber waviness through microscopic observations. As the mathematical models proposed in this thesis rely on the initial geometry of the fibers within the prepreg, having an improved image recognition software to determine the mean waviness should be investigated. Currently, the imaging recognition software used in this study is only able to determine the mean angle of misalignment for all fibers in the image and determining the sinusoidal waveform on an individual fiber is a manual process. Development of an image recognition software would allow for more accurate application of the equation proposed to solve for effective Young's modulus. The software would need to be able to determine the mean wavelength and amplitude of each fiber strand within the microscopic image. Potentially, the mathematical equation can be built into the software to calculate the effective modulus of the prepreg at its current waviness. Considering that the application of the equation proposed in this thesis is reliant on microscopic images, implementation of a more sophisticated software to replace current rudimentary measurements can greatly improve the application of the equation.

Chapter 9: References

[1] Z. Bin Wang, Z. Y. Han, H. Lu, and H. Y. Fu, "A review of tensioner for automated fiber placement," in *Advanced Materials Research*, 2013, vol. 740, pp. 183–187.

[2] J. Frketic, T. Dickens, and S. Ramakrishnan, "Automated manufacturing and processing of fiber-reinforced polymer (FRP) composites: An additive review of contemporary and modern techniques for advanced materials manufacturing," *Addit. Manuf.*, vol. 14, pp. 69–86, 2017.

[3] D. O. Evans, M. M. Vaniglia, and P. C. Hopkins, "Fiber placement process study," in *International SAMPE Symposium and Exhibition (Proceedings)*, 1989, vol. 34, no. pt2, pp. 1822–1833.

[4] E. Oromiehie, B. G. Prusty, P. Compston, and G. Rajan, "Automated fibre placement based composite structures: Review on the defects, impacts and inspections techniques," *Compos. Struct.*, vol. 224, no. May, p. 110987, 2019.

[5] K. Croft, L. Lessard, D. Pasini, M. Hojjati, J. Chen, and A. Yousefpour, "Experimental investigation of effect of automated fiber placement defects in composite structures," in *International SAMPE Symposium and Exhibition (Proceedings)*, 2010.

[6] M. Hojjati, J. Chen, A. Yousefpour, and M.-A. Octeau, "Automated fibre placement (AFP) of aerospace composite structures," in *24th Annual Technical Conference of the American Society for Composites 2009 and 1st Joint Canadian-American Technical Conference on Composites*, 2009, vol. 2, pp. 1005–1013.

[7] C. Kassapoglou and J. Hammer, *Design and analysis of composite structures with manufacturing flaws*, vol. 35, no. 4. 1990.

[8] F. Heinecke and C. Willberg, "Manufacturing-Induced Imperfections in Composite Parts Manufactured via Automated Fiber Placement," *J. Compos. Sci.*, vol. 3, no. 2, p. 56, 2019.

[9] R. Harik, C. Saidy, S. J. Williams, Z. Gurdal, and B. Grimsley, "Automated fiber placement defect identity cards: Cause, anticipation, existence, significance, and progression," *Int.*

SAMPE Tech. Conf., vol. 2018-May, no. January, 2018.

[10] P. J. Schubel, "Cost modelling in polymer composite applications: Case study – Analysis of existing and automated manufacturing processes for a large wind turbine blade," *Compos. Part B Eng.*, vol. 43, no. 3, pp. 953–960, 2012.

[11] D. Leutz, M. Vermilyea, S. Bel, and R. Hinterhölzl, "Forming Simulation of Thick AFP Laminates and Comparison with Live CT Imaging," *Appl. Compos. Mater.*, vol. 23, no. 4, pp. 583–600, Aug. 2016.

[12] L. M. Dangora, C. Mitchell, K. D. White, J. A. Sherwood, and J. C. Parker, "Characterization of temperature-dependent tensile and flexural rigidities of a cross-ply thermoplastic lamina with implementation into a forming model," *Int. J. Mater. Form.*, vol. 11, no. 1, pp. 43–52, 2018.

[13] T. G. Gutowski, Z. Cai, S. Bauer, D. Boucher, J. Kingery, and S. Wineman, "Consolidation Experiments for Laminate Composites," *J. Compos. Mater.*, vol. 21, no. 7, pp. 650–669, 1987.

[14] K. Potter, "Bias extension measurements on cross-plied unidirectional prepreg," *Compos. Part A Appl. Sci. Manuf.*, vol. 33, no. 1, pp. 63–73, 2002.

[15] D. H. J. A. Lukaszewicz and K. Potter, "Through-thickness compression response of uncured prepreg during manufacture by automated layup," *Proc. Inst. Mech. Eng. Part B J. Eng. Manuf.*, vol. 226, no. 2, pp. 193–202, Feb. 2012.

[16] H. Alshahrani and M. Hojjati, "A theoretical model with experimental verification for bending stiffness of thermosetting prepreg during forming process," *Compos. Struct.*, vol. 166, pp. 136–145, 2017.

[17] H. Alshahrani and M. Hojjati, "A new test method for the characterization of the bending behavior of textile prepregs," *Compos. Part A Appl. Sci. Manuf.*, vol. 97, pp. 128–140, 2017.

[18] J. Wang, A. C. Long, and M. J. Clifford, "Experimental measurement and predictive modelling of bending behaviour for viscous unidirectional composite materials," *Int. J. Mater. Form.*, vol. 3, no. 2, pp. 1253–1266, Sep. 2010.

[19] W. Zhang *et al.*, “Experimental Methods to Characterize the Woven Composite Prepreg Behavior During the Preforming Process,” in *Proceedings of the American Society for Composites--Thirty-First Technical Conference*, 2016.

[20] K. Potter, C. Langer, B. Hodgkiss, and S. Lamb, “Sources of variability in uncured aerospace grade unidirectional carbon fibre epoxy preimpregnate,” *Compos. Part A Appl. Sci. Manuf.*, vol. 38, no. 3, pp. 905–916, Mar. 2007.

[21] P. Hubert and A. Poursartip, “Method for the direct measurement of the fibre bed compaction curve of composite prepregs,” *Compos. Part A Appl. Sci. Manuf.*, vol. 32, no. 2, pp. 179–187, 2001.

[22] T. G. Clapp and H. Peng, “Buckling of Woven Fabrics: Part II: Effect of Weight and Frictional Couple,” *Text. Res. J.*, vol. 60, no. 5, pp. 285–292, 1990.

[23] K. Potter, “In-plane and out-of-plane deformation properties of unidirectional preimpregnated reinforcement,” *Compos. Part A Appl. Sci. Manuf.*, vol. 33, no. 11, pp. 1469–1477, 2002.

[24] P. Boisse, N. Hamila, E. Vidal-Sallé, and F. Dumont, “Simulation of wrinkling during textile composite reinforcement forming. Influence of tensile, in-plane shear and bending stiffnesses,” *Compos. Sci. Technol.*, vol. 71, no. 5, pp. 683–692, 2011.

[25] O. J. Nixon-Pearson, J. P. H. Belnoue, D. S. Ivanov, K. D. Potter, and S. R. Hallett, “An experimental investigation of the consolidation behaviour of uncured prepregs under processing conditions,” *J. Compos. Mater.*, vol. 51, no. 13, pp. 1911–1924, 2017.

[26] S. Erland, T. J. Dodwell, and R. Butler, “Characterisation of inter-ply shear in uncured carbon fibre prepreg,” *Compos. Part A Appl. Sci. Manuf.*, vol. 77, pp. 210–218, 2015.

[27] Y. Wang, D. Ivanov, J. P. H. Belnoue, J. Kratz, B. C. Kim, and S. R. Hallett, “Experimental characterisation of in-plane shear behaviour of uncured thermoset prepregs,” no. June, pp. 24–28, 2018.

[28] D. F. Sentis *et al.*, “Tensile behaviour of uncured sheet moulding compounds: Rheology and flow-induced microstructures,” *Compos. Part A Appl. Sci. Manuf.*, vol. 101, pp. 459–

470, Oct. 2017.

[29] F. Liu, Y. Wang, X. Xue, and H. Yang, “Temperature dependence of the viscosity of epoxy acrylate-tripropylene glycol diacrylate binary mixtures,” *E-Polymers*, vol. 15, no. 6, pp. 447–450, 2015.

[30] Cytec Engineered, “Cycom 977-2 Epoxy Resin System -Technical Data Sheet,” *Cytec - Eng. Mater.*, pp. 1–4, 2012.

[31] S. W. Yurgartis, “Measurement of small angle fiber misalignments in continuous fiber composites,” *Compos. Sci. Technol.*, vol. 30, no. 4, pp. 279–293, 1987.

[32] A. L. Stewart and A. Poursartip, “Characterization of fibre alignment in as-received aerospace grade unidirectional prepreg,” *Compos. Part A Appl. Sci. Manuf.*, vol. 112, pp. 239–249, 2018.

[33] K. Potter, B. Khan, M. Wisnom, T. Bell, and J. Stevens, “Variability, fibre waviness and misalignment in the determination of the properties of composite materials and structures,” *Compos. PART A-APPLIED Sci. Manuf.*, vol. 39, no. 9, pp. 1343–1354, Sep. 2008.

[34] D. Wilhelmsson and L. E. Asp, “A high resolution method for characterisation of fibre misalignment angles in composites,” *Compos. Sci. Technol.*, vol. 165, pp. 214–221, 2018.

[35] P. J. Joyce, D. Kugler, and T. J. Moon, “A technique for characterizing process-induced fiber waviness in unidirectional composite laminates - Using optical microscopy,” *J. Compos. Mater.*, vol. 31, no. 17, pp. 1694–1727, 1997.

[36] M. Herráez *et al.*, “Computational micromechanics evaluation of the effect of fibre shape on the transverse strength of unidirectional composites: An approach to virtual materials design,” *Compos. Part A Appl. Sci. Manuf.*, vol. 91, pp. 484–492, 2016.

[37] D. Kuksenko, H. J. Böhm, and B. Drach, “Effect of micromechanical parameters of composites with wavy fibers on their effective response under large deformations,” *Adv. Eng. Softw.*, vol. 121, pp. 206–222, 2018.

[38] M. R. Garnich and G. Karami, “Finite Element Micromechanics for Stiffness and Strength

of Wavy Fiber Composites," *J. Compos. Mater.*, vol. 38, no. 4, pp. 273–292, 2004.

[39] T. D. Sheet, "CYCOM 977-2 and 977-2A."

[40] J. Patel and P. Peralta, "Characterization of deformation localization mechanisms in polymer matrix composites: A digital image correlation study," in *Conference Proceedings of the Society for Experimental Mechanics Series*, 2017, no. 200869, pp. 243–246.

[41] B. Pan, K. Qian, H. Xie, and A. Asundi, "On errors of digital image correlation due to speckle patterns," *ICEM 2008 Int. Conf. Exp. Mech. 2008*, vol. 7375, no. August 2009, p. 73754Z, 2008.

[42] B. Drach, D. Kuksenko, and I. Sevostianov, "Effect of a curved fiber on the overall material stiffness," *Int. J. Solids Struct.*, vol. 100–101, pp. 211–222, 2016.

[43] "Tenax ®-J HTS40 E13 3K 200tex (G30-500 3K HTA-7C EP03) HTS40 E13 6K 400tex (G30-500 6K HTA-7C EP03) HTS40 E13 12K 800tex (G30-500 12K HTA-7C EP03) Tenax ®-E HTS40 F13 12K 800tex (HTS5631 800tex f12000 t0) HTS40 F13 24K 1600tex (HTS5631 1600tex f24000 t0)," 2008.

[44] P. Cartraud and T. Messager, "Computational homogenization of periodic beam-like structures," *Int. J. Solids Struct.*, vol. 43, no. 3–4, pp. 686–696, 2006.

[45] L. POTIER-FERRY M; SIAD, "Homogénéisation géométrique d'une poutre ondulée," *Comptes rendus l'Académie des Sci. Série 2, Mécanique, Phys. Chim. Sci. l'univers, Sci. la Terre*, 1992.

[46] E. Syerko, A. A. Diskovsky, I. V. Andrianov, S. Comas-Cardona, and C. Binetruy, "Corrugated beams mechanical behavior modeling by the homogenization method," *Int. J. Solids Struct.*, vol. 50, no. 6, pp. 928–936, Mar. 2013.

[47] N. Buannic and P. Cartraud, "Higher-order effective modeling of periodic heterogeneous beams. I. Asymptotic expansion method," *Int. J. Solids Struct.*, vol. 38, no. 40–41, pp. 7139–7161, 2001.

[48] "Silicone Rubber," *AZoM*, 2001. [Online]. Available: https://www.azom.com/article.aspx?ArticleID=920. [Accessed: 09-Jun-2020].

[49] “Properties: Silicone Rubber,” *AZoM*, 2001. [Online]. Available: https://www.azom.com/properties.aspx?ArticleID=920. [Accessed: 09-Jun-2020].

[50] H. Miyagawa, C. Sato, T. Mase, E. Drown, L. T. Drzal, and K. Ikegami, “Transverse elastic modulus of carbon fibers measured by Raman spectroscopy,” *Mater. Sci. Eng. A*, vol. 412, no. 1–2, pp. 88–92, 2005.